



PREDIS

Deliverable 4.8

Characterization of magnesium phosphate cement and low-cost magnesium phosphate cement

Date 28.6.2024 Version Final

Dissemination level Public

Lead author

Raúl Fernández

UAM – Universidad Autónoma de Madrid, Spain

email raul.fernandez@uam.es



This project has received funding from the Euratom research and training programme 2019-2020 under grant agreement No 945098.

Project acronym PREDIS	Project title PRE-DISposal management of radioactive waste	Grant agreement No. 945098
Deliverable No. D4.8	Deliverable title Characterization of magnesium phosphate cement and low-cost magnesium phosphate cement	Version Final
Type Report	Dissemination level Public	Due date M46
Lead beneficiary KIPT, CNRS, ORANO, CSIC, UAM		WP No. 4
Main author Raúl Fernández (UAM)	Reviewed by Abdessalam Abdelous (IMT), WP4 Leader	Accepted by Maria Oksa (VTT), Coordinator
Contributing author(s) KIPT: Sergey Sayenko, Vladimir Shkuropatenko, Yevhenii Svitlychnyi; CNRS: Kim-Khanh Le, Davide Rodrigues, Sylvie Delpech, Céline Cannes; ORANO: Lavinia Stefan; CSIC: Carla Fernández-García, María Cruz Alonso; UAM: Mikel Dieguez, Pilar Padilla-Encinas, Jaime Cuevas, Ana Isabel Ruiz, Raúl Fernández		Pages 67

<p>Abstract</p> <p>Deliverable D4.8 reports the main activities performed by the research groups involved in the subtasks 4.6.1 'Geopolymer' and 4.6.2 'Cement-based materials' of the PREDIS project (CSIC, CNRS, KIPT, ORANO and UAM) focused on the optimization of a magnesium potassium phosphate cement (MKPC) formulation and the study and development of a low-cost MKPC, in both cases with the objective to encapsulate radioactive metals, although most efforts have been led towards aluminium.</p> <p>Several key issues have been dealt, including the nature of MgO and the possibility to replace dead-burned magnesia by reactive magnesia, the nature of filler materials and their contribution to the MKPC properties, the magnesium to phosphate ratio, the influence of different retarders and the study of the pore ion content and the curing conditions.</p> <p>The properties of MKPC are very dependent of the specific formulations, and subtle changes of ratios or components can largely vary their characteristics. Nevertheless, it has been observed that blast furnace slag, volcanic ash and wollastonite can be used as fillers with similar or even better performance than fly ash, commonly considered as a reference filler.</p> <p>As the phosphate is highly soluble but MgO is not, a formulation considering a stoichiometric ratio would lead to excess of both unreacted precursors, causing efflorescence and weakness in the microstructural properties of MKPC matrices. The magnesium to phosphate ratio should, therefore, be increased to the maximum possible without compromising the passivation zone of the reactive metals. The pore solution is mainly dominated by phosphates, borates, and potassium, that decrease their concentration with the increasing magnesium to phosphate ratio but increase the pH.</p> <p>The use of reactive magnesia not only reduces the overall costs but also demonstrated that due to its higher specific surface, is able to better complete reaction with KH_2PO_4, leaving less anhydrous MgO in the material.</p> <p>The study has revealed that several retarders can be used, not only alone but also in combination. However, further studies need to be performed to better understand their effect on the hydration mechanisms.</p>

<p>Coordinator contact Maria Oksa VTT Technical Research Centre of Finland Ltd Kivimiehentie 3, Espoo / P.O. Box 1000, 02044 VTT, Finland E-mail: maria.oksa.@vtt.fi Tel: +358 50 5365 844</p>
--

Notification

The use of the name of any authors or organization in advertising or publication in part of this report is only permissible with written authorisation from the VTT Technical Research Centre of Finland Ltd.

Acknowledgement

This project has received funding from the Euratom research and training programme 2019-2020 under grant agreement No 945098.

TABLE OF CONTENTS

1	INTRODUCTION.....	6
1.1	Main goals.....	7
1.2	Activities carried out.....	7
2	OPTIMIZATION OF MAGNESIUM PHOSPHATE CEMENT FORMULATIONS.....	7
2.1	UAM: development and optimization of magnesium phosphate cement formulations for encapsulation of aluminium.....	7
2.1.1	Materials and methods.....	8
2.1.2	Main findings on the MPC formulations.....	9
2.1.3	Recommendations.....	24
2.2	CSIC: optimization and characterization of MKPC formulations.....	25
2.2.1	Main goals.....	25
2.2.2	Materials used and samples description.....	26
2.2.3	Main findings: design of an optimal and stable MKPC matrix.....	28
2.2.4	Effect of M/P ratio on macro and microstructural properties of MKPC.....	37
3	LOW-COST MAGNESIUM PHOSPHATE CEMENTS.....	44
3.1	CNRS and ORANO: developing a low-cost magnesium phosphate cement formulation for nuclear waste stabilization.....	44
3.1.1	Materials and methods.....	44
3.1.2	Results.....	45
3.1.3	Discussion and conclusions.....	54
3.2	KIPT: effect of mineralogical additives on the structure, the physical and mechanical properties of MKPC.....	55
3.2.1	Initial materials and sample preparation.....	56
3.2.2	XRD analysis of MKPC samples.....	57
3.2.3	Microstructural study of MKPC samples.....	58
3.2.4	Study of mechanical properties.....	60
3.2.5	Samples with high content of BFS.....	61
3.2.6	Tests with reactive and hard burnt MgO.....	61
3.2.7	Conclusions.....	62
4	DISSEMINATION.....	62
	ACKNOWLEDGMENTS.....	64
	REFERENCES.....	65

1 Introduction

In the domain of radioactive waste management, a common approach to safely prepare low and intermediate-level radioactive wastes for disposal is to encapsulate them within a cement matrix [1]. Portland Cements (PC) has frequently been used due to its cost-effectiveness and stability after hydration [2]. However, the varied nature of radioactive wastes, particularly from the dismantling of old nuclear reactors, presents a unique challenge. Some of these wastes contain metallic aluminium, an amphoteric metal that forms a protective oxide layer in neutral conditions but becomes soluble in strongly alkaline environments, such as those created by PCs [3,4]. This solubility leads to ongoing corrosion, releasing dihydrogen gas and potentially causing container damage [5]. Therefore, the key criterion for encapsulating aluminium waste focuses on controlling hydrogen production.

Magnesium phosphate cements (MPCs) have been proposed as alternative cementitious systems to conventional PC systems for the encapsulation of low and intermediate level radioactive wastes containing reactive metals, due to a lower internal pH (4-9). The high alkalinity of PC systems can induce corrosion of metals such as aluminium, beryllium and uranium. In addition to the low pH, preserving the passivation zones of these metals (aluminium passivation in the pH range 3-9; beryllium 6-13), MPCs demand lower water than PC, set at shorter time and may lead to higher early compressive strength. The use of MPC allows the incorporation of significant quantities of metallic wastes into the cement package, making it a more cost-effective option, as fewer packages need to be produced.

The process to prepare MPC is based on a reaction between MgO, which is often subjected to high-temperature calcination to reduce reactivity [6], a soluble acid phosphate salt and water, according to reaction 1, to produce K-struvite ($\text{MgKPO}_4 \cdot 6\text{H}_2\text{O}$) as the main reaction product.



Although early works on MPCs used ammonium polyphosphates, e.g. [7], monopotassium phosphate (KH_2PO_4) has emerged as the more practical source of phosphate, avoiding the release of noxious ammonia during the setting and hardening. Monopotassium phosphate is usually sold as a fertilizer (MKP) with large purity and affordable price. The cement produced is, therefore, termed as magnesium potassium phosphate cement (MKPC).

A low amount of chemical retarder is normally added in the reaction to delay the acid-base reaction, control the setting time and limit the temperature rise. The most commonly used retarders include boric acid and borax [8,9], but other chemicals (thiosulphates, tripolyphosphates, alginates) are also investigated [10].

Various composites might be added as fillers to improve the mechanical strength, the chemical resistance and to reduce costs. Coal fly ash (FA) and blast furnace slag are the most commonly used fillers in MKPC matrices due to their morphology and small size, able to enhance the fluidity in the mixture and contribute to the mechanical strength of the cement [11]. Nevertheless, the availability of FA is being recently reduced as it is generated as a by-product in coal-based thermal power plants that are being shut down worldwide to reduce carbon emissions and meet climate targets. Similarly, the availability of blast furnace slag will significantly decline, globally, due to the transition of the iron and steel industry to a low-carbon steelmaking. Therefore, an increasing interest in the study of novel types of fillers is generated for the improvement of properties and quality/cost ratio of MKPC.

Most of the raw materials used to prepare MKPCs are either of high purity (such as the acid activator or the retarder), either from a few providers when it comes to dead-burned MgO. The use of such raw materials is understandable when it comes to investigating a novel cement matrix and its hydration mechanisms. However, from an industrial point of view this can lead to an increased overall price for the metric ton.

The high cost of MPCs presents a significant barrier to a larger industrial use. One of the main raw materials used in MPC preparation is dead-burned MgO which is available from limit number of

suppliers, leading to elevated costs. Furthermore, dead-burned MgO is primarily obtained through a high-temperature treatment process of high-quality natural magnesite, typically conducted at temperatures ranging from 1300 to 1700 °C. This process not only consumes an important amount of energy but also results in environmental pollution. Since magnesite consist mainly of magnesium carbonate, the calcination process results in the release of significant amounts of CO₂.

Addressing this issue requires the exploration of alternative sources of MgO to reduce the high CO₂ emissions associated with dead-burned MgO production and MgO price. As a solution, a low-cost MPC formulation (LC-MPC) has been considered, using reactive MgO instead of dead-burned (DB) MgO.

Reactive MgO, also known as caustic calcined MgO, is produced through a calcination process at temperatures below 900 °C. Lower calcination temperatures result in more affordable MgO prices. One notable characteristic of this type of MgO is its moderate to high chemical reactivity [12]. Its wide usage includes application in fertilizers, animal feed, and as a fundamental component for various MgO chemicals essential for the production of paper, ceramics, and cements.

For LC-MPC, the use of reactive MgO is not only advantageous in terms of price but also has good advantages in terms of durability and a lower carbon footprint. Additionally, with its specific surface area being 100 times greater than that of DB MgO, reactive MgO becomes significantly more accessible for participating in the formation of the hydrate phase. Consequently, less anhydrous MgO remains in the matrix thereby reducing long-term durability concerns and the potential for elevated pH levels if MgO continues to react.

Thus, the objective is to decrease the MKPC cost. A screening of the different phosphate and MgO sources was initially proposed. The influence of the purity of the raw materials on the properties of MKPC-based matrices were investigated, as well as the feasibility to design such matrices by valorising wastes.

1.1 Main goals

Guidelines for sub-tasks 4.6.1 (formulation) and sub-tasks 4.6.2 (cost optimization) considered to specifically address:

- The role of MgO, including the use of both, hard-burned and reactive MgO
- The role of the Mg/P ratio
- The role of the water/(MgO + KH₂PO₄) ratio
- The filler nature and the filler/(MgO + KH₂PO₄) ratio
- The role of retarders, including their combination
- The MKPC curing conditions

1.2 Activities carried out

This document outlines the contribution and main achievements obtained within the work performed in subtask 4.6.1, focused on the optimization of MPC formulations for encapsulation of reactive metals and 4.6.2 focused on the cost-optimization of MPC.

2 Optimization of magnesium phosphate cement formulations

2.1 UAM: development and optimization of magnesium phosphate cement formulations for encapsulation of aluminium

It was initially agreed by all groups involved in task 6 to consider a reference MKPC mortar formulation to begin the studies. This formulation was optimized for encapsulation of metallic aluminium and corresponds to formulation M1 in [13]. The cement formulation is composed by MgO

and KH_2PO_4 in equimolar stoichiometry. Boric acid was added as a retarder, and the water/cement mass ratio was equal to 0.51 (cement = $\text{MgO} + \text{KH}_2\text{PO}_4$). A high quality MgO source permitted good fluidity and workability.

Table 1. MKPC mortar formulation defined as a reference for all the studies (mass of components are expressed to obtain 1 L of cement). Mass ratio indicates the reagent/ $(\text{MgO} + \text{KH}_2\text{PO}_4)$ ratio

Reference starting reagents	Mass (g)	Mass ratio
MgO (MAGCHEM 10CR, hard burnt 95.3 wt.%)	131.39	-
KH_2PO_4 (KristaTM, 98 wt.%)	443.58	-
Sand MI 0.1/1.2 (Sibelco, 99,3 wt.% SiO_2)	574.97	1
Fly ash (class F, low CaO content)	574.97	1
Boric acid (H_3BO_3)	11.50	0.02
H_2O (distilled water)	293.24	0.51

Based on the characteristics presented by the MKPC prepared by this formulation, activities performed under task 4.6.1 involved:

- The acquisition of raw materials from different sources (MgO , KH_2PO_4 , fillers, retarders and sand) and characterization of their physical, chemical and mineralogical properties.
- Evaluation of cement pastes and mortars characteristics by modifying components and ratios in the MPC formulations
- Evaluation of the reactivity of metallic aluminium encapsulated in MKPC and PC.

2.1.1 Materials and methods

Materials:

Four different MgO have been used, supplied by Martin Marietta Inc (USA) and Magnesitas Navarras (Spain). The KH_2PO_4 was provided by Yara and Seminsa, sold as a high-purity (98%) commercial fertilizer MKP (mono-potassium phosphate). A laboratory-grade boric acid with a purity of >99.5% wt.%, was used as setting retarder. Coal fly ash (low calcium-Class F) was provided by the Cordemais thermal power station in France, operated by Électricité de France S.A. Volcanic ash was collected at the island of La Palma (Canary Islands, Spain). It was produced as a consequence of the volcanic eruption that took place from September to December 2021 at the Cumbre Vieja volcano. Wollastonite (CaSiO_3) was provided by Crimidesa. Pumice (volcanic rock) was provided by Kremer. Two different types of metakaolin (MK) were provided by Imerys and IMCD. In general, both MK samples were quite similar in chemical composition and mineralogy. Normalized quartz sand was purchased in agreement with EN 196-1 grain size distribution, ranging from 0.08 to 2 mm.

Methods:

Workability of cement pastes and mortars was measured by means of the mini-slump test, using an open cone of 57 mm in height and 19 mm in diameter at the top and 38 mm at the base. The slump area was calculated using ImageJ software. The setting time was tested using an automatic Vicat Needle Matest Vicatronic E044N (Matest, Italy) according to the ASTM-C191 norm. The pH of cement pastes suspensions was measurement at different ages (1, 2, 7, 15, 30, 90 and 180 days). XRD analyses were performed on MPC powder samples after 7, 28 and 90 days with a Bruker D8 instrument (Bruker Corporation, Billerica, Massachusetts, USA) with a copper anode X-ray tube ($\lambda(\text{K}\alpha_1) = 1.54056 \text{ \AA}$), measured at a 2θ angle from 3° to 70° with a step size of 0.02.

SEM-EDX studies were carried out with a JEOL JM-6400 microscope coupled to a LINK LZ_5 EDX analyser on MPC samples cured for 28 days. The voltage used was 20 kV and the samples were coated with gold, with an average layer of 15 nm.

Cement mortars of $4 \times 4 \times 16 \text{ cm}^3$ were prepared to measure compressive strengths after 7, 28 and 90 days with a Matest Compression E161-03N tester (Matest, Italy) according to the European norm EN 196-1:2016. Also using those same prismatic dimensions, but using three gang moulds, the dimensional stability was measured in cement mortars using a Matest Length Comparator E077 (Matest, Italy) after 7, 28 and 90 days. Each presented value of compressive strength and length change was averaged from three individual samples.

X-ray computed microtomography (XCT) was used to observe the physical changes that occurred at the metal/matrix interface region using a Nikon CT-SCAN-XT H-160. A total of 1600 images were taken for each analysis performed. The data were processed using DragonFly® 2022 software which allowed the generation of 2D and 3D images as well as porosity percentages.

2.1.2 Main findings on the MPC formulations

2.1.2.1 Role of magnesium oxides

Five different magnesium oxides were tested. The reference MgO was a hard burnt 95.3 wt.% MgO (determined by X-ray fluorescence; XRF) imported from USA. The XRF analysis indicated minor presence of Ca, P and (<2 wt.%) and Si, Fe and Al (<0.6 wt.%). The BET specific surface area was < 1 m²/g. Other four magnesium oxides with lower quality were obtained from Spain as the product price was negligible compared to the costs associated to shipment and duties of the imported material. The Spanish magnesites products with decreasing quality contained a) 70.9 wt.% MgO, b) 68.8 wt.% MgO, c) 57.3 wt.% MgO and d) 54.6 wt.% MgO. All of them were original from the same quarry and included increasing Ca content with the decreasing MgO (from 15 to 25 wt.%). The XRD analyses confirmed presence of dolomite, calcite, quartz and iron oxides in the mineralogy.

Several MKPC pastes formulations were tested with these five MgO sources, considering a Mg/P molar ratio within the range 1-1.7 (mass ratio 0.3-0.5). Other variables included addition of boric acid as retarder (0, 1 or 2 wt.%), fly ash in filler/cement mass ratios 0, 0.7 and 1, and water in water/cement mass ratios 0.2 and 0.4. Although water content is normally expressed in the literature as water/cement or water/solid mass ratio, it is important to consider that for a stoichiometric reaction at least 5 molecules of water are required for each KH₂PO₄ molecule to produce K-struvite. That should be the minimum water content added to the mixture. A formulation with a filler/cement = 1; Mg/P molar ratio = 1 and water/cement mass ratio = 0.4 contributed with 3.9 molecules of water per molecule of KH₂PO₄, that was insufficient to produce K-struvite.

At low Mg/P molar ratio (Mg/P = 1) the lower quality MgO produced good workability but no setting after 24 h, while the higher quality MgO produced bad workability and rapid setting.

Out of all the tested formulations, and due to better workability, cement setting and mechanical strength, it was decided to consider the formulation shown in Table 2 as reference MKPC paste.

Table 2. MKPC paste reference formulation (mass of components are expressed to obtain 1 L of cement).

Reference starting reagents	Mass (g)
MgO (MAGCHEM 10CR, hard burnt 95.3 wt.%)	90.55
KH ₂ PO ₄ (KristaTM, 98 wt.%)	305.69
Fly ash (class F, low CaO content)	396.24
Boric acid (H ₃ BO ₃)	5.43
H ₂ O (distilled water)	202.08

Components ratios in the formulation:

MgO/KH₂PO₄ molar ratio = 1; mass ratio = 0.3

H₂O/(MgO + KH₂PO₄) molar ratio = 2.50; mass ratio = 0.51

Fly ash/(MgO + KH₂PO₄) mass ratio = 1

H₃BO₃/(MgO + KH₂PO₄) mass ratio = 0.01

H₂O/KH₂PO₄ molar ratio = 5

However, two key issues were identified and investigated in deeper detail.

The availability of FA is becoming limited. As mentioned in section 1, the progressive shut down of power plants worldwide is reducing the generation of FA in benefit of the reduction of global CO₂ emissions but reducing thereby the reserves of this material. As the future trends seems to evolve in that direction, the search of alternative filler materials results necessary.

In addition, this MKPC reference formulation produced efflorescence on the surface of the cured samples after 1 day and specimens showed low strength. Although, theoretically, the equimolar reaction between MgO and KH₂PO₄ should be able to exhaust both chemical reagents and produce K-struvite, MgO does not completely disaggregate, therefore reducing its availability to react with the phosphate. For this reason, the use of MKPC in the construction sector, where the achievement of alkaline pH is unimportant, considers mixtures with high Mg/P ratios in benefit of the mechanical strength and minimisation of efflorescence. The Mg/P molar ratios can usually vary from 3 to >10 (e.g. [14,15]).

Both aspects, the role of fillers and the Mg/P ratio are described in sections 2.1.2.2 and 2.1.2.3.

2.1.2.2 Role of fillers

Five different silicate and aluminosilicate materials were initially acquired and characterized to be used as fillers in MKPC formulations: fly ash, wollastonite, pumice and 2 different metakaolins. An additional sixth material, volcanic ash, was also included.

Coal fly ash (class F-low calcium) had a particle size distribution of $d_{10} = 7 \mu\text{m}$, $d_{50} = 31 \mu\text{m}$, $d_{90} = 163 \mu\text{m}$, and mineral composition dominated by quartz, mullite and amorphous phases.

Wollastonite (CaSiO₃), according to the XRD analysis, also contained quartz (SiO₂), albite (NaAlSi₃O₈) and calcite (CaCO₃), and in minor proportion K-feldspar (KAlSi₃O₈), muscovite (KAl₂(AlSi₃O₁₀)(OH)₂), diopside (MgCaSi₂O₆) and gypsum (CaSO₄.H₂O). The particle size distribution showed a multimodal frequency with $d_{10} = 6.3 \mu\text{m}$, $d_{50} = 41.3 \mu\text{m}$, $d_{90} = 216 \mu\text{m}$.

Pumice was received with a grain size of <40 μm . The mineralogy contained mostly silica rich glass and a minor number of silicates, such as alkali feldspar, quartz, and biotite.

Two different types of metakaolin (MKA and MKB) were studied. MKA contained 95 wt.% of particles < 80 μm , while MKB contained 68 wt.% of particles of <2 μm . Both MK samples were quite similar in mineralogical composition, mainly including amorphous aluminosilicates, anatase, and quartz.

Volcanic ash was collected at the island of La Palma (Canary Islands, Spain). It was produced as a consequence of the volcanic eruption that took place from September to December 2021 at the Cumbre Vieja volcano. The eruption emitted more than 10 million cubic meters of ash and pyroclastic materials that deposited covering large extensions of the island's surface. The particle size distribution presented monomodal frequencies, with $d_{10} = 158 \mu\text{m}$, $d_{50} = 444 \mu\text{m}$, $d_{90} = 844 \mu\text{m}$. The mineralogy showed ferromagnesian minerals presenting a low degree of crystallization (olivine, pyroxene, forsterite, augite, amphibole), with the addition of silica minerals (tridymite, cristobalite), mullite, plagioclases (anorthite, albite), Fe and Ti oxides (rutile, magnetite) and amorphous components.

The chemical composition of all the fillers measured by XRF can be observed in Table 3.

Table 3. Chemical composition and specific surface area of filler materials (wt.%). FA: fly ash; PM: pumite; MKA: metakaolin A; MKB: metakaolin B; VA: volcanic ash. SSA = specific surface area, measured by the BET method of nitrogen adsorption

Component	FA	WO	PM	MKA	MKB	VA
SiO ₂	52.9	41.2	55.4	57.3	52.9	35.33
Al ₂ O ₃	21.9	5.0	17.7	37.0	43.2	11.27
CaO	3.8	43.3	1.2	0.1	0.02	13.5
Fe ₂ O ₃	10.6	3.7	3.3	1.6	0.5	18.8
MgO	1.6	2.5	-	0.3	-	7.1
K ₂ O	1.8	1.6	9.7	0.7	0.2	2.1
Na ₂ O	1.2	1.3	10.2	-	0.3	4.9
TiO ₂	1.0	0.5	0.3	2.4	2.5	4.9
P ₂ O ₅	0.2	-	0.04	-	0.1	1
F ⁻	-	-	0.5	-	-	-
Cl ⁻	-	-	0.4	-	-	-
∑ others	0.8	0.9	1.3	0.5	0.3	0.8
SSA* (m ² /g)	11.7	6.5	2.7	21.3	12.6	0.6

Several MKPC pastes samples were prepared with the different fillers at water/cement mass ratio of 0.40. Cement mortars were also prepared but the water/cement ratio had to be increased to values in the range 0.51 to 0.75 to allow good workability and homogeneous hydration of the mortars. Figure 1 presents the aspect of prismatic cement mortars casted in 4 × 4 × 16 cm³ moulds. Some efflorescence can be observed on some samples, clearly visible on the surface of the MKB mortar.



Figure 1. Visual aspect of MKPC mortars containing (from left to right): metakaolin A, metakaolin B, wollastonite, pumice and volcanic ash.

Table 4 presents the designed mix proportions of MKPC pastes and mortars, including the filler, MgO, KH₂PO₄, water, H₃BO₃ and sand.

Table 4. Formulations of MKPC pastes and mortars. FA: fly ash; PM: pumite; MKA: metakaolin A; MKB: metakaolin B

Filler	MgO/KH ₂ PO ₄ (molar)	H ₂ O/cement (mass)	Filler/cement (mass)	Sand/cement (mass)	H ₃ BO ₃ /cement (mass)
Mortars					
FA	1.00	0.51	1.00	1.00	0.02
WO		0.51	1.00		
PM		0.75	1.00		
PM		0.51	0.40		
MKA		0.65	1.00		
MKA		0.51	0.40		
MKB		0.51	0.40		
Pastes					
FA	1.00	0.40	1.00	0.00	0.02
WO			1.00		
PM			0.40		
MKA			0.40		
MKB			0.40		

cement: MgO+KH₂PO₄

The results of setting time of the fresh pastes are shown in Table 5. In general, MKPC are known to exhibit shorter setting times than OPC, although slow setting leads to faster strength development. All the formulations had similar setting times except for the formulation WO, with a final setting time significantly longer than the rest of the formulations produced with an addition of filler. It was found that all formulations with fillers had shorter final setting times than those obtained for MKPC alone (5.8 h), likely due to an increase in the contact surface area in the presence of filler, which increases the reactivity of the cement.

The flow areas of the cement pastes resulted between 34 cm² and 42 cm² for all the formulations. These results indicated that the workability was suitable for the manipulation of the fresh mixture and its pouring into moulds. For the formulations PM 0.4, MKA 0.4 and MKB 0.4 it was only possible to incorporate 40% of filler, with respect to the cement content, due to the higher porosity and larger

capacity of water retention by the fillers. At higher contents of filler, the mixtures were excessively dry and exhibited poor workability.

Table 5. Setting time and workability results of the MKPC mortars.

Formulation	Initial setting time (h)	Final setting time (h)	Flow area (cm ²)
FA	2.0	4.0	34
WO	3.2	6.2	41
PM 0.4	2.2	2.6	39
MKA 0.4	2.0	2.4	42
MKB 0.4	1.7	2.1	37
No filler	5.2	5.8	81

The formulation with PM at filler/cement ratio = 1 revealed the lowest values of compressive strength after 7, 28 and 90 days of curing due to the higher amount of water (water/cement mass ratio = 0.75), being discarded due to its low strength and consistency.

The compressive strength for the mortar with MKA after 90 days of curing was 41 MPa, despite the high water/cement mass ratio (0.65). Nevertheless, a high amount of water may be undesirable due to the formation of hydrated intermediate phases instead of K-struvite, discarding this formulation from further analyses. The formulations with FA and WO showed compressive strengths of 41 and 34 MPa at 90 days, respectively (Figure 2a).

The results of compressive strength for the second batch of MKPC mortars PM, MKA and MKB with a filler/cement mass ratio = 0.40 and water/cement mass ratio = 0.51 are shown in Figure 2b. The three formulations revealed similar compressive strengths after 90 days of curing and are comparable to those found using FA.

The compressive strength of all formulations increased gradually with curing time, with a 52% higher strength for the WO formulation after 90 days of curing with respect to 7 days, and 31%, 28%, 18%, and 1.7% for the FA, and the formulations with MKA, MKB, and PM at filler/cement ratio = 0.4, respectively. These increases in compressive strength with time indicated the continuity of the K-struvite growth and a more condensed structure, resulting in an improvement in the mechanical properties of the MKPC.

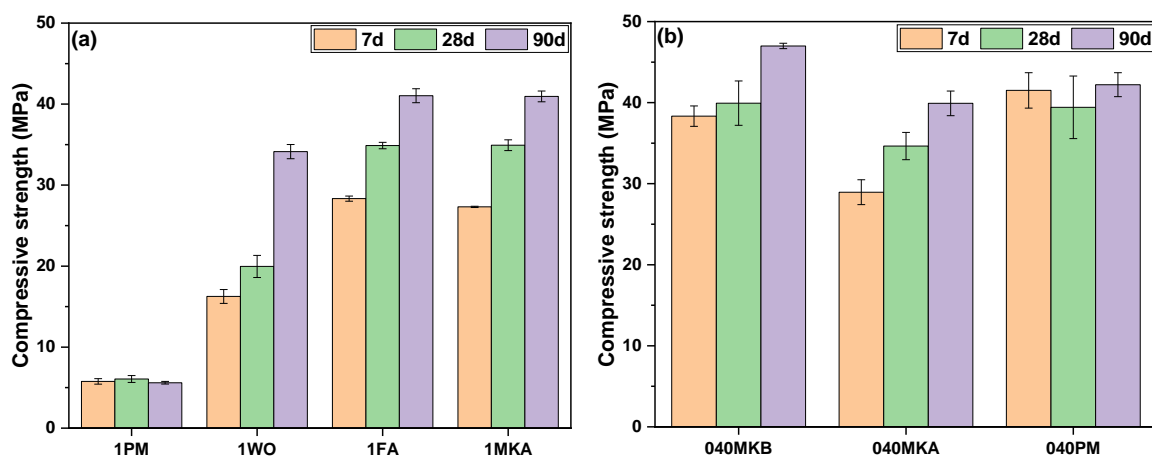


Figure 2. Compressive strength of MKPC (a) mortars at filler/cement mass ratio = 1 and variable water/cement ratio; (b) mortars with a fixed filler/cement ratio = 0.4 and water/cement ratio = 0.51.

The length change of mortars with a water/cement mass ratio = 0.51 and a filler/cement mass ratio = 1 for WO and 0.40 for PM, MKA, and MKB was calculated by measuring the length change after 7, 28, and 90 days of isolated curing into plastic bags at 20 °C (Figure 3). For the FA formulation, it was not possible to measure the dimensional stability due to the limited availability of this material in our study that did not allow us to prepare an additional cement mortar.

The major relative length change (%) was measured for the formulation MKA (filler/cement ratio = 0.4) with a percentage of expansion of around 1.1% after 7 and 28 days of curing, followed by a shrinkage to 0.9 % after 90 days. A similar trend was found for the MKB sample filler/cement ratio = 0.4), but with a lower percentage of expansion, below 0.4% after 90 days of curing. For the samples WO and PM, the increase in expansion from 7 to 28 days was not observed. A continuous decrease was observed from the original length as a function of time, although these length changes were very low, indicating excellent dimensional stability.

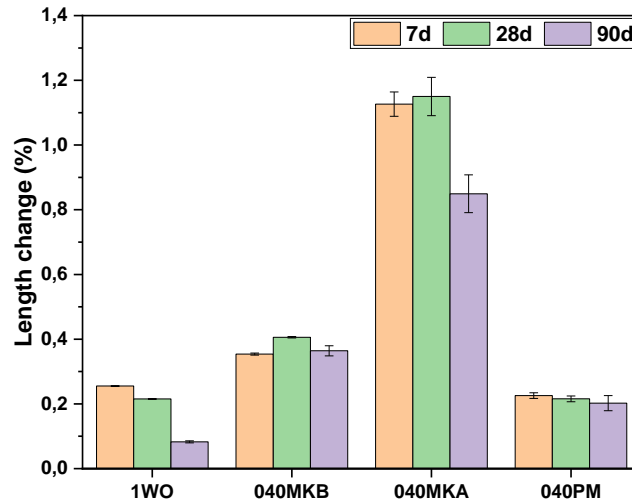


Figure 3. Length expansion of MKPC mortars with a mass ratio $H_2O/cement = 0.51$ and a mass ratio filler/cement = 1 for WO and 0.40 for PM, MKA and MKB.

Figure 4 shows the results of pH evolution in the suspensions of MKPC pastes with a 1:1 solid/liquid ratio as a function of the curing time, up to 160 days. At the initial time ($t = 0$), all formulations showed a pH in the range of 5-6, controlled mainly by the weak acids dissolved in aqueous phase of the fresh MKPC paste.

The formulations with the fillers FA, PM, MKA, and MKB showed very similar pH values between a range of 7 and 7.6 for the first 90 days of curing, corresponding the pH range of the aluminium passivation zone. The higher pH was measured for the formulation with WO due to the possible partial dissolution of the wollastonite, adding Ca and generating a more alkaline medium that could contribute to increase the pH to the actual range of 8-8.3.

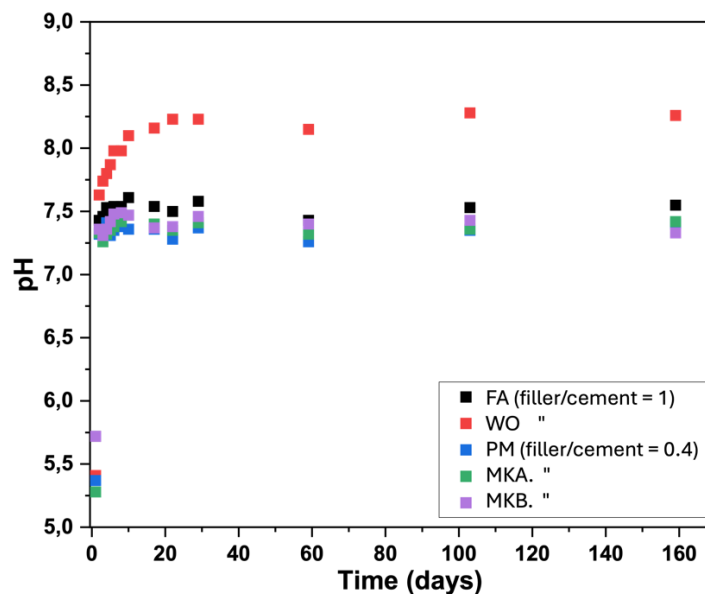


Figure 4. pH of MKPC paste suspensions with a solid/liquid ratio of 1:1.

The main hydration product for all formulations observed by XRD was attributed to crystalline K-struvite. A small reflection of unreacted MgO was also detected in all formulations; nonetheless, no presence of KH_2PO_4 was observed, except for the formulation MKA at filler/cement ratio = 0.4 after 28 days, but was no longer present after 90 days of curing, indicating the continuous hydration reaction (Figure 5).

A decrease in the reflections attributed to MgO was observed after 90 days, again suggesting the continuity of the hydration reaction. Furthermore, no evidence of the formation of hydrate intermediates, such as $\text{Mg}_2\text{KH}(\text{PO}_4)_2 \cdot 15\text{H}_2\text{O}$, were found.

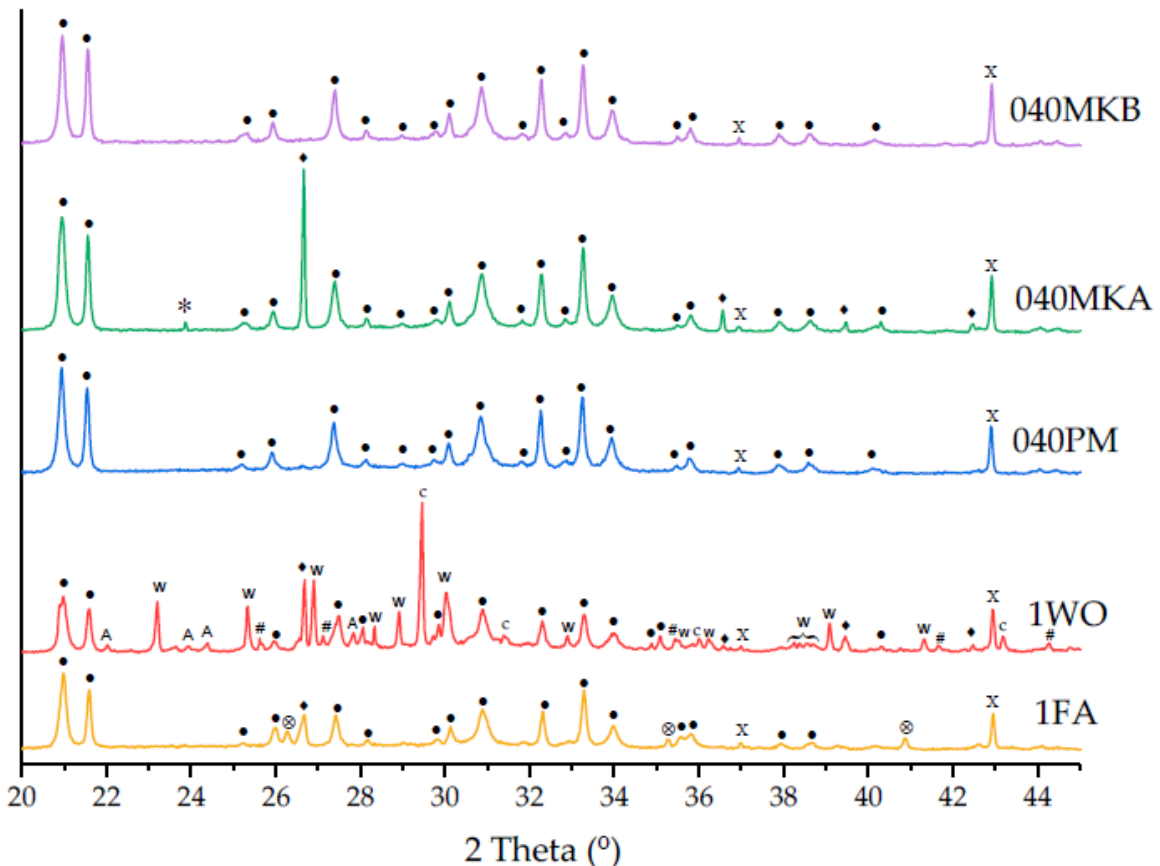


Figure 5. XRD patterns of MKPC pastes after 28 days of curing. •: K-struvite; X: MgO; W: wollastonite; ♦: quartz; *: KH_2PO_4 ; ⊗: mullite; c: calcite; #: microcline; A: albite.

Crystals of K-struvite can be observed by SEM in all formulations, intergrowing with the filler materials. Punctual EDX analyses on K-struvite crystals presented small amounts of Si and Al (<1%), denoting a low incorporation of these elements in the MKPC matrix, where Mg, K and P were dominant, and the Mg/P and K/P atomic ratios remain close to 1 in agreement with the K-struvite theoretical stoichiometry.

K-struvite can develop various morphologies depending on the location where it formed. In the pores of the MKB sample, K-struvite grew into large tabular crystals (Figure 6). The morphology presented well developed crystal aggregates with networks of layered K-struvite crystals surrounded by amorphous metakaolin fulfilling the space between layers. This could explain the higher compressive strength of the MKPC blended with this filler by developing a denser microstructure filling the cracks and generating a less porous structure. Also, the development of crystal growth of the K-struvite crystals layered in random orientation could lead to a higher mechanical strength due to the absence of potential weakened planes in the structure of the MKPC.

In confined regions, K-struvite tends to adopt less regular but denser aggregated crystals, as observed in the PM sample (Figure 7). Non-crystalline aluminosilicates particles (in orange) attributed to pumice and unreacted MgO (green spots) could be observed. The latter indicating its

incomplete reaction, in agreement with the results obtained by the XRD. Nonetheless, for both cases, pumice and metakaolin, a good bonding between the filler and the MKPC matrix and absence of new mineral phases was observed.

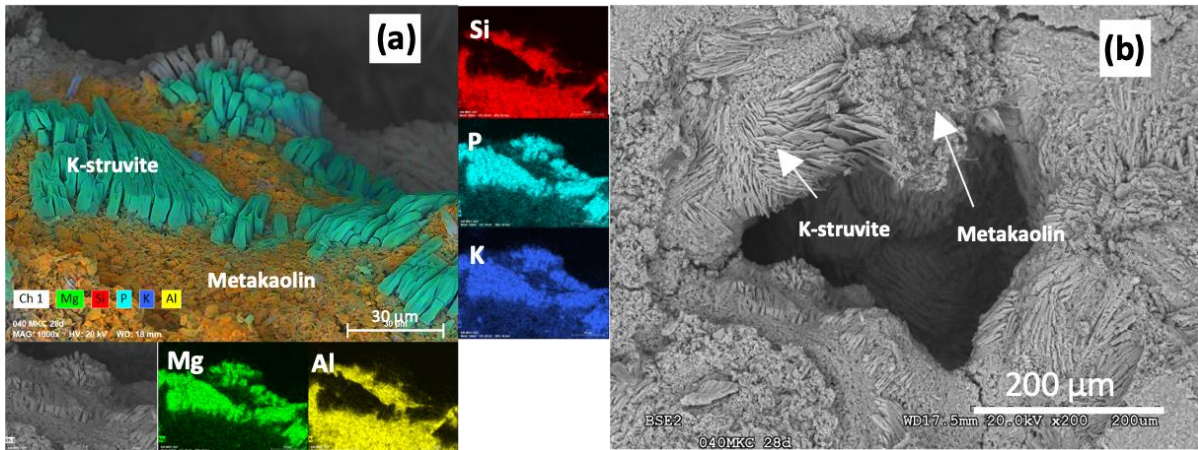


Figure 6. SEM images of MKPC pastes with MKB. (a) K-struvite growing on a metakaolin bed and chemical content of selected elements indicated in colour, and (b) large tubular crystal of K-struvite growing near metakaolin at the inner surface of a cement pore.

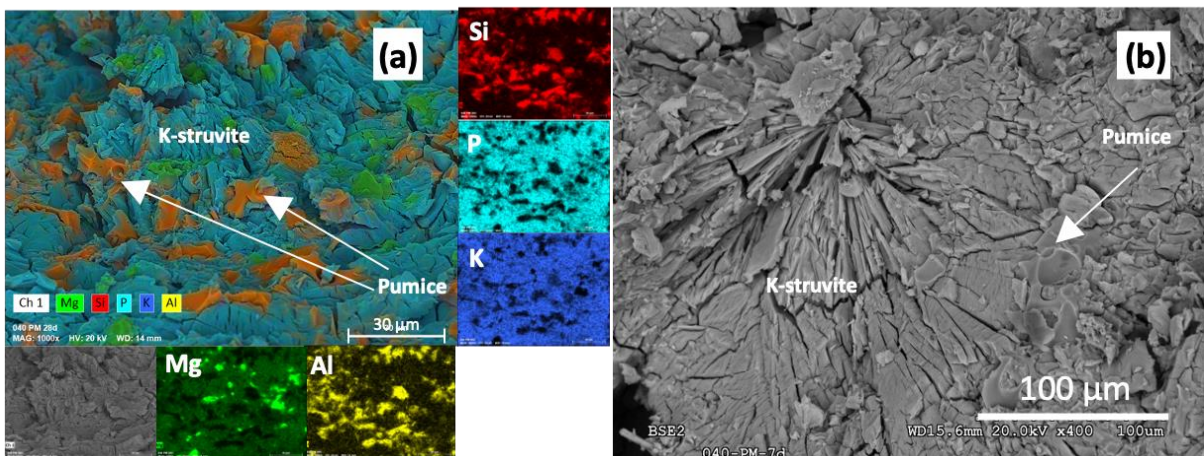


Figure 7. SEM images of MKPC pastes with PM. (a) K-struvite with pumice particles and excess of unreacted MgO, and (b) dense crystal habit of K-struvite.

Similar structures were found for the MKPC formulations with WO and FA fillers. In the pastes prepared with WO (Figure 8a) rod shape crystals of wollastonite were observed embedded in the MKPC matrix. Glassy morphologies were also found in this sample (see dashed red square markers in Figure 8b). Punctual EDX semi-quantitative analyses of these areas were performed, finding relatively high content of Ca (between 3 and 10 %) and S (between 1.8 and 13.7 %), possibly attributed to secondary minerals of the filler.

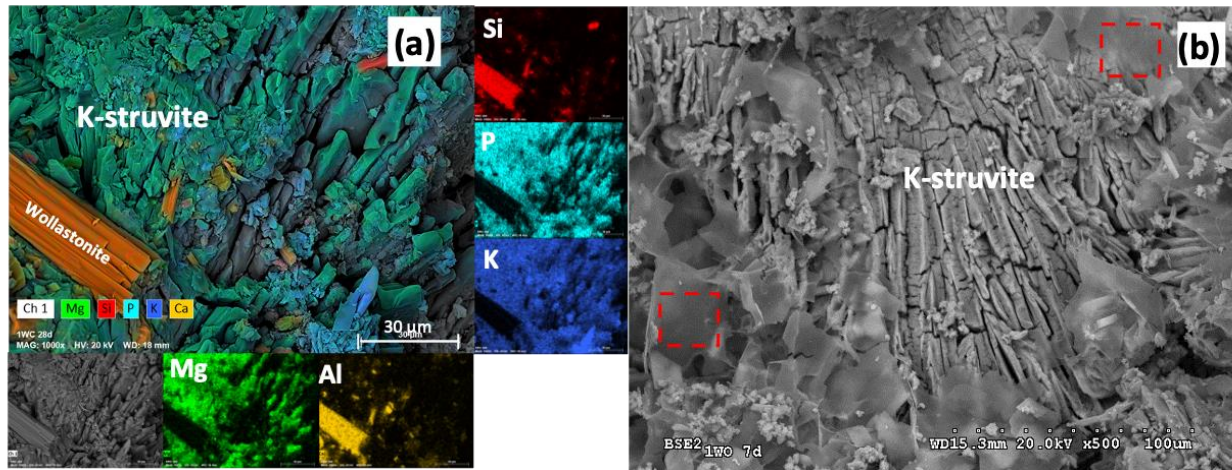


Figure 8. SEM images of MKPC pastes with WO (a) K-struvite with wollastonite (orange), and b) K-struvite habit and glassy Ca, S-enriched morphologies (shown within the dashed red squares).

All the filler materials showed favourable results for their use in MKPC cements for the encapsulation of radioactive metal waste. The wollastonite filler, being a natural commercial material of large and local availability, low cost and being able to be incorporated in a higher proportion in the MKPC mixture, was particularly attractive to substitute fly ash.

Volcanic ash was evaluated in a later stage while determining the significance of the magnesium to phosphate molar ratio.

2.1.2.3 Role of magnesium to phosphate ratio

This section evaluates the Mg/P molar ratio, increasing the reference ratio from 1 to 2, 3 and 4 M, using the most promising filler out of the fillers studied before, wollastonite, and volcanic ash, as this material became available at the beginning of 2022 and some preliminary characterization also indicated a promising behaviour as filler. Fixed MKPC formulations were used for this evaluation, considering that the filler/cement ratio decreased accordingly to the increasing Mg/P molar ratio. Filler/cement mass ratios = 1.06, 0.74 and 0.5 were used for the Mg/P molar ratios = 2, 3 and 4 M, respectively. The H_3BO_3 /cement mass ratio was 0.02, and two types of H_2O /cement ratios were used: 0.3 (for MKPC pastes) and 0.4 (for MKPC mortars). The sand/cement mass ratio was 1 in the mortars.

Similar initial and final setting times were observed with volcanic ash for the formulations with Mg/P molar ratio = 2 and 3 M, but when the ratio was increased to 4 M, a slightly increased setting time was observed. In the case of wollastonite, the initial setting time was similar for 2 and 4 M and shorter than for 3 M. The final setting time was also faster for 4 M, indicating a change in trend from 3 to 4 M (Table 6).

Table 6. Setting time of MKPCs using either volcanic ash (VA) or wollastonite (WO).

Formulation	Initial setting time (h)		Final setting time (h)	
	VA	WO	VA	WO
2M	1.8	2.0	2.5	5.2
3M	1.8	3.4	2.5	5.4
4M	2.5	2.0	2.9	3.0

In general, the compressive strength increased with the curing time. This increase was better appreciated in the samples with wollastonite, where the strength improved by 112% from 7 to 90 days for 2 M, 52% for 3 M and 77% for 4 M. In samples prepared with volcanic ash, the strength after 7 days was initially higher than with wollastonite, but the improvement with time up to 90 days was lower, 26% for 2 M, 18% for 3 M and 17% for 4 M (Figure 9).

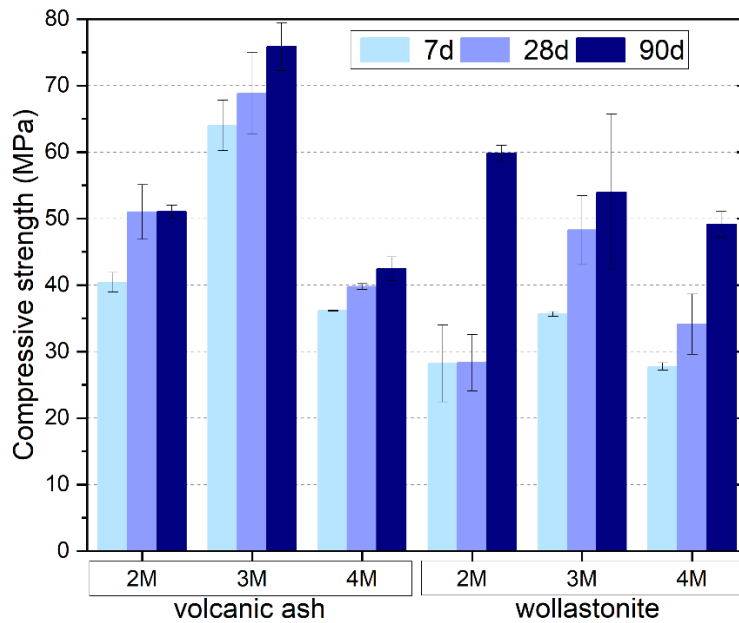


Figure 9. Compressive strength of MKPC mortars.

In comparison with the results obtained before, for the formulations with Mg/P = 1 and w/c in the range of 0.51–0.75, the compressive strength achieved in the present study was higher for all formulations, indicating the net effect obtained by increasing the Mg/P ratio and decreasing the w/c ratios.

The length change of the mortars was measured after 7, 28 and 90 days, and the results are shown in Figure 10. In general, the length changes were not much affected by either the Mg/P ratio or the curing time, after 7 days, for the formulations prepared with volcanic ash, but were highly variable for the formulations prepared with wollastonite. It was observed that the presence of wollastonite caused a shrinkage that increased with the hydration time, being higher for the Mg/P molar ratio of 4 M.

This effect was also observed with the 4 M formulation with volcanic ash. For 3 M, an expansion of 0.28% was determined after 28 days, followed by a shrinkage of 0.25% after 90 days. For 2 M, there was an expansion of 0.31% after 28 days, which was similar after 90 days (Figure 10).

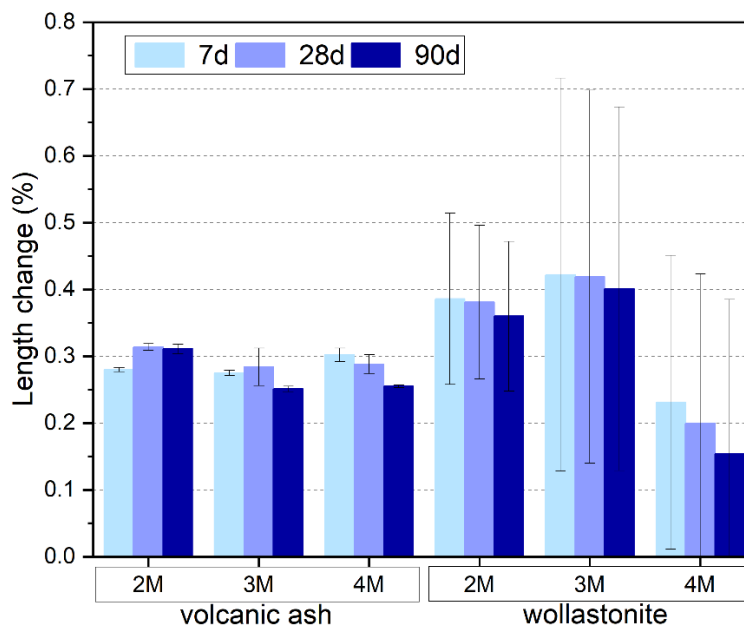


Figure 10. Length expansion of MKPC mortars.

Figure 11 shows the pH evolution over 90 days. The pH remained in a range between 7.5 and 9.5 for all the formulations except for the 3 M with wollastonite, which temporarily reached a pH = 10.5 after 15 days, and for the three formulations with volcanic ash, after 24 h, that were below pH 5.8, although the pH increased to over 7.8 after 48 h.

Apart from punctual pH variation, within certain range, both filler materials influenced similarly on the pH, and there was an evident increase of pH with the increase of the Mg/P molar ratio in the MKPC formulations, that seemed to stabilize in a range close to 8 at 2 M, 8.7-9.2 at 3M and 9.3 at 4M after 90 days.

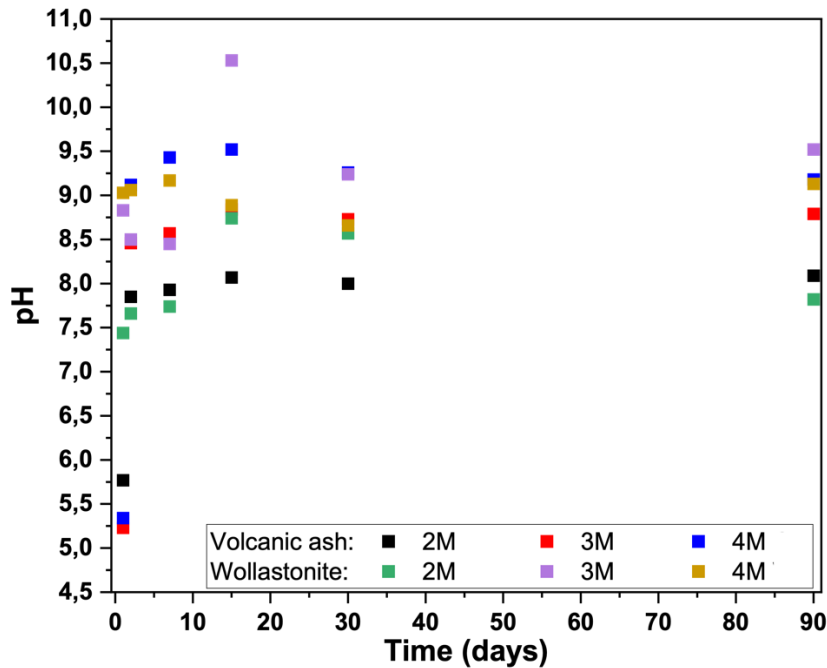


Figure 11. pH evolution of MKPC pastes suspensions as a function of time.

Independently of the formulation, the main reaction product observed in all X-ray diffractograms was K-struvite, whose reflections intensities increased with the curing time.

Calcite was observed in all samples with wollastonite, with decreasing intensity with the increasing curing time. The rest of the minerals initially present in wollastonite and volcanic ash could also be observed in the MKPCs, although their XRD intensities were much lower compared to the large and sharp reflections of K-struvite and MgO. With both fillers, unreacted periclase (MgO) was observed, while KH_2PO_4 could not be identified (Figure 12).

The semi-quantitative analyses performed using Rietveld refinement indicated an increase in both minerals, K-struvite and periclase, with the increasing Mg/P ratio, independently of the filler used. Thus, the K-struvite formed after 90 days for the Mg/P molar ratios of 2, 3 and 4 M represented 57, 60 and 65 wt.% with wollastonite, and 47, 58 and 65 wt.% with volcanic ash. The excess of periclase was semi-quantified within the range of 11–14 wt.% at 2 M, 14–18 wt.% at 3 M and 18–22 wt.% at 4 M, considering the formulations with both fillers and including the three curing times (Table 7).

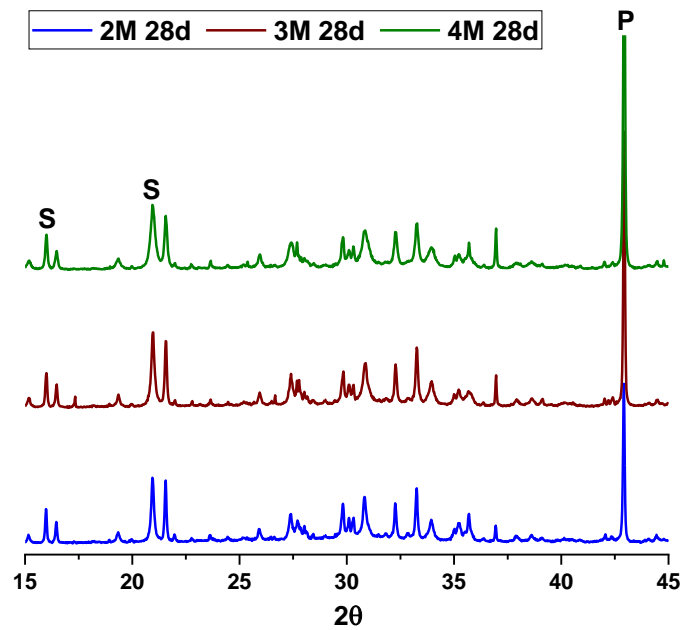


Figure 12. XRD patterns of MKPC pastes with volcanic ash after 28 days of curing. S: K-struvite; P: MgO.

Table 7. Rietveld quantification performed on the samples at 2, 3 and 4 M with volcanic ash after 90 days.

		K-struvite (wt.%)	Periclase (wt.%)
Volcanic ash after 90d	2M	47	11-14
	3M	58	14-18
	4M	65	18-22

The SEM-EDX analysis was limited to studying the morphology and compositions of the mineral phases present in the cement paste samples cured for 28 days.

The main reaction product was K-struvite. As the analyses were performed on polished sections, the morphology of the K-struvite crystals was better observed when they were grown in cavities. K-struvite was identified as a tabular crystal growing in pores, whereas when growing in confined areas, its morphology presented more irregular crystals.

The formation of large struvite crystals in different pores was generally observed for both fillers. In general, as the Mg/P molar ratio increased, the size of the crystals increased, and the faces became better defined. At 2 M, the formulations with wollastonite presented incipient crystal growth (Figure 13a), although the crystal habit could not be well differentiated. Prismatic crystals were better defined at 3 M (Figure 13b) and the size was increased at 4 M (Figure 13c).

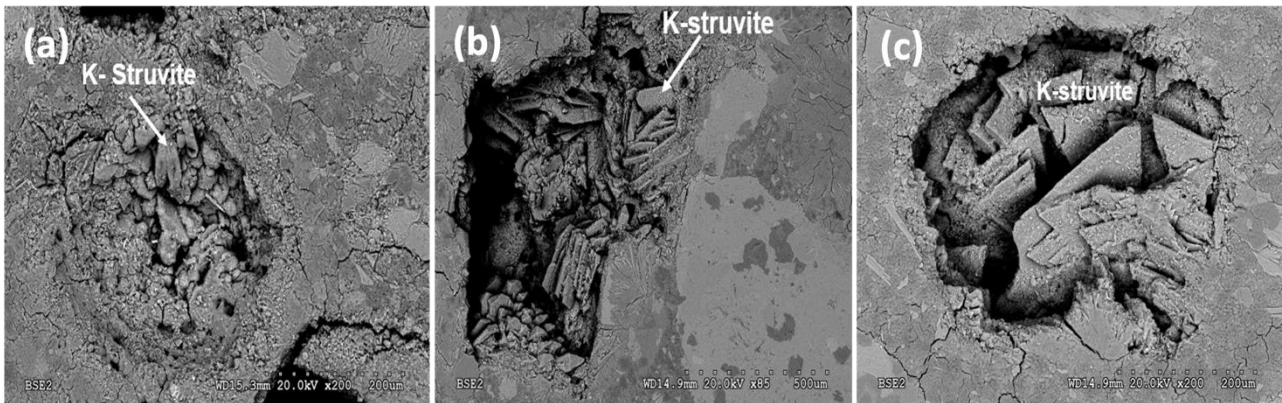


Figure 13. SEM images of MKPC pastes prepared with wollastonite at Mg/P molar ratios of (a) 2 M, (b) 3 M and (c) 4 M.

The MKPC formulations including volcanic ash presented K-struvite crystals with irregular tabular morphologies at the three Mg/P molar ratios, although the crystal sizes were not much larger at higher Mg/P ratios (Figure 14a, b and c).

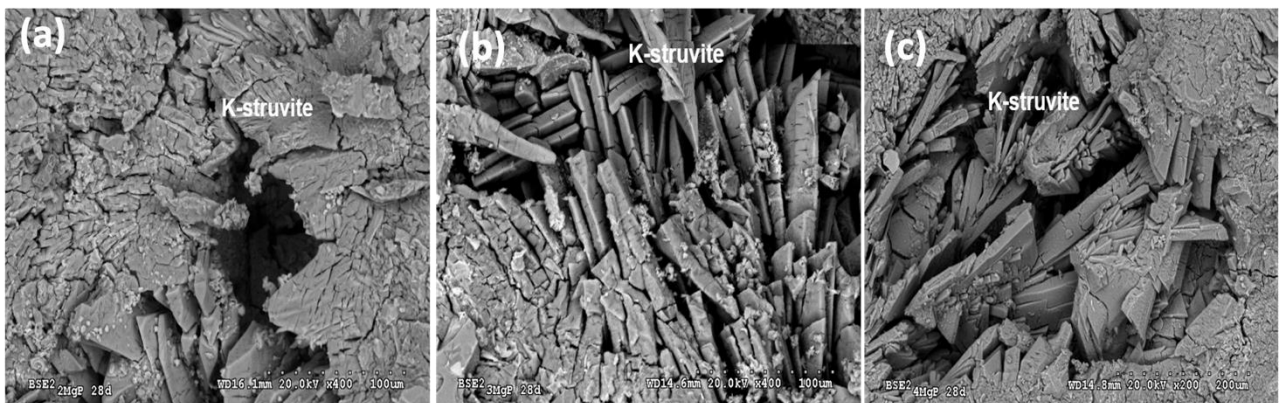


Figure 14. SEM images of MKPC pastes prepared with volcanic ash at Mg/P molar ratios of (a) 2 M, (b) 3 M and (c) 4 M.

The chemical atom ratios (%) of Mg, K and P determined by SEM_EDX analyses on selected locations corresponding to the MKPC matrices are presented in Figure 15 in a ternary plot. Carbon and oxygen were excluded from each analysis and the atomic ratios were recalculated up to 100%. Other elements (mostly Si, Al, Ca, Fe and Na, and minor quantities of Ti, Mn, S, Cl, Zr and Zn) were not excluded. The data presented in Figure 15 (133 analyses) only account for those analyses presenting a sum of Mg + K + P > 90%. This considers some potential interference of the elements forming the surrounding minerals, mixed with the MKPC matrix or potentially included in the K-struvite composition, and could slightly affect the atom ratios, as the total sum of these three elements might be below 100%. Nonetheless, the interference was minimal, since the sum of Mg + K + P \geq 99% for 65% of these analyses and was \geq 95% for 92% of them.

Independently of the Mg/P molar ratio and the filler used in the formulations, the data indicated that the atomic ratio of Mg/K/P found in most of the compositions was near the stoichiometric 1:1:1 molar ratio, characteristic of K-struvite. Some dispersion of the data towards high Mg ratios and, consequently, low K and P ratios, was observed with the increasing Mg/P molar ratio, mostly attributed to an excess of unreacted MgO.

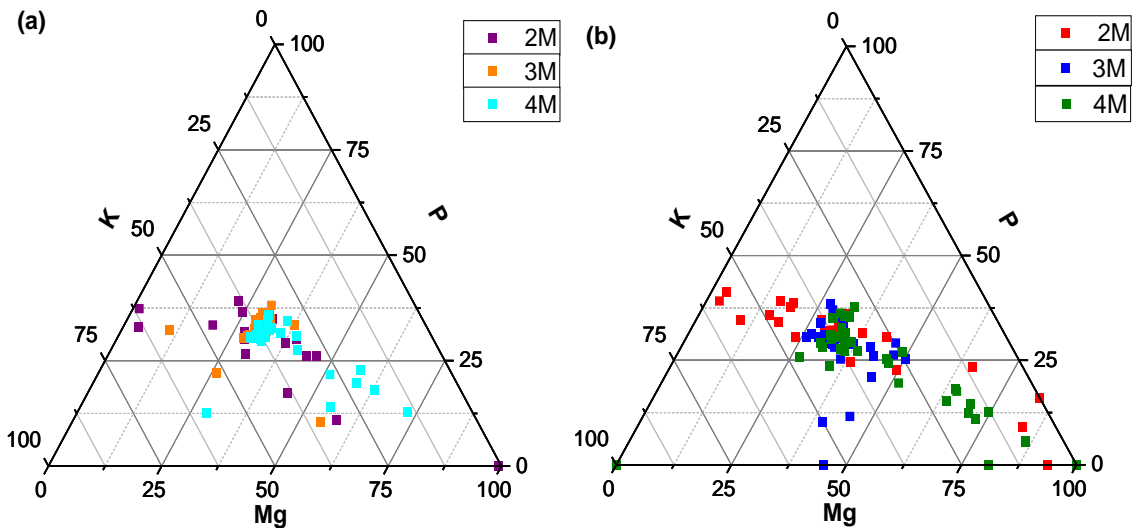


Figure 15. Percentages of Mg, K and P in MKPC pastes after 28 days curing, measured via semi-quantitative EDX analyses. (a) Volcanic ash, (b) Wollastonite.

As expected, it was observed that the increasing Mg/P molar ratio prevented unwanted efflorescence on the MKPC.

2.1.2.4 Role of retarder

To evaluate the role of two different retarders a comparison between boric acid and sodium thiosulphate ($\text{Na}_2\text{S}_2\text{O}_3$) was performed for a MKPC formulation.

Cement pastes and mortars were prepared using the following MKPC formulations: Mg/P = 3 M; water/cement mass ratio = 0.3 (for cement pastes) and 0.4 for cement mortars; filler/cement mass ratio = 0.74, retarder/cement mass ratio = 0.02 and sand/cement mass ratio = 0 (for cement pastes) and 1 for cement mortars. The MgO used was MAGCHEM 10 CR and the filler was volcanic ash.

The setting was much faster with $\text{Na}_2\text{S}_2\text{O}_3$. It was not possible to perform the mini-slump test due to the low fluidity of the cement paste with this formulation.

It was observed that the presence of thiosulphate accelerated the setting process, starting at 12 minutes and ending at 17 minutes, while, with boric acid, the start of setting occurred at 108 minutes and ended at 150 minutes.

When the Vicat needle mold was unmolded with the thiosulphate paste, the surface of the material was destroyed. Small white aggregates corresponding to monopotassium phosphate indicated a poor mixing process due to the lack of fluidity of the material.

The compressive strength achieved with $\text{Na}_2\text{S}_2\text{O}_3$ after 7 and 28 days was 29 ± 2 MPa and 32 ± 2 MPa, respectively, while the strength achieved using boric acid after 7 and 28 days was much higher, 64 ± 4 MPa and 69 ± 6 MPa, respectively.

The length change of mortars was determined after 7 and 28 days. A larger elongation was observed for the formulation with $\text{Na}_2\text{S}_2\text{O}_3$, reaching 0.8 % after 28 days while the sample with H_3BO_3 reached 0.28%.

The pH was measured for cement pastes suspensions only over 15 days. Both formulations displayed similar pH values, although the formulation with boric acid remained below pH 9 after 15 days while the formulation with sodium thiosulphate reached a value of 9.3.

For this particular MKPC formulation, the better results were obtained with boric acid, but the study demonstrated the impact of using different retarders.

2.1.2.5 MPC-Al and PC-Al reactivity

With the objective to evaluate the reactivity of a MKPC and make a direct comparison with a PC, the technique of micro X-ray computed tomography (μ -XCT) was used. It helped to observe the physical changes occurring at the metal/matrix interface region without disturbing the cement samples. Pure Al sheets with dimensions 2 x 2 cm² were embedded in MKPC and PC cement pastes. Samples were analyzed just after 1 week after setting, to consider the initial stage, and after 4 months in the case of the PC and 1 year in the case of the MKPC to study the evolution with time. A total of 1600 images were obtained for each analysis performed and the images were processed to generate 3D volumes.

The MKPC paste formulation included volcanic ash as filler and exhibited a Mg/P molar ratio = 1.

The 3D images (Figure 16) display the Al sheets (shown in grey in the center) with the porosity distribution of the inner cement matrices. The pores around the plate and at the edge of the matrix increased slightly with hydration time. In the case of the MKPC paste, less porosity was observed in the cement matrix.

The PC porosity observed was homogeneously distributed throughout the matrix, whereas the MKPC samples showed a high porosity in the outer contour of the monoliths.

A high porosity was observed around the aluminium plate in the PC pastes at both, initial a final time. That was initially attributed to an inadequate insertion of the aluminium sheet in the cement paste. Therefore, the PC paste with Al was prepared again and the XCT analysis performed after 7 days evidenced a very similar result, which could indicate a very large hydrogen production at short time, caused by corrosion on the surface of the aluminium sheet, which slightly increased with time. That was not observed in the case of MKPC.

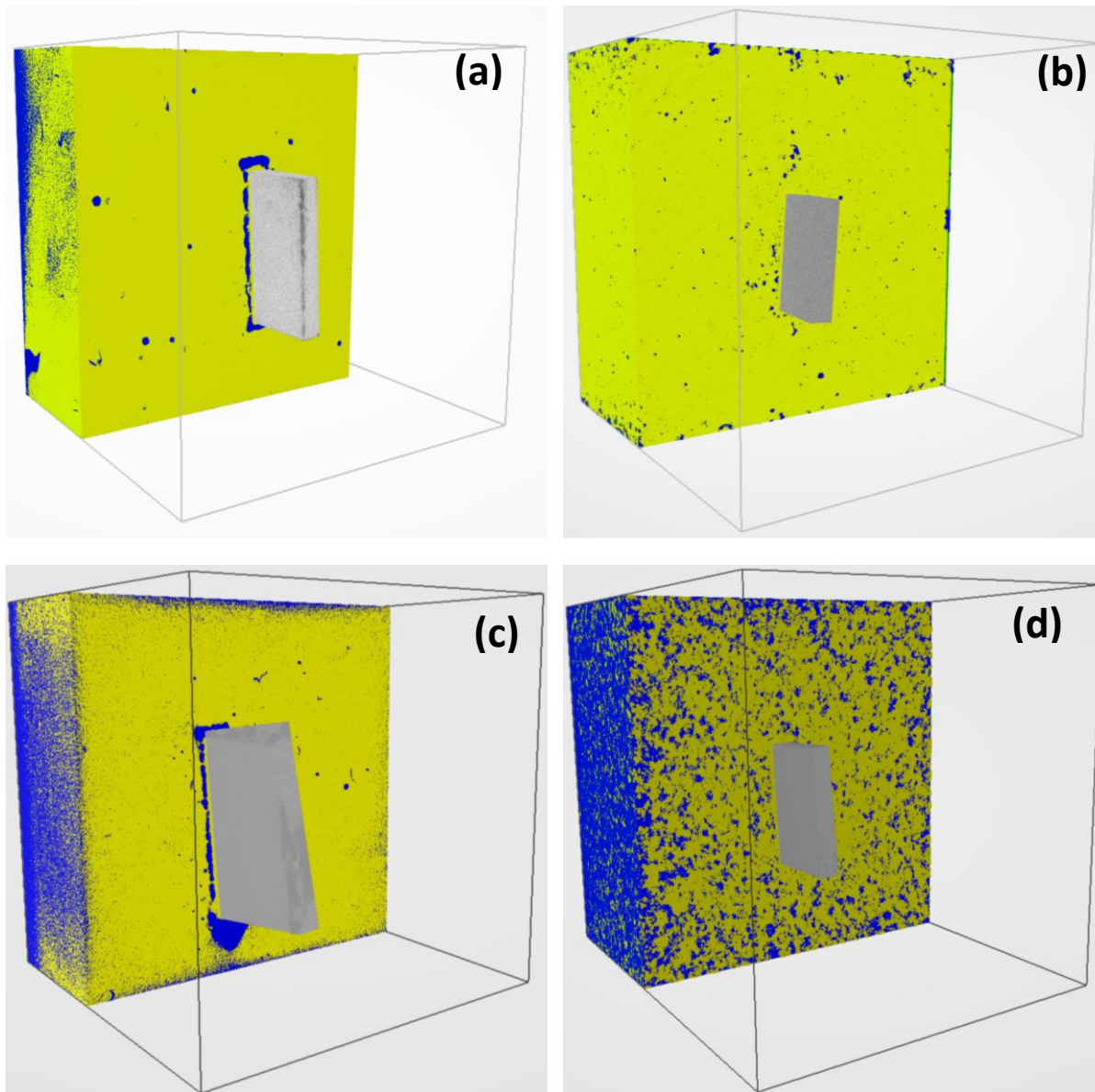


Figure 16. 3D XCT images: (a) CEM I $t = 7$ days, (b) MKPC $t = 7$ days, (c) CEM I $t = 4$ months, (d) MKPC $t = 1$ year. Blue colour = porosity; yellow = matrix, grey = Al plate.

2.1.3 Recommendations

For encapsulation of reactive metals, a prevailing neutral to low alkaline pH is an important condition that must be ensured in a MKPC formulation, thus preventing potential corrosion. The porewater pH, measured as a powder suspension in water, is highly influenced by the MgO content. The reference formulation considered in Table 1 presented a Mg/P molar ratio = 1 (Mg/P mass ratio = 0.3). Increasing the MgO content increased the pH but, accordingly, improved the mechanical strength and prevented or mitigated efflorescence. Therefore, a compromise must be found on this respect. A formulation with at least a Mg/P molar ratio = 2 would be recommended to improve mechanical properties and reduce potential efflorescence. Formulations with higher Mg/P could compromise the pH, reaching regions where Al is not passivated. In addition to the Mg/P ratio the pH has been observed to be influenced by the filler material, very probably by the content in carbonates and soluble traces included in the filler.

Adding filler materials increased the amount of inert solid in the mixture, which in turn reduced the highly exothermic heat generated by the acid-base reaction. The appropriate external morphology of filler particles can improve the workability of cement pastes and lead to higher mechanical strength

in the resulting cement compared to not using filler. Moreover, fillers are typically less expensive than the main components of MKPC (MgO and KH_2PO_4). Therefore, it may be beneficial to consider highly abundant materials with a well-defined composition. Volcanic ash has shown good characteristics to be incorporated into MKPC formulations, however the distribution of this material and its homogeneity is not guaranteed. Commercial olivine could be an alternative to explore in future works.

The formulation should include the minimum amount of water to generate K-struvite as the main reaction product. As the stoichiometry between MgO, KH_2PO_4 and H_2O is 1:1:5, but Mg could be in excess, the molar ratio $\text{H}_2\text{O}/\text{KH}_2\text{PO}_4$ should be considered. A formulation considering $\text{Mg}/\text{P} = 1$, filler/cement mass ratio = 1 and $\text{H}_2\text{O}/\text{KH}_2\text{PO}_4$ molar ratio 5:1 corresponds to a water/solid mass ratio 0.25.

Magnesium phosphate cements are recognized for their fast-setting properties. The setting time of the cement can be significantly delayed by adding a retarder. There is no real need to develop a fast-setting cement for the encapsulation of reactive metals compared to traditional Portland cement. The absence of a retarder has been observed to result in a rapid exothermic reaction, leading to high initial heat generation, fast setting, and efflorescence on the cement paste. Therefore, it is recommended to add a retarder. It has been observed that the type of retarder influences the fluidity of the cement paste before it sets.

2.2 CSIC: optimization and characterization of MKPC formulations

CSIC and UAM contributed to the subtasks T4.6.1 in close collaboration, sharing materials, planning experiments and integrating and discussing results. The work performed by CSIC alone is described in this section 2.2.

2.2.1 Main goals

To guarantee the stability of MKPC matrices for Al immobilisation, the CSIC contribution in present work was structured in to two main topics:

- 1) Effect of the MgO characteristics and moisture curing in 1M MKPC matrices using FA as filler.
- 2) Influence of the $\text{MgO}/\text{KH}_2\text{PO}_4$ (M/P) molar ratio in the physical and chemical properties of MKPC matrices to design a stable and optimal formulation for metal immobilisation.

The physico-chemical processes involved in the MKPC matrices was studied by analyzing physical properties, such as mechanical compressive strength and pore structure and the mineralogy of solid phases and pore chemical composition in cement paste and mortar systems. Table 8 summarises the main parameters, test conditions, systems, and methods studied by CSIC in D4.8.

Table 8. Description of the work performed by CSIC to study MKPC physico-chemical stability.

Type matrix	M/P ratio	w/s ratio	Type MgO	Moisture curing condition			Time (day)	Property	
								Physical	Chemical
MKPC pastes	1M	0.3	MN, 83%	100%RH			30	-	XRD
	2M		MM, 98%	Water immersion	100%RH	Isolated	50	Mechanical compressive strength	XRD Pore pH Pore ion
	3M								
MKPC mortars	1M	0.51	MM, 98%	Water immersion			600	MIP	XRD Pore pH Pore ion
				Isolated			90	MIP EIS	XRD Pore pH Pore ion
	100%RH			MIP					
	2M								
3M									

2.2.2 Materials used and samples description

2.2.2.1 Raw materials

Hard-burnt magnesia (MgO) from Martin Marietta Magnesia Specialties (MM, 97% purity) and from Magnesitas Navarras (MN, 83% purity), were used to prepare MKPC cementitious materials. The chemical composition by FRX technique of both MgOs is included in Table 9. Significant difference in MgO content is detected, higher for MM-MgO, which shows a high purity range than MgO-MN. However, periclase as main mineral phase with a well-defined crystalline microstructure is detected in the XRD pattern for both MgO in Figure 17-left. A low-cost KH_2PO_4 (98% purity) from fertilizer industry supplied by Yara (Krista TM), and a retarder H_3BO_3 (>96% purity) from VWR Chemicals to delay the acid-basic reaction and control the setting time were also introduced.

In addition, fly ash (FA) type F from different sources was introduced as inert filler material to enhance the fluidity in the mixture, limit the temperature rise during setting time and shrinkage risk. The chemical compositions of both FA are also included in Table 9. Slightly differences between both FA are in SiO_2 and Fe_2O_3 content, with similar Al_2O_3 and CaO content. However, a similar vitreous microstructure due to an amorphous hump is identified in the XRD patterns in Figure 17-right, with mullite and quartz as main mineral phases. Ferric secondary phases as hematite are also detected.

Table 9. Chemical composition of the raw materials (in %wt.).

Material	Na ₂ O	K ₂ O	CaO	SiO ₂	Al ₂ O ₃	Fe ₂ O ₃	MgO	SO ₃	CaO _{free}	CO ₂	NiO
MgO-MM	-	-	1.1	1.0	0.4	0.2	96.6	0.01	-	0.7	0.01
MgO-MN	-	-	10.9	3.7	0.4	3.0	81.6	-	-	-	0.09
FA-1	1.2	1.8	3.3	62.7	22.8	5.7	1.6	0.8			
FA-2	0.4	1.6	4.4	44.9	23.7	19.4	1.0	0.5	-	-	-

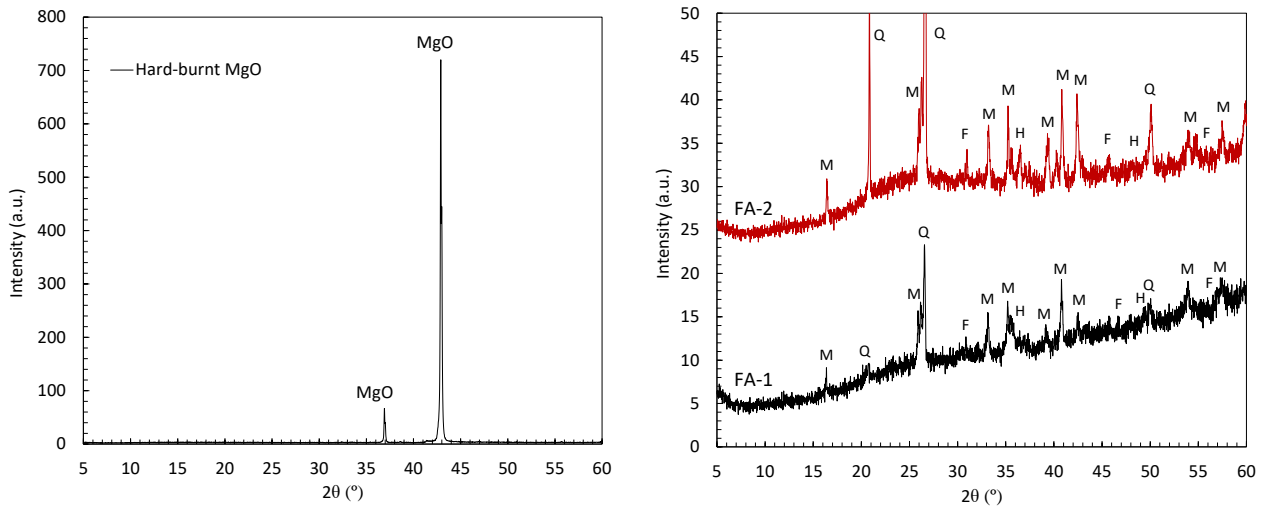


Figure 17. XRD patterns of hard-burnt MgO (left) and both FA type F (right). Legend: MgO: Periclase; M: Mullite; Q: Quartz; F: Fe₃O₄; H: Hematite.

2.2.2.2 MKPC mortar and cement paste preparation

Prismatic samples of MKPC 1 x 1 x 6 cm³ cement pastes (Figure 18-a) and 5 x 5 x 5 cm³ mortars (Figure 18-b) were prepared using different MgO/KH₂PO₄ (M/P) ratio of 1, 2 and 3 M for matrix characterization tests presented in

Table 8. Additionally, 1 M M/P ratio MKPC mortars with two stainless-steel meshes embedded were designed to study the pore connectivity of MKPC matrix from the electrical properties presented in D4.11 (sample type in Figure 18-c).

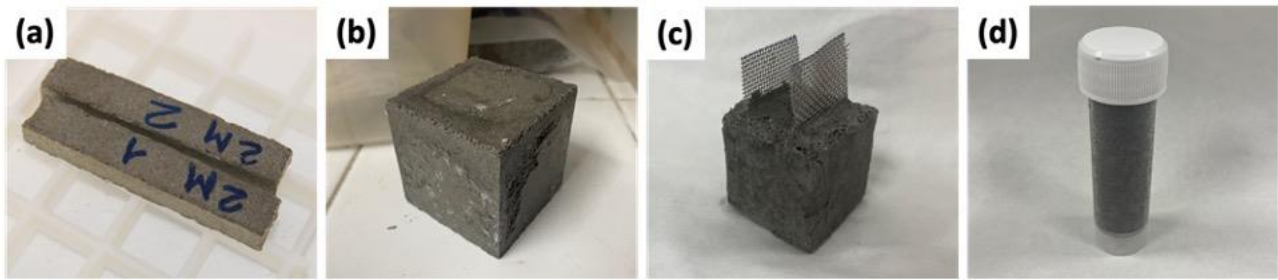


Figure 18. Type of MKPC samples and geometry: a) prismatic 1 x 1 x 6 cm cement paste; b) prismatic 5 x 5 x 5 cm mortar system; c) 3 x 3 x 3 cm mortar system with stainless-steel embedded; and d) cylindrical mortar isolated system.

Dosages used in this study are given in

Table 10 according to [13]. Mix ratios of different compounds are summarized in Table 11. A water/solid (w/s, in mass ratio) of 0.5 for mortars and 0.3 for pastes were used. For mortars samples, a standardized graded sand with a 99% silica content was incorporated in the proportions given in Table 11. Specimens were cured at a room temperature of 22 ± 2 °C under three moist curing conditions: (1) immersed in water, (2) in a chamber at 100% relative humidity (RH), and (3) isolated, in sealed plastic containers (sample type in Figure 18-d), also identified as endogenous curing.

Table 10. Formulation dosages for MKPC cement paste and mortars for different MgO/KH₂PO₄ (M/P) molar ratio (1L batch).

Compound (mass, g)	M/P ratio = 1M		M/P ratio = 2M		M/P ratio = 3M	
	Mortar	Paste	Mortar	Paste	Mortar	Paste
MgO	70	100	110	170	140	210
KH ₂ PO ₄	232	332	183	282	155	232
Sand (\leq 2mm)	302	-	293	-	295	-
Fly ash (FA)	302	432	293	452	295	442
H ₃ BO ₃	6	9	6	9	6	9
Distilled water	154	130	149	136	150	133

Table 11. Mix ratios for MKPC cement pastes and mortars.

Material	MgO/KH ₂ PO ₄	H ₂ O/solid	FA/solid	Sand/solid	H ₃ BO ₃ /solid
	(molar ratio)	(mass ratio)			
Mortar	1,2,3	0.5	1.00	1.00	0.02
Paste	1,2,3	0.3	1.00	0.00	0.02
Solid: MgO + KH ₂ PO ₄ ; FA: fly ash					

2.2.2.3 MKPC matrix characterization methodology

Compressive strength was performed over 28 days in paste systems under the three curing conditions (100%RH, isolated and immersed in water) following the UNE-EN 196-1 standard [16]. Four replicate samples were prepared for each curing to obtain the experimental deviations.

To characterize the MKPC microstructure, total porosity and pore size distribution were analyzed in mortar specimens by mercury intrusion porosimetry (MIP), while the mineralogy was determined in paste and mortars by X-ray diffraction (XRD) under the different curing at 7, 28, 50, 70 and 90 days. For both techniques, the chemical reaction was stopped by immersion a piece of sample in isopropanol during 24h to remove the excess of liquid water.

To understand the pore network connectivity based on the electrical properties, electrochemical impedance spectroscopy (EIS) in a frequency range between 10⁵ to 0.01 Hz was carried out in 1M MKPC mortars with two embedded stainless-steel meshes (see Figure 1-c) over 90 days in isolated and 100%RH. Five samples were prepared for each condition to assess the experimental errors.

Pore pH and pore ion composition (PIC) was obtained following the procedure described in [17]: a piece of MKPC mortar or paste sample from the three curing conditions was ground to 80 μ m and a 1:1 solid/liquid suspension using deionized water was prepared. After 5-minute stirring, the solution was filtered, and the pH was determined at several curing ages (7, 28, 50, 70 and 90 days). In addition, ICP-OES was employed to obtain the ionic composition of the filtered solution (P, B, Mg, K, Ca, S, Na, Al, Fe, Si, and Ca).

2.2.3 Main findings: design of an optimal and stable MKPC matrix

2.2.3.1 MgO characteristics and curing on 1M MKPC stability with FA as filler





To optimize the 1M M/P ratio MKPC formulation, the performance of two types of MgO with different purity grades was evaluated: MgO from Martin Marietta (referred as MgO-MM) with a 97% purity and MgO from Magnesitas Navarras (referred as MgO-MN) with an 83% purity. Cylindrical 1M MKPC cement pastes were prepared according to

Table 10, using both MgO. The stability of these samples was assessed over one-week curing period at 100%RH.

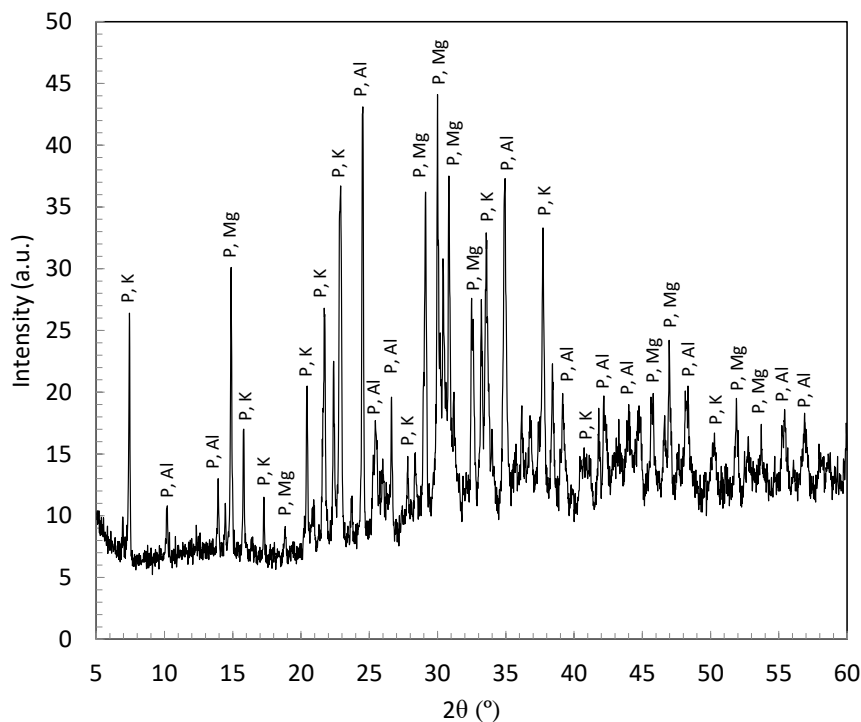
Table 2 presents the 1M MKPC pastes with MgO-MM at 1 and 7 days (Table 2-a and Table 2-b), as well as those made with MgO-MN at 1 and 7 days (Table 2-c and Table 2-d).

Significant differences in performance were observed between the two MgO after 1 day at 100%RH. MgO-MN exhibited significant white efflorescences on the surface of the samples. In contrast, the MgO-MM samples displayed fewer instabilities. After 7 days, significant volumetric changes associated with these efflorescences were evident in the MKPC pastes with MgO-MN, which were less pronounced in those with MgO-MM, although in both cases volumetric damages occurred.

Table 12. 1M MKPC pastes using MgO-MM and MgO-MN at 1 day and 7 days under 100%RH.

Type	MgO – MM (97%)		MgO – MN (83%)	
Time	1 day	7 days	1 day	7 days
Paste systems				
	(a)	(b)	(c)	(d)

The crystalline composition of the white efflorescence was analyzed by XRD, mainly identified to be constituted of magnesium and potassium phosphates. These efflorescences, accompanied by volumetric changes, are compromising the microstructural stability of MKPC matrices and the mechanical strength required to ensure an optimally stable matrix for a suitable Al immobilization.









*Figure 19. XRD pattern of the white efflorescences in 1M MKPC pastes at 100%RH curing.
Legend: P, Al: aluminium phosphates ($AlPO_4$); P, Mg: magnesium phosphates ($H_{16}MgP_2O_{10}$,
 $H_8Mg_7P_2O_{16}$, H_7MgPO_7); K, P: potassium phosphates ($H_8K_4P_4O_{16}$, $H_{16}K_6P_6O_{20}$).*

Although both types of MgO induce physico-chemical instabilities, better performance was observed with MgO-MM, which was selected for its use in the preparation of MKPC cementitious materials. In order to determine the cause of these instabilities, the effect of the amount of moisture during curing condition was evaluated. 1M MKPC pastes were prepared (see

Table 110) under three different curing conditions (water immersion, 100%RH and isolated in sealed plastic vials) following the architecture depicted in Figure 118-a.

Table 13 shows the 1M MKPC pastes under the three curing conditions at 2 and 7 days of testing. It can be observed that a greater amount of instability, showing as efflorescences and volumetric changes, are detected under high moisture conditions, particularly when immersed in water (see Table 13-a), followed by 100% RH curing (see Table 13-b). Moreover, these instabilities become more pronounced over curing time at 7 days. Better behavior is detected when there is a lack of moisture from curing under isolated curing at 2 and 7 days (see Table 13-c). This confirms that moisture from curing plays an important role in the physical and chemical stability of these MKPC matrices.

Table 13. 1 M MKPC pastes at 2 and 7 days under water immersion, 100%RH and isolated curing.

1M MKPC pastes (MgO-MM, 97% purity)			
Curing type	Water immersion	100%RH	Isolated
	(a)	(b)	(c)
2 days			
7 days			

The effect of moisture curing on MKPC physico-chemical stability is being analyzed now in the macro and microstructure properties to find a stable and optimal MKPC matrix for AI long-term storage. Different properties were analyzed as defined in

Table 8:

- Physical properties: Mechanical strength

Figure 20 includes the mechanical strength of MKPC pastes at 1M M/P ratio after 28 days under the three-moisture curings: water immersion, 100%RH and isolated or endogenous curing in sealed plastic containers. The standard deviation is also included.

As described previously, the moisture content during curing has a significant influence in the physical stability of 1M MKPC matrix. Under high moisture conditions such as water immersion, the lowest compressive strength value is detected (7.33 MPa) followed by 100%RH curing (8.6 MPa) where higher deformations and efflorescences were observed, Table 13. An excess of soluble phosphates in the matrix is favoured by the high moisture content in the pores, resulting in the appearance of efflorescences and associated cracking, which reduces the mechanical performance. The greater dispersion found in 1M MKPC paste at 100% RH curing is probably a consequence of the greater instability at the time of measurement.

A certain increase in isolated curing was observed with values of 8.75 MPa. Due to a lack of water in the pores, the acid-base reaction is not complete and more unreacted phases would contribute to a reduction in the porosity and volume shrinkage in MKPC matrices, generating a denser structure. However, under all curing conditions, strengths of less than 10 MPa are observed, which is related to the poor stability of the 1M MKPC matrix due to the higher MgO content in the initial formulation.

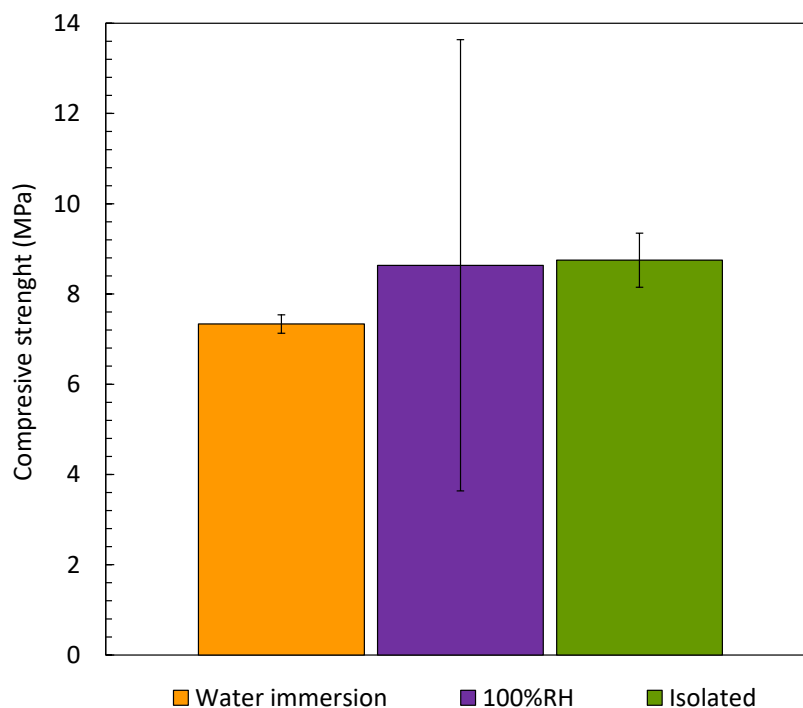


Figure 20. Compressive strength and standard deviations of MKPC pastes at 1M M/P ratio under water immersion, 100%RH and isolated condition after 28 days of testing.

- Physical properties: Pore network and connectivity

Pore network microstructure was analysed in 1M M/P ratio MKPC mortars at the end of the test under the three curing conditions in order to understand the main differences found in mechanical strength depending on the curing moisture content.

The pore volume distribution and total porosity and pore size proportions are observed in Figure 21-left and in Figure 21-right, respectively. A multimodal distribution is detected in Figure 21-left for the 1M MKPC mortars in the three curing conditions, where the small and intermediate pore sizes are dominant compared to the large pore sizes. However, a higher number of pores are found under

high moisture curing conditions than under endogenous curing. As a result, a higher total porosity is detected in Figure 21-right with values of 12.31% and 12.26% under water immersion and 100%RH respectively, which shows a larger number of capillary pores ($\approx 5\%$ for pores < 0.01 to $0.1\mu\text{m}$).

Lower total porosity is observed in isolated curing condition (8.69%, in Figure 21-right), with respect to 100%RH and water immersion. The proportion of capillary pores (2% for pores $< 0.1\mu\text{m}$) is lower in the isolated systems as also observed in Figure 21-left.

The content of water in pores can have a significant effect on the evolution of reaction components in the development of MKPC microstructures. However, these differences in pore size and distribution are not appreciated in compressive strength (Figure 20), which are very similar but lowers at higher moisture content. Furthermore, in isolated curing, the pore water is consumed without any addition, being insufficient to allow the acid–base reaction to progress adequately, reducing the porosity and increasing the mechanical performance due to the presence of higher levels of unreacted products.

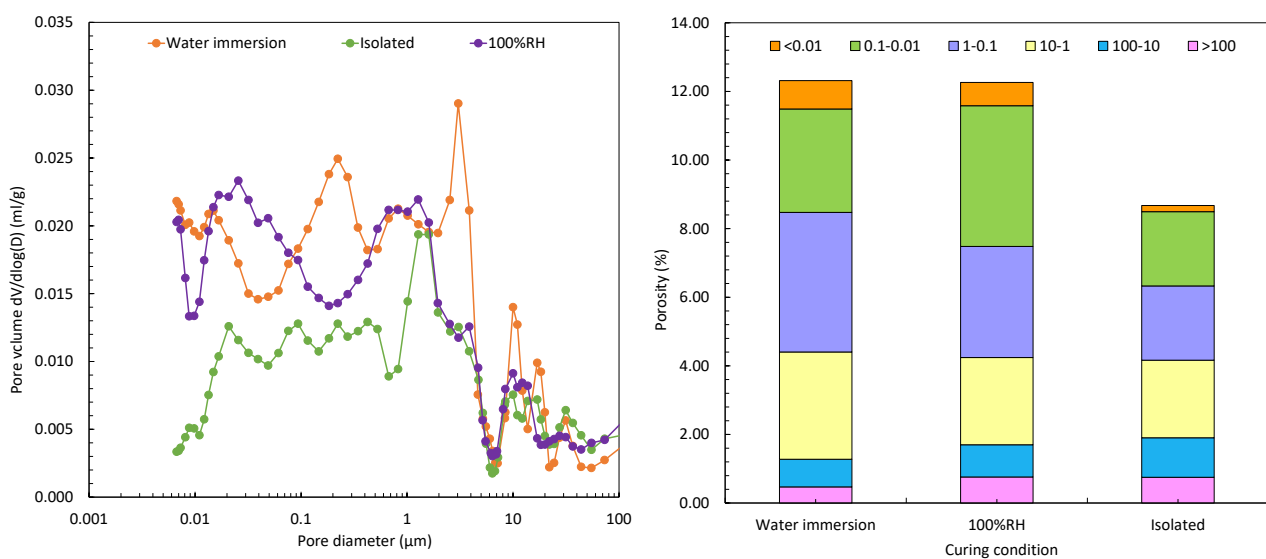


Figure 21. Pore volume distribution (left) and total porosity and pore size proportions (right) in 1M MKPC mortars under water immersion, 100%RH and isolated condition at the end of the test.

The synergy between dielectric properties and pore network is evaluated with EIS, to provide more information about the MKPC matrix at microstructural level. Figure 22-a and Figure 22-b show the EIS response of 1M MKPC mortars under isolated and 100%RH respectively over 70 days curing.

The high-frequency domain in an EIS diagram is attributed to the properties of the cement matrix in terms of the pore network: solid phase, disconnected pores, and the electrical resistance (R_e) of connected pores. Zoomed areas of the Nyquist diagram are represented in Figure 22-c and Figure 22-d, which correspond to the high-frequency domain up to 105 Hz for isolated and 100%RH curing, respectively. The inflection point close to the real impedance (Z') axis was used to determine the R_e evolution with the maturity of the matrix.

Under isolated conditions (see Figure 22-c), R_e increases with time with a shift towards lower frequencies at the inflection point of the high frequency domain. This is attributed to the progression of the acid-base reaction due to pore water consumption as defined in D4.11. Conversely, at 100%RH (see Figure 22-d), only a slight shift in the high frequency region of the Nyquist plot is observed at the end of the test, without a significant increase in R_e over time, which is associated with a better electrical conductivity response through a higher pore water content, also analysed in D4.11.

Different EIS capacitive response in terms of electrochemical behaviour related to the diameter of the Nyquist semicircle is also detected at low and intermediate frequencies over time for both curing,

related to the connectivity of the pore network of the bulk matrix. A dependence of the apparent dielectric constant on the pore network was associated with the diameter of the Nyquist semicircle. Under 100%RH, a decrease in the diameter of the semicircle associated with a decrease in the dielectric constant is detected in Figure 22-b, with lower capacitive over time being related to a good pore network in the matrix as found in Figure 21. On the other hand, an increase in the diameter of the semicircle related to an increase in the capacitive matrix behaviour was observed for the isolated condition in Figure 22-a, resulting in poor connectivity in the pore network by a lower number of pores in Figure 21.

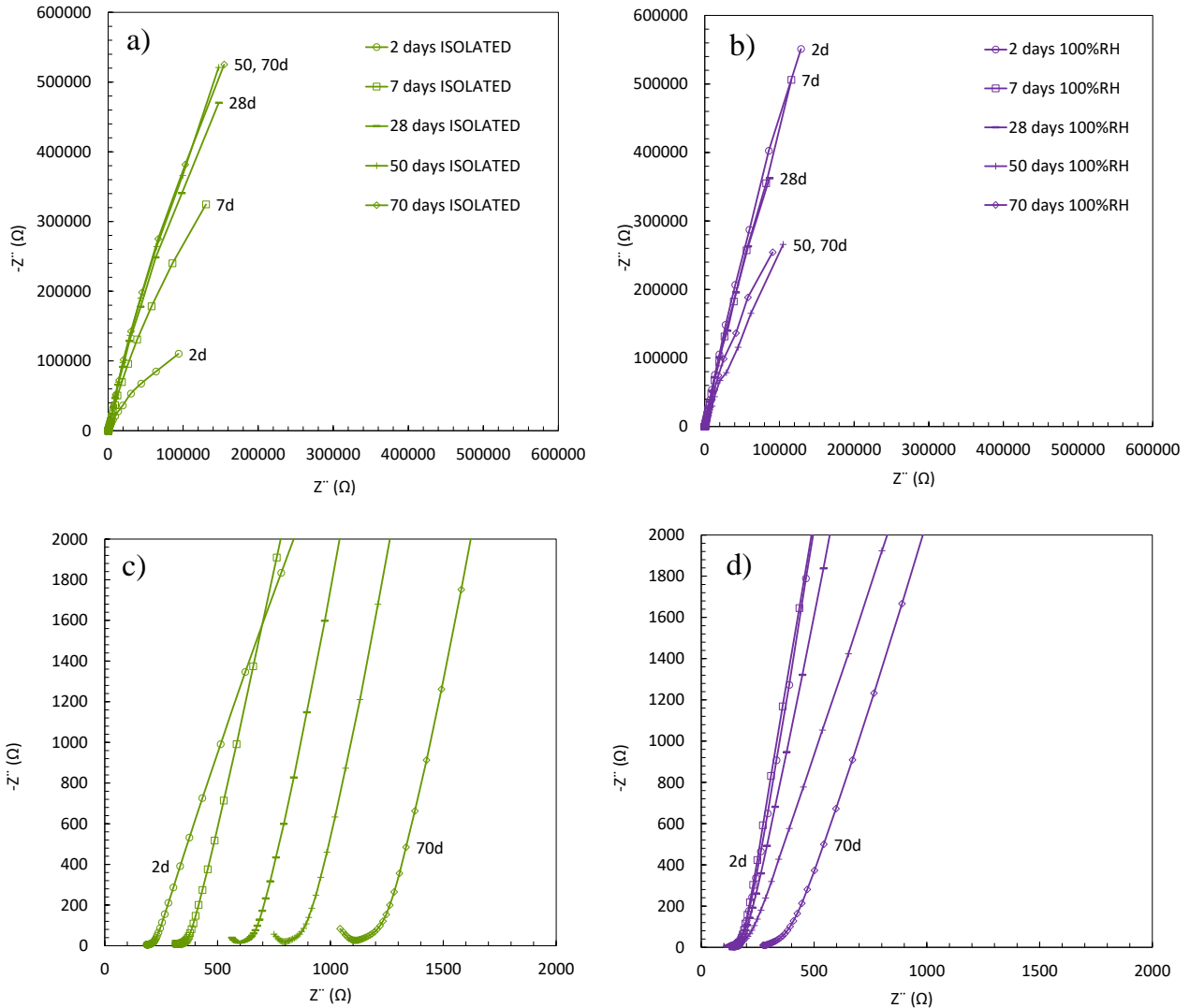


Figure 22. EIS response for 1M MKPC mortar [18]: (a) Nyquist plots in isolated curing at low frequency, (b) Nyquist plots in 100%RH at low frequency, (c) Nyquist plots in isolated curing at high frequency, and (d) Nyquist plot in 100%RH at high frequency.

- Chemical properties: Solid phases

The chemical microstructure in terms of solid phases of MKPC matrices is influenced by the pore moisture content during curing.

Figure 23 includes the main mineral phases of 1M MKPC mortars at the end of the test determined via XRD technique considering the effect of the moist availability during curing: isolated, 100%RH and water immersion. K-struvite is detected as the main mineral phase in the three systems with residual periclase formation. In addition, quartz and mullite coming from the FA and sand in mortar preparation were identified. At higher moisture content (100%RH and water immersion), the MKPC acid–base reaction is expected to be favoured, and the main reflections of K-struvite with lower residual periclase were detected at 20.99° and 36.46° , respectively.

On the contrary, under isolated curing, K-struvite and more defined reflections of unreacted MgO were detected at 20.83° and 36.46° , respectively, probably because the water amount for the reaction progress is not enough.

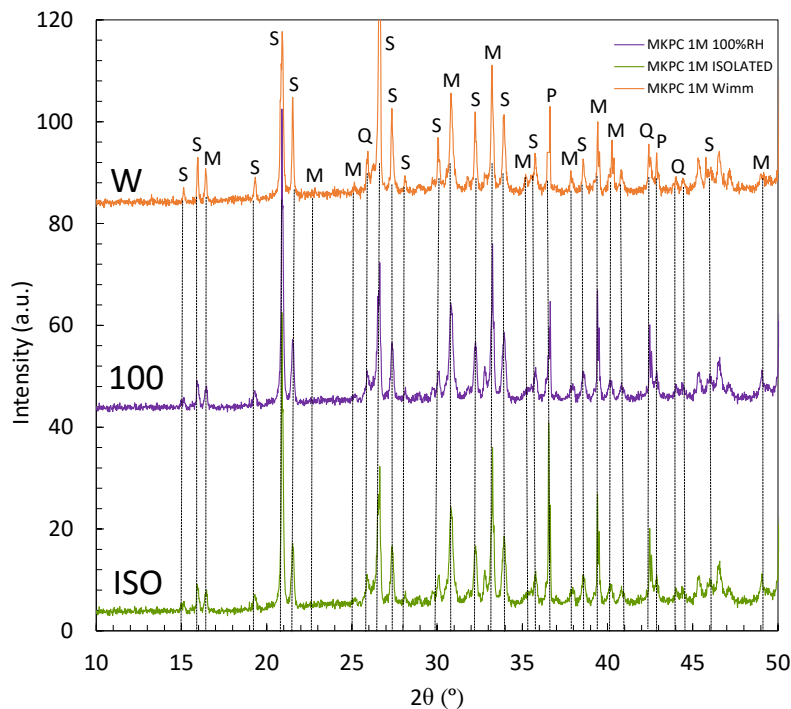


Figure 23. XRD pattern of 1M MKPC mortars in water immersion, at 100%RH and isolated curing after 28 days. Legend: S (K-struvite); P (Periclase); Q (Quartz); and M (Mullite).

- Chemical properties: pH and ion evolution in the pore solution

The pore pH of the 1M MKPC mortar and paste pore solution under the three curing conditions was analysed in Figure 24 to understand the effect of the moisture during curing in the chemical stability of these type of matrices.

Main differences between mortars and pastes are related to the higher w/s ratio in mortar preparation, which influence the solubility of the main crystalline phases. An increase in the pore pH evolution is detected for the three-moisture content. In all 1M MKPC systems, near neutral pH values are observed at the initial stage. However, there are significant differences as curing progresses. At high moisture content, in water immersion curing, a significant increase is observed after 50 days of testing due to a lixiviation phenomenon from the pore solution to the external curing water, increasing the pH from 7 to 8.79 (also analysed in D4.11). However, in the 100% RH curing, no risk of leaching, final pH values of 8.6 and 8.1 are observed in mortar and paste samples respectively, with a slight evolution over time. Isolated curing gives the lowest pH value of around 7.8 after stabilisation at 28 days of testing. The slight difference between the three curing conditions is explained by differences in the pore ion content, which is related to the reaction progress.

An analysis of the main ions in the pore solution at the beginning and at the end of the test was carried out via ICP-OES, as shown in Table 14; evaluating the evolution of phosphate, borates, magnesium, potassium and sulphur of 1M MKPC mortars in water immersion, 100%RH and isolated curing.

As defined previously by XRD, under high moisture curing (water immersion and 100%RH), the acid-base reaction is complete due to the constant moisture supplied from curing for the reaction to progress. In this term, a significant decrease of the main ions in the pore solution is related to the formation of K-struvite as main mineral phase as observe in the XRD pattern (Figure 23). In the isolated media, the MKPC acid-base reaction is not complete due to a lack of external moisture

supplying more P, S, K, Mg, and B in the pore solution than in 100%RH and water immersion condition showing a non-evolution over time. Higher ion contents in isolated condition would indicate that unreacted phases remain in the pore solution due to the acid-base reaction not being complete due to insufficient water in the media.

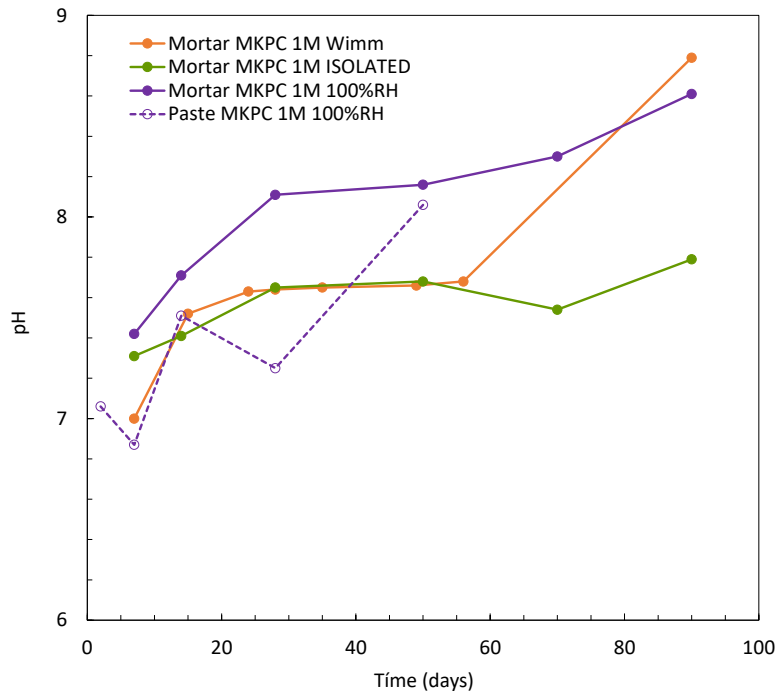


Figure 24. Pore pH evolution in 1M M/P ratios of MKPC mortars or cement pastes under water immersion, 100%RH and at isolated curing condition.

Table 14. Pore ion evolution for 1M MKPC mortars immersed in water, isolated and at 100%RH.

Curing condition	Water immersion		100%RH		Isolated	
	Initial	Final	Initial	Final	Initial	Final
Phosphate (P, ppm)	6572.00	520.00	4803.48	829.10	6768.05	4766.77
Borate (B, ppm)	199.00	56.62	369.26	131.22	506.96	520.31
Magnesium (Mg, ppm)	60.00	10.70	82.71	41.74	109.06	104.35
Potassium (K, ppm)	28108.00	1024.09	13345.10	2464.65	19453.50	15123.60
Sulphur (S, ppm)	99.00	132.81	908.71	141.80	1436.63	1444.42

As can be seen in Table 14, higher contents of S ions are detected in the pore solution of 1M MKPC mortars in all curing conditions. These sulphur ions are attributed to the FA used as a filler in this type of matrices.

In order to understand the possible influence of fly ash on the physico-chemical stability of MKPC matrices, the effect of FA in the presence of the main ions of MKPC matrices (borates and phosphates) was evaluated to analyse if there are changes in pH and to confirm the presence of S ions in the MKPC pore solution derived from FA. For present study, three type of aqueous solutions were prepared: (1) distilled water + FA, (2) distilled water + FA + KH_2PO_4 and (3) distilled water + FA + H_3BO_3 . Analyses were performed after 5 min and after 24 hours of stirring.

Figure 25 shows the S ion content in ppm in the three aqueous solutions. In the presence of only FA, no S ions are identified after 24 hours stirring. However, in the presence of the main ions of MKPC matrices, significant differences are identified. In a boron media, S ion content of 300 ppm is detected without changes after 24 hours stirring. On the other hand, in a phosphorous media, a significant increase of the S ion content is observed after 24 hours from 300 to 500 ppm. In this context, S ions in MKPC matrices are derived from the FA used a filler.

The pH evolution is observed in Figure 25-right. In all media, the pH increases to more alkaline values after 24h stirring. However, in the presence of phosphates, the lowest pH value (≈ 5) is detected. In this context, the S ions from the FA used as a filler in MKPC matrices have an influence in the pore pH evolution to more alkaline values over time.

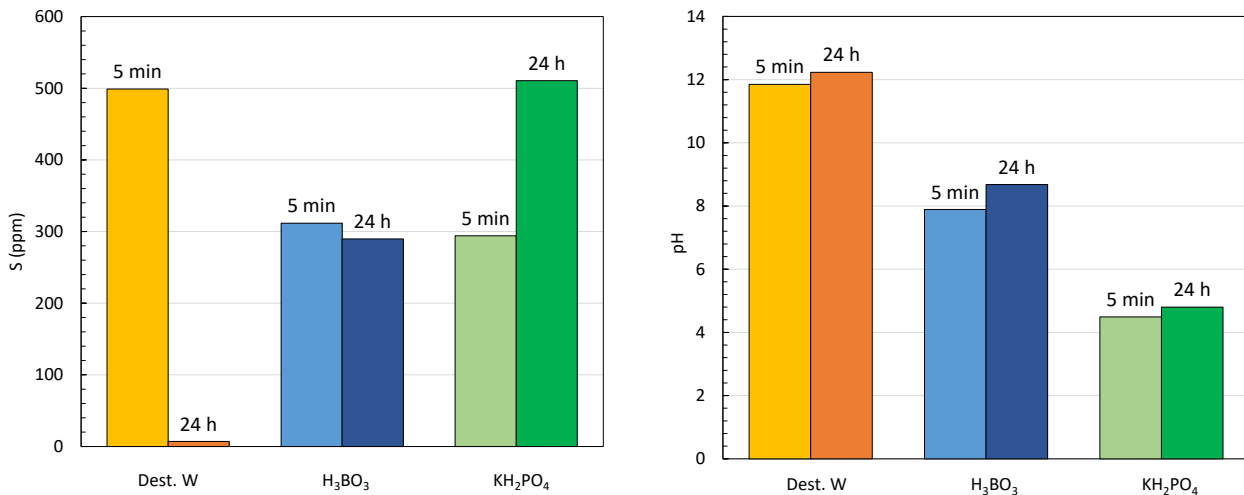


Figure 25. S ion content (in ppm) (left) and pH evolution (right) at 5 min and 24 hours stirring in boron and phosphorus solutions with FA.

2.2.3.2 Main conclusions

The main conclusions obtained by CSIC about the influence of the moisture curing on the physico-chemical stability of MKPC matrices are:

- Higher moisture content in the matrix supplied by the curing environment allows higher instabilities in MKPC matrix due to the rapid dissolution of the excess of soluble phosphates at 1M M/P ratio formulation, which leach out and crystallize as white efflorescences.
- The 1M M/P ratio exhibits lower strengths in the three curing conditions, yielding matrix instabilities and phosphate efflorescences.
- The acid–base reaction is complete under high moisture condition with the formation of K-struvite and minor residual periclase in the 1M microstructure. A decrease of the main ions in the pore solution exists due to the formation of the main mineral phases, increasing the pore pH over curing time.
- S ion content in pore solution is attributed to the FA used as a filler, which increase the pore pH of 1M MKPC matrix to more alkaline values.
- In endogenous or isolated curing, the reaction does not progress completely due to the lack of water in the system, with more dissolved ions in the pore solution and more unreacted products, showing more near neutral pH values.
- A better pore network is observed at higher moisture content showing more capillary pores than in isolated condition, which improve the physical stability of MKPC matrices. However, no relation with mechanical strength is detected.

Although the isolated environment provides better physical stability, curing at 100% RH has been selected for the MKPC matrices to ensure the complete progression of the acid-base reaction through a continuous supply of water in the pores providing a better chemical stability. In addition, 1M MKPC matrices have a better physical performance than under water immersion condition.

Table 15 summarizes the main conclusions obtained from CSIC in order to evaluate the influence of the pore moisture content from curing on the stability of 1M MKPC matrices.

Table 15. Main conclusions in the evaluation of moisture curing on MKPC physico-chemical stability.

Effect of moisture curing		Isolated	100%RH	Water immersion
		<i>1M M/P ratio</i>	<i>1M M/P ratio</i>	<i>1M M/P ratio</i>
Property	Mechanical strength	Low (8.75 MPa)	Low (8.6 MPa)	Low (7.33 MPa)
	Pore structure	Low porosity	Higher porosity and capillary pores	
	Pore connectivity	Poor	Better	-
	Mineral phases	K-struvite, residual MgO	Main K-struvite, lower residual MgO	
	Pore pH	Neutral pore pH (≈ 7) Slight evolution	Pore pH (≈ 8) Slight evolution	Higher pH (≈ 9) Lixiviation
	Pore ion content	Higher P, Mg, K and B No progress reaction Lack pore water	Less P, K, Mg and B in pore solution. Progress of acid-base reaction Enough pore water	

2.2.4 Effect of M/P ratio on macro and microstructural properties of MKPC

Since MgO contributes to certain instabilities as observed in section 4.1, the current objective aims to increase the MgO/KH₂PO₄ (M/P) ratio in order to evaluate its effect on the physicochemical stability of the MKPC matrices. MKPC pastes with MgO-MM were prepared using different M/P ratio at 1, 2 and 3M (see

Table 110) under 100%RH curing, selected to better identify instabilities, following the architecture depicted in Figure 118-a.

Table 16 shows the 1, 2 and 3M M/P ratio MKPC pastes at 2 and 7 days under 100%RH curing. It can be observed that a greater amount of instabilities, such as efflorescences and volumetric cracks, are detected with the 1M formulation (see


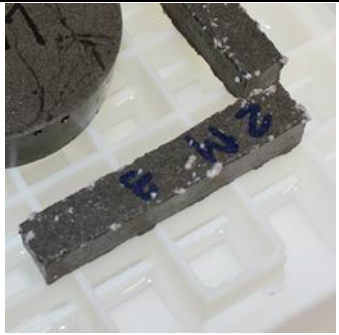



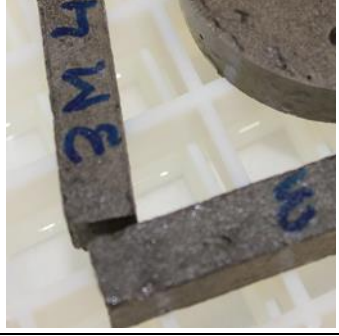
Table 16-a) which are more pronounced with curing advance. Contrary, with the increase of the M/P ratio at 2 and 3M, higher amount of MgO and less KH_2PO_4 is introduced in the paste preparation, as observed in

Table 110. The physico-chemical instabilities observed in 1M MKPC pastes are less evident at higher M/P ratio (see

Table 16-b at 2M and

Table 16-c at 3M) also with curing time. This confirms that the M/P ratio plays an important role in the physical and chemical stability of MKPC matrices.

Table 16. MKPC pastes with 1, 2 and 3M M/P ratio at 2 and 7 days under 100%RH curing.

MKPC pastes (MgO-MM, 97% purity) at 100%RH			
M/P ratio	1M	2M	3M
	(a)	(b)	(c)
2 days			
7 days			

Due to these observations, the effect of the M/P ratio on the physico-chemical stability of MKPC is now being analyzed at both macro and microstructural level to design an optimal MKPC matrix for a stable long-term Al immobilization. Different properties were analyzed as defined in

Table 8:

- Physical properties: Mechanical strength

To understand the effect of the M/P ratio on the MKPC physical stability, Figure26 shows the mechanical strength response of 1, 2 and 3M MKPC pastes after 28 days at 100%RH condition. The standard deviation is also included.

As observed in Figure26, higher M/P ratios allow higher compressive strengths (30 and 25 MPa for 2M and 3M, respectively). This better mechanical performance is related to the pore structure or the solid phases in the microstructure, which will be discussed below. Conversely, lower compressive strengths were found at 1M M/P content (8.6 MPa) in accordance with the development of volume deformations and phosphate efflorescences as shown in

Table 16 under 100%RH curing. The greater dispersion found in 1M at 100% RH is probably a consequence of the greater instability of this matrix, which causes the excess of phosphates from the initial formulation to leach out of the cement paste in the form of efflorescences favoured by the high moisture content in the pores.

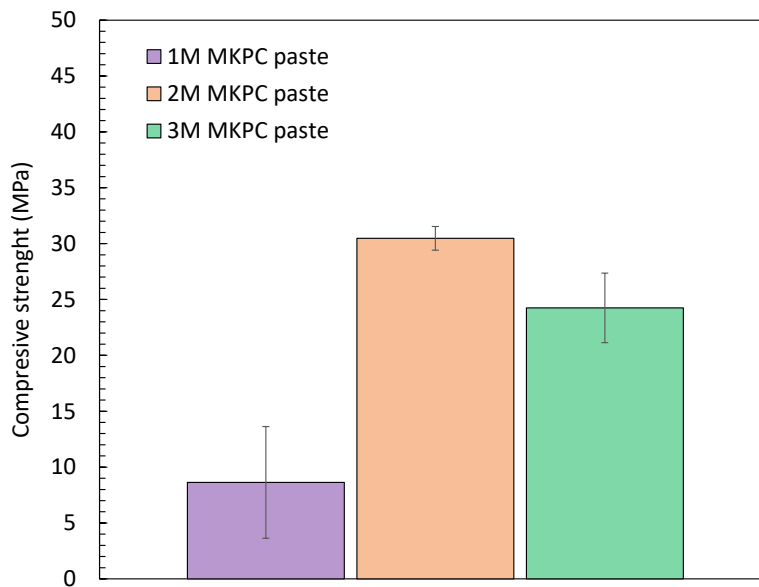


Figure 26. Compressive strength and standard deviations of MKPC pastes at different M/P ratio (1, 2 and 3M) under 100%RH condition after 28 days of testing.

- Physical properties: Pore network

To understand the differences on mechanical strength depending on the M/P ratio, total porosity was evaluated in 1M and 3M MKPC mortars under 100%RH, as observed in Figure27. In addition, the evaluation of the pore size distribution during MKPC maturity is fundamental to understand the pore connectivity in relation to the advance of the acid-base reaction at microstructural level.

An increase in total porosity is detected for all M/P ratio over curing advance. However, higher values are identified at higher M/P ratio at the end of the test. Values of about 10% in 1M (see Figure27-left) and 12% in 3M (see Figure27-right) are detected. This total porosity does not fit well with the higher compressive strengths at higher M/P ratio in Figure26. As a result, to understand the effect of total porosity on mechanical strength development, the pore size distribution is also considered. As observed in Figure27, an increase in capillary pores ($< 0.1\mu\text{m}$) are observed at higher M/P ratios (1M: 3.2% and 3M: 5.2%), which contribute to a densification of the matrix, giving higher mechanical strength at higher M/P ratios.

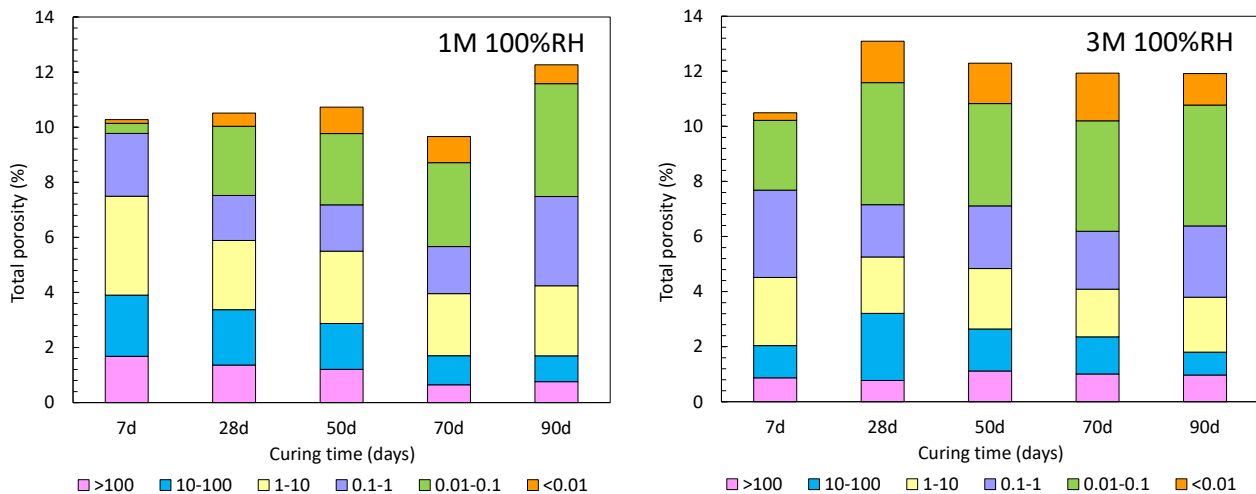


Figure 27. Total porosity and pore size distribution evolution in μm over 90 days at 100%RH condition from 1M (left) to 3M (right) M/P ratio [18].

- Chemical properties: Solid phases

The chemical microstructure of MKPC matrices can be affected by the M/P ratio in the solid phases, type, and amount of reacted and unreacted products in function of sample maturity.

Figure 28 shows the XRD patterns of 1, 2 and 3M M/P ratio at 100%RH over 90 days, including the crystalline phases that constitute to the microstructure. K-struvite is detected as main mineral phase for all systems. Diffraction reflections corresponding to quartz and mullite are detected, coming from the FA and sand used in mortar preparation.

As observed, at higher M/P ratio (2 and 3M) more residual periclase is detected due to more MgO and less phosphate amount in the MKPC initial formulation (

Table 110). The coexistence of both mineral phases contributes to the densification of the matrix microstructure, which improves the strength performance in Figure26 at higher M/P ratio. In addition, the increase in capillary pores over time (see Figure27-right) indicates the progressive formation of the solid phases that densify the matrix. On the contrary, less intense diffraction peaks of residual periclase are identified at the lower M/P ratio of 1M, due to the lower amount of MgO in the initial MKPC formulation and higher soluble phosphate in the form of white efflorescences and instabilities, showing the lowest mechanical performance in Figure26.

The influence of the M/P ratio on matrix maturity is now analysed in the XRD patterns for 1 and 3M MKPC mortars over 90 days at 100%RH condition, shown in Figure29.

Figure29-left shows that for 1M M/P ratio, periclase diffraction peaks practically disappear after 28 days of curing, indicating that practically all MgO has reacted with phosphates to form K-struvite. This is not the case of 3M M/P ratio in Figure29-right, where intense diffraction reflections of residual periclase are identified at all curing ages. In this context, the advance of matrix maturity has been attributed with the advance of MgO and KH_2PO_4 reaction and the formation of K-struvite.

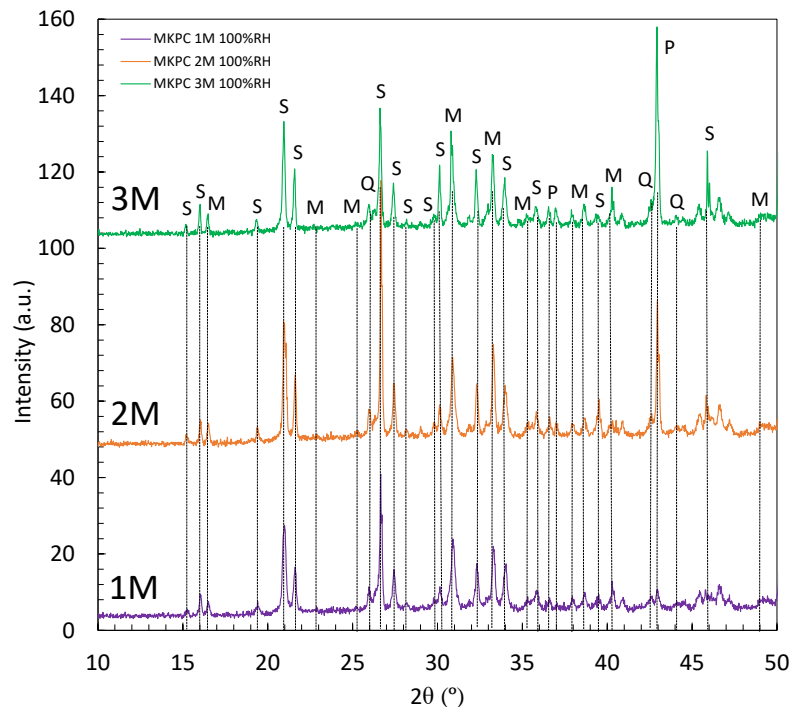


Figure 28. XRD pattern of MKPC mortars at 1, 2 and 3M M/P ratio at 100%RH condition over 90 days. Legend: S (K-struvite); P (Periclase); Q (Quartz); and M (Mullite).

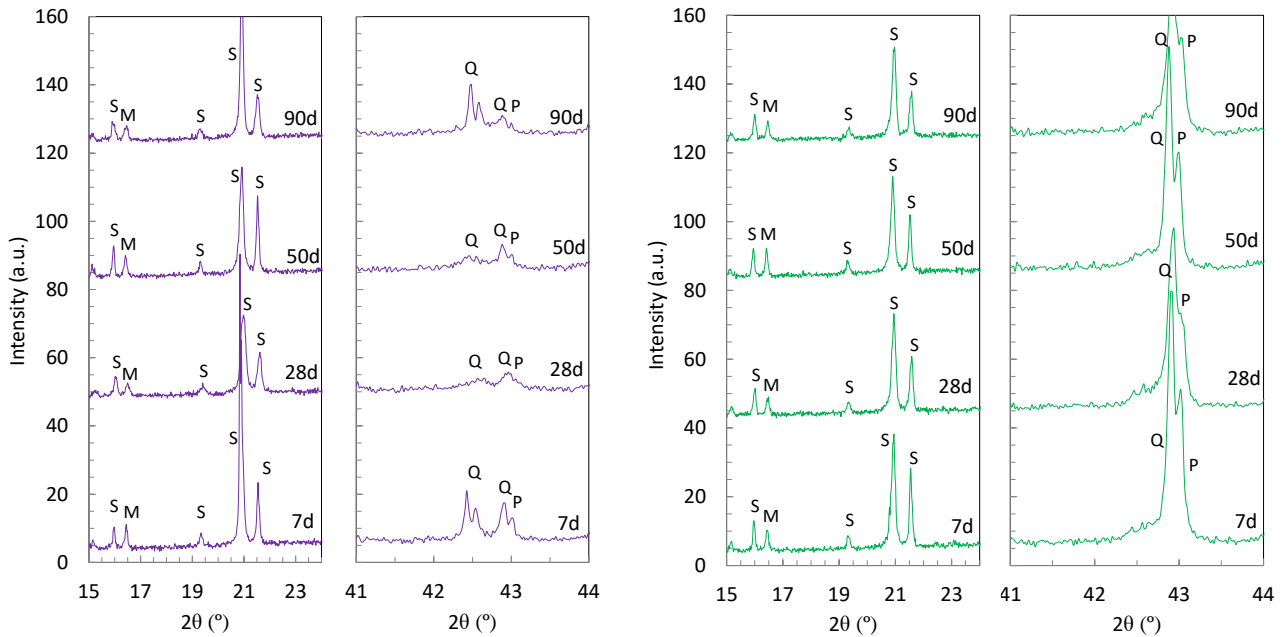


Figure 29. XRD patterns of MKPC mortars at 100%RH over 90 days at 1M (left) and 3M (right) M/P ratio [18]. Legend: S (K-struvite); P (periclase); Q (Quartz); and M (mullite).

- Chemical properties: pH and ion evolution in the pore solution

With regard the chemical composition of MKPC matrices, the pH of the liquid pore media is analysed to better understand the reaction mechanism of MgO and KH_2PO_4 to form the main product K-struvite, which also affects the chemical stability of the cementitious matrix for Al immobilisation.

The effect of the M/P ratio (1, 2 and 3M) on the pore pH was evaluated in cement pastes and mortars, shown in Figure30.

There is a clear increase in pore pH values with increasing M/P ratio in both pastes and mortars. The differences between the two cementitious materials are related to the fact that mortars are initially prepared with higher w/s ratios (Table 111), which can affect the solubility of the different phases and increase the pore pH. However, an increase evolution is detected for all M/P ratios in both systems. A stabilization is found after 28 days curing with values of 8.7 and 9.5 in pastes, and 10.3 and 10.5 in mortars for 2M and 3M M/P ratio, respectively. At the lower M/P ratio of 1M, near neutral pH values are observed with final values of 8.6 and 8.1 in mortars and pastes respectively, with a slight evolution over time.

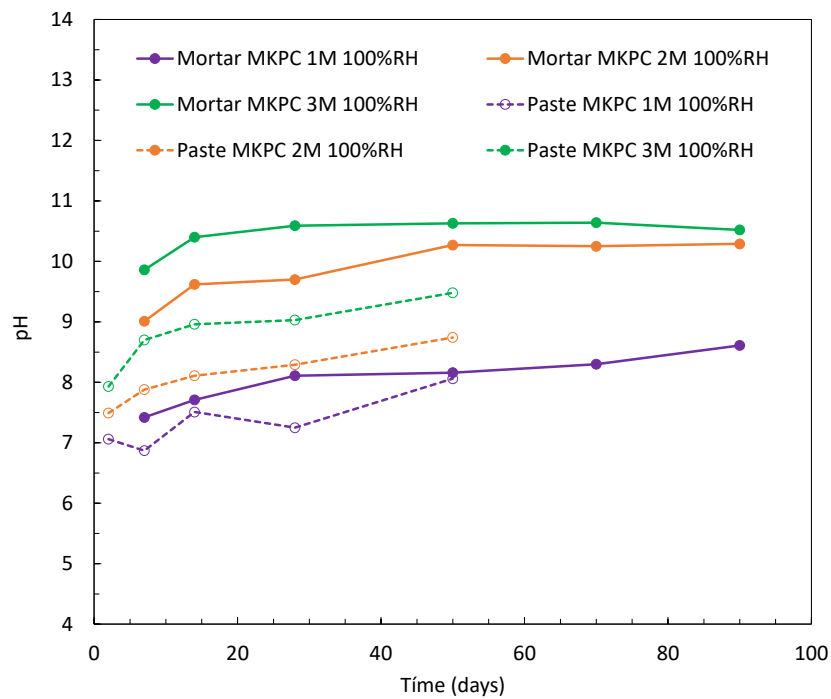


Figure 30. Pore pH evolution in 1, 2 and 3 M M/P ratio MKPC mortar and pastes at 100%RH.

The MKPC microstructural changes as a function of the M/P ratio are in chemical equilibrium with the evolution of the pore ion content. An analysis of the main ions in the pore solution at the beginning and at the end of the test was carried out via ICP-OES, as shown in Table 217; evaluating the evolution of phosphate, borates, magnesium, potassium and sulphur of 1, 2 and 3 M M/P ratio MKPC mortars at 100%RH for over 90 days.

As observed in Table 27, a higher phosphate content is detected in the early stages at lower M/P ratio, which explains the lower pH values in Figure30. A significant decrease in P ions is observed over time at all M/P ratio, associated with the progress of the acid-base reaction. K-struvite is formed as the main reaction product (see Figure28), as evidenced by the decrease in K ions in 1, 2 and 3M pore solution. Low levels of Mg ions are detected at all ratios due to the MgO reacting to form K-struvite with curing advance. However, a slightly higher Mg content is detected in the 1M formulation due to the presence of phosphate efflorescences. B ions decreased over time, but no clear effect of M/P ratio is inferred.

In addition, Table 27 (red lines) shows high levels of S-ions at all M/P ratios due to the use of FA as a filler in MKPC matrices, which contributes to the modification of the chemical microstructure by the increase in pore pH (see 4.1).

Table 27. Pore ion evolution for 1, 2 and 3M M/P ratio MKPC mortars at 100%RH.

MgO/KH ₂ PO ₄ ratio	1M		2M		3M	
	Initial	Final	Initial	Final	Initial	Final
Phosphate (P, ppm)	4803.48	829.10	880.88	20.33	72.01	5.50
Borate (B, ppm)	369.26	131.22	318.86	152.14	361.54	92.97
Magnesium (Mg, ppm)	82.71	41.74	12.49	17.96	12.65	11.65
Potassium (K, ppm)	13345.10	2462.65	4137.34	1115.17	2713.83	949.64
Sulphur (S, ppm)	908.71	141.80	630.66	193.57	595.62	145.11

2.2.4.1 Main conclusions

The main conclusions obtained by CSIC about the effect of M/P ratio in the physico-chemical stability of MKPC matrices are:

- The physico-chemical stability of the MKPC matrices in terms of microstructural properties show a high dependence of the M/P molar ratio used in the initial formulation.
- Lower M/P ratio of 1M shows higher initial phosphate amount and lower strengths, giving matrix instabilities and phosphate efflorescences. The increase of M/P ratios allow higher capillary pores which contribute to increase the matrix mechanical strength in all moisture curing conditions.
- In addition, at higher M/P ratios, the coexistence of K-struvite and MgO increase the mechanical strengths, also related with the K-struvite micromorphology that is fully developed at higher M/P ratios.
- The pore solution is mainly dominated by phosphates, borates, and K while low Mg content. The pore ion content decrease with the M/P ratio due to the acid-base reaction progresses over curing time.
- The content of phosphate contributes to control the pH in in the pore solution that increase with the increase of M/P ratio.

Since the 1 M formulation generates numerous instabilities, manifested as white efflorescences and volumetric changes, a new formulation is to be selected by increasing the M/P ratio. At high M/P ratios, there is a significant improvement in the mechanical properties of the MKPC matrices. However, an increase in the pore pH associated with a significant decrease in the main ions in the pore solution results in low chemical stability.

Therefore, based on the results presented in section 4.2, an M/P ratio between 1M and 2M is chosen. This ratio allows maintaining high physical stability and optimal pH values within the passivity range for long-term immobilisation of radioactive Al.

Table 38 summarises the main conclusions obtained from the CSIC studies in order to evaluate the effect of the M/P ratio on the stability of MKPC matrices for long-term Al immobilisation.

Table 38. Main conclusions obtained in the evaluation of M/P ratio on MKPC stability.

Effect M/P molar ratio		1M	2M	3M
		<i>100%RH</i>	<i>100%RH</i>	<i>100%RH</i>
Property	Mechanical strength	Low (8.6 Mpa) Efflorescence + crack	High (30 Mpa) No instabilities	High (25 Mpa) No instabilities
	Pore structure	Porosity (10%) Less Capillary pores	Porosity (\approx 11%) Capillary pores	High porosity (\approx 12%) High capillary pores
	Mineral phases	Less MgO residual Main K-struvite	High MgO residual Main K-struvite	High MgO residual Main K-struvite
	Pore pH	pH neutral (\approx 8)	High pH (\approx 9.5)	High pH (\approx 10.5)
	Pore ion content	High initial P content Pht. efflorescences Ions decrease	Lower P content Ions decrease Complete reaction	Lower P content Ions decrease Complete reaction

3 Low-cost magnesium phosphate cements

3.1 CNRS and ORANO: developing a low-cost magnesium phosphate cement formulation for nuclear waste stabilization

The primary objective of the study performed by CNRS and ORANO was to develop a low-cost formulation of MPC for the purpose of stabilizing aluminium waste on an industrial scale. This development involved the use of reactive MgO as the primary component and explored the use of thiosulphate, either alone or in combination with boric acid, as retarders, with the aim of identifying the optimal proportion of these additives within the LC-MPC mortar. The goal was to formulate and evaluate the optimized MPC formulations that possessed comparable characteristics to the reference MPC such as fluidity, workability, setting time, and mechanical strength. To achieve this, it was first needed to evaluate the impact of the retarder on setting time and mechanical strength. Additionally, XRD analysis were also performed to ensure the formation of hydrates similar to those found in the reference MPC formulation to ensure their binding role.

3.1.1 Materials and methods

3.1.1.1 Raw materials and mortars preparation

Two types of MPC mortars were prepared:

- MPC mortars with reactive MgO (called R1-R10) at different ratios of thiosulphate/cement, with or without adding 2 wt.% of boric acid.
- MPC mortars with DB MgO (D1-D10) at same ratios of retarder/cement as (R1-R10) samples for comparison.

D6 is the reference MPC formulation.

The design parameters for the mixes containing reactive magnesia were kept the same as those chosen for the initial formulation (Table 19).

Table 19. Grout mix general parameters and different retarder % of MPC samples with reactive MgO (R) and DB MgO (D)

Grout mix parameters		Mortar	Sodium thiosulphate (wt.% cement)	Borax (wt.% cement)
Mg/P (molar)	1	R1, D1	0	0
w/c	0.51	R2, D2	0.03	0
S _{sand/c}	1	R3, D3	0.05	0
S _{fly ash/c}	1	R4, D4	0.08	0
		R5, D5	0.1	0
		R6, D6	0	0.02
		R7, D7	0.03	0.02
		R8, D8	0.05	0.02
		R9, D9	0.08	0.02
		R10, D10	0.1	0.02

Raw materials used are listed in Table 20.

The mixing process is described as follows:

- Weigh and mix dry powders (MgO, KH₂PO₄, fly ash, sand) for 5 minutes in a Turbula.
- Dissolve the boric acid in distilled water, once the boric acid has been well dissolved, add the sodium thiosulphate to obtain mixing water.
- Add the premixed powders to the mixing water while stirring at a slow speed (100 rpm). Mix for 2 minutes at medium speed (600 rpm) and then 3 minutes at high speed (1200 rpm).

Table 20. Raw materials

Reagent	Reference, Supplier	Purity (wt.%)	Specific surface (m ² /g)
Reactive MgO	AK98VHR, Timab	97.3	90
DB MgO	Magchem 10CR, Martin Marietta Magnesia	98.3	0.9
KH ₂ PO ₄	ACS reagent, Sigma-Aldrich	99	
Fly ash	Class F-low Cao content, EDF CORDEMAIS		1.5
Boric acid	VWR	>99.5	
Sodium thiosulphate pentahydrate	ACS reagent, Sigma-Aldrich	99.5	
Sand	MIOS 0.1-1.2 mm, SIBELCO	SiO ₂ ≥98	

For compression strength tests, MPC mortars were cast in plastic moulds with dimensions of 4 × 4 × 4 cm³, demoulded after 24 h and then cured in plastic zipped bag at room temperature to the specified age.

3.1.1.2 Analytical methods

The setting time of MPC mortars was measured by automatic Vicat apparatus according to NF EN 196-3. The compressive strength was determined from triplicate 4 cm cube mortars after 7 days of curing using a Proviq 500kN automatic hydraulic machine. The solid samples after compression tests were ground to obtain a very fine powder. Diffractograms were acquired using a BRUKER diffractometer on previously ground samples. The acquisition was performed over a range from $2\theta = 5^\circ$ to $2\theta = 70^\circ$ with steps of 0.017° and a measurement time equivalent to 0.625 s per step. The obtained diffractograms were processed with the EVA software. Before being exploited, they underwent three pre-processing operations:

- The subtraction of the contribution of the K α 2 line of copper.
- The subtraction of the background.
- A very slight smoothing (smooth factor = 0.05).

Quantitative analysis was performed using the Rietveld method with the MAUD software.

3.1.2 Results

3.1.2.1 Some preliminary considerations

There are several grades of magnesium oxide, as a function of the calcination temperature. Magnesite ores are calcined at temperatures varying between 600 and 1400°C, resulting in MgO

with different reactivities. Hard (dead) and medium burnt MgO reacts slowly and incompletely with available water to form $\text{Mg}(\text{OH})_2$, while soft burnt MgO reacts fast and completely. There is a direct link between the sintering temperature, and the specific surface of the end-product, as shown in Table 21. Of course, higher sintering temperatures lead to higher prices for the MgO.

Table 21. Effect of calcination temperature on the surface area and reactivity of industrially obtained MgO [19].

Calcination temperature [°C]	Specific surface area [m^2/g]
650	17.40
800	14.62
1000	7.92
1200	2.13
1400	0.44

The link between surface area and early age properties is straightforward: the higher it is, the faster the reaction takes place and setting time, hydration heat and fluidity are heavily degraded.

There is an important difference of specific surface between reactive and dead burned magnesia that were used for the present study, of a factor equal to 100. Soft burnt magnesia reacts very quickly, presents a highly exothermic reaction with a flash set, which does not allow the industrial use.

The design parameters for the mixes containing reactive magnesia were kept the same as those chosen for the initial formulation (see Table 19). This was made for comparison purposes. However, reactive magnesia occupies a higher volume than dead burned magnesia as shown in Figure 31.



Figure 31. Equal mass of reactive MgO and DB MgO.

It should be noted that there is a possibility of further optimization of the formulation by reducing the overall volume of cement used in the mix, and thus lowering the prices per cubic meter. It is already known that the reaction between DB MgO and KH_2PO_4 is not complete even for low Mg/P ratios. As found by Qiao [20], only 41% reacted MgO is found in the microstructure for Mg/P = 2 (21% for Mg/P = 4 and 8.5% for Mg/P = 10). Even though MgO and KH_2PO_4 are supposed to present a stoichiometric reaction, this is not the case, as the mix will set, and non-reacted anhydrous MgO and KH_2PO_4 will remain in the matrix. This has several drawbacks:

- Seen the high prices for both MgO and KH_2PO_4 , total hydration should be aimed. K-struvite, the hydration product, will be the cement paste that links together the stiff elements present in the mix, such as sand and fly ash.

- If anhydrous MgO can bring some strength to the matrix, this is not the case for highly soluble KH_2PO_4 ; at a molar ratio Mg/P equal to 1 for a cement paste (aggregates not included), the total volume occupied by KH_2PO_4 is of 37% (Figure 32). If all MgO does not react (which seems to be the case) an important volume of high price reagent will remain in the matrix, with no utility for the properties of the hardened paste.
- Moreover, the presence of non-reacted KH_2PO_4 could affect durability of the matrix. Previous studies have shown that for low Mg/P ratios efflorescence is observed as well as swelling and decrease in mechanical strength of the samples [21]. This was linked to the presence of unreacted phosphates in the porosity of the matrix, especially in presence of water (Figure 33).

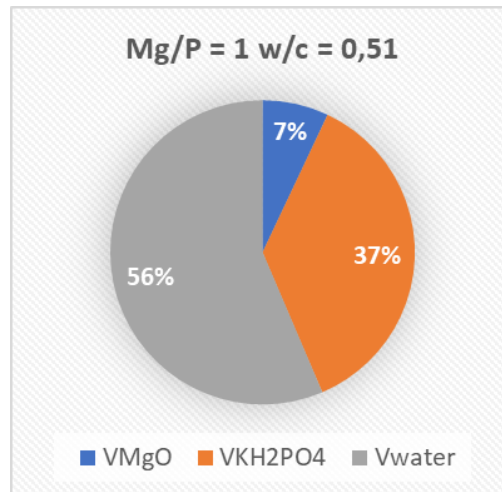


Figure 32. Volume phases for a cement paste (Mg/P = 1, w/c = 0.51).

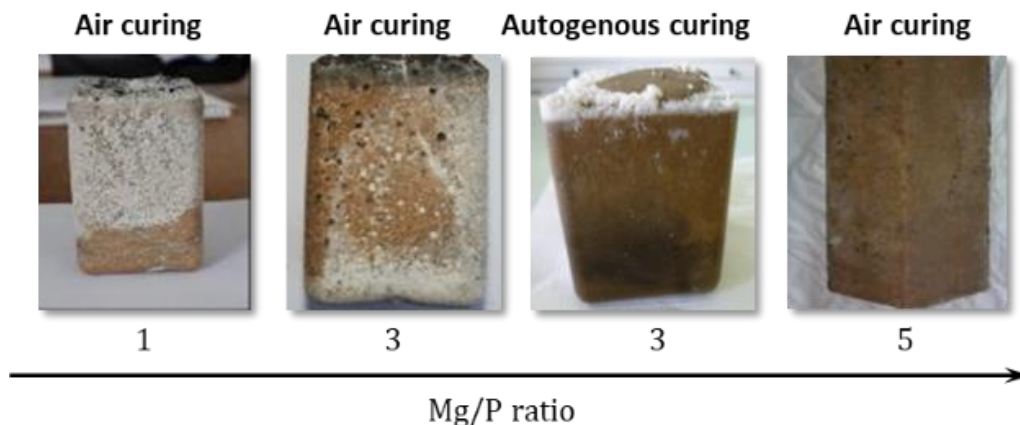


Figure 33. Efflorescence observed for different samples function of Mg/P ratio (w/c = 0.2) [21].

Using a reactive magnesia could have some advantages:

- Having a higher specific surface will enhance the degree of hydration and lower the anhydrous part remaining in the microstructure.
- From a durability point of view, the absence of KH_2PO_4 could avoid efflorescence and dimensional instability of the samples.
- The use of reactive magnesia can also lower the overall price of the material.

However, the use of reactive magnesia is not possible unless proper retarders are used. Classic retarders like borax are inefficient when dealing with reactive MgO. Previous work has shown that an efficient retarder for reactive magnesia could be sodium thiosulphate [22]. This approach was proven effective in delaying the hydration reaction of reactive MgO, thus providing sufficient time for industrial cement applications. Indeed, Figure 34 illustrates that the use of borax is ineffective, whereas thiosulphate has the capability to mitigate the rapid setting time observed in MPC prepared with reactive MgO.

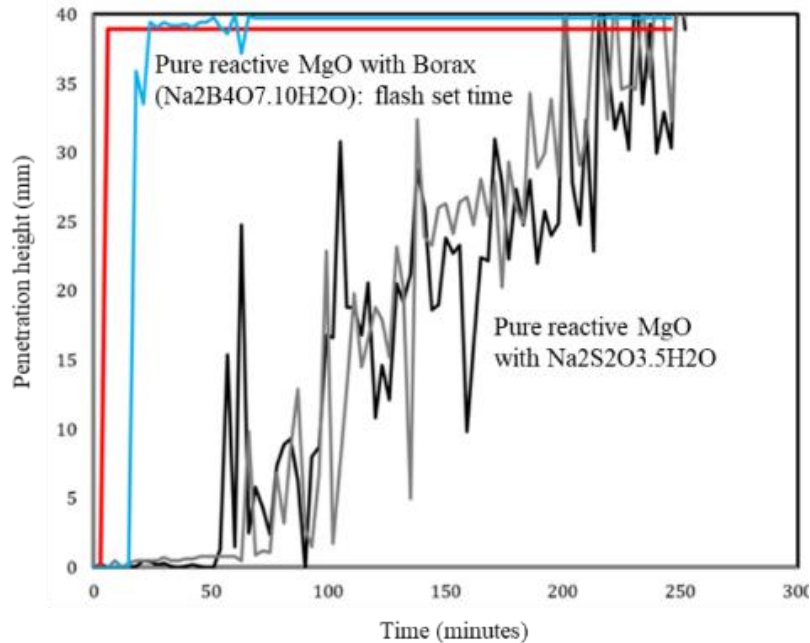


Figure 34. Comparison between setting time of reactive MgO retarded with borax and sodium thiosulphate [22].

The present experimental campaign aims to investigate the potential use of sodium thiosulphate as a retarder when reactive magnesia replaces dead burned magnesia in the initial mix.

3.1.2.2 Experimental results

For samples using reactive MgO, mixing was impossible when 2wt.% boric acid was used alone as retarder (Figure 35). Loss of fluidity is due to the much higher specific surface of reactive MgO compared to DB MgO and boric acid is not an efficient retarder in this case. The mixture was too reactive, and the setting was too fast. Good fluidity of the mixture was found when thiosulphate was added as retarder. It was observed that fluidity increased with the concentration of thiosulphate. When used alone as retarder, at least 5wt.% of thiosulphate is required to have good fluidity. However, in presence of 2wt.% of boric acid, good workability can be achieved with less than 5wt.% thiosulphate. With DB MgO, the fluidity and workability of samples were good under all conditions: with or without boric acid and with different thiosulphate contents.

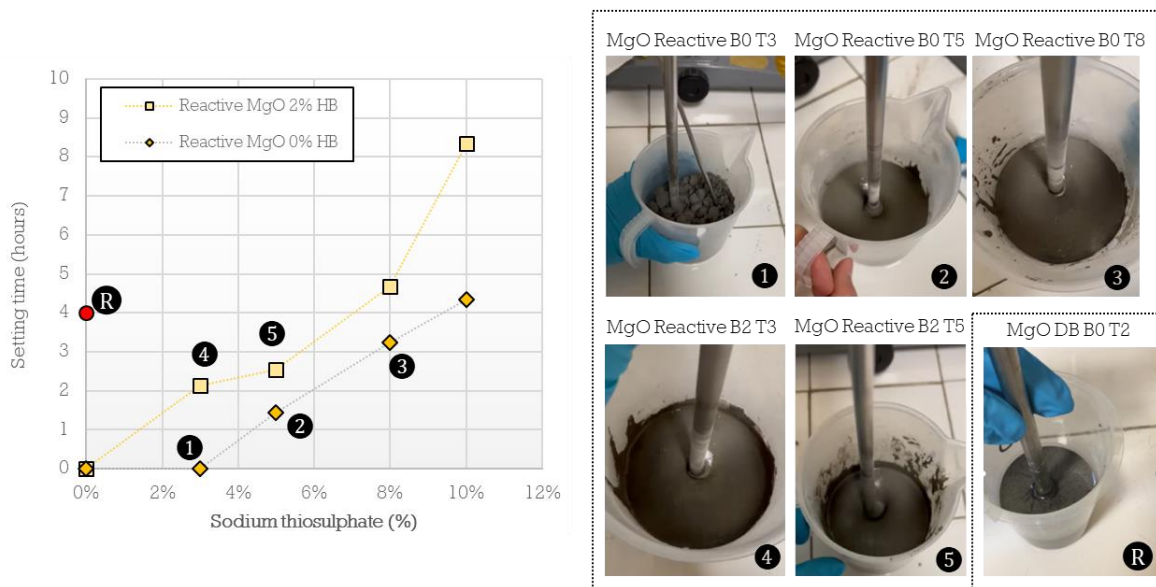


Figure 35. (left) Final setting time for reactive magnesia mixes with and without boric acid, function of sodium thiosulphate wt.% added (dot in red represents the reference mix, with dead burned MgO) and (right) mixing tests.

In what concerns setting time, the results were coherent with previous observations concerning the retard effect of sodium thiosulphate in the mix with reactive MgO. The addition of sodium thiosulphate allowed, in the absence of boric acid, to delay the setting of mortar (see Figure 35). However, in absence of boric acid, the minimum content of sodium thiosulphate is of 7% for a setting time of about an hour and a half. Results were significantly better when 2wt.% of boric acid was used. For 2wt.% of boric acid and 3wt.% of sodium thiosulphate, setting time exceeded 2 hours, which was a good result especially considering that even with significantly higher percentages of boric acid alone, reactive magnesia still exhibited flash set. The reference formulation, with dead burned magnesia and 2wt.% boric acid content the setting time was around 4 hours. This was obtained for reactive magnesia for 2wt.% of boric acid and 8wt.% of sodium thiosulphate.

However, it should be noted that the reactive magnesia mix should be optimized in terms of initial mass of MgO (and consequently of KH_2PO_4) in the composition. To ensure a more accurate comparison, it would be preferable to design the mix at a consistent final volume of hydrates over a constant initial mass of cement. However, this aspect will be investigated in subsequent phases of the study, as the initial phase was intended to establish the parameters for future experimental campaigns.

Sodium thiosulphate was equally tested on dead burned magnesia mixes, and results are shown in Figure 36. For mortars using MgO DB, in presence of boric acid, the addition of thiosulphate increased the setting time starting from 5wt.% content. When the content of thiosulphate ≥ 8 wt.%, setting time of more than 13 hours was observed. In the absence of boric acid, a higher quantity of sodium thiosulphate was required to achieve the same setting time as the reference grout. It can be considered that in both cases, the retarding effect worked better when combining thiosulphate and 2wt.% boric acid.

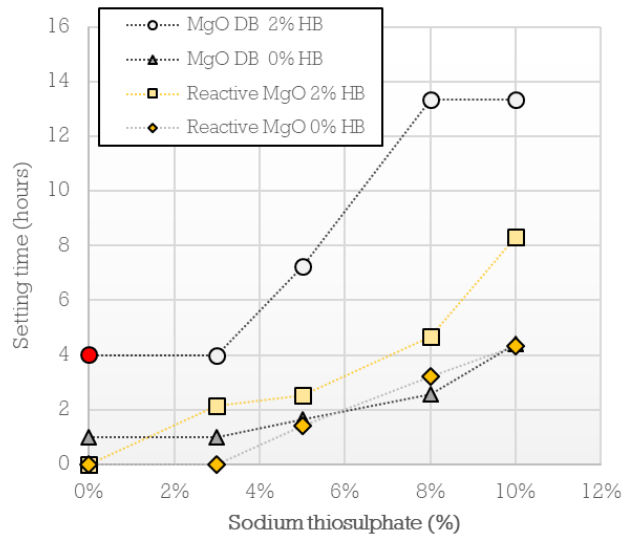


Figure 36. Final setting time for dead burned and comparison with reactive magnesia mixes with and without boric acid, function of sodium thiosulphate wt.% added (dot in red represents the reference mix, with dead burned MgO).

A simple method for measuring temperature, for preliminary comparison, was implemented. Five minutes after mixing, temperature was measured by a probe immersed in the mixture, and results are shown in Figure 37. Higher temperatures were recorded for samples containing reactive MgO (65 °C) compared to those prepared with DB MgO (30 °C). Again, such results were expected because grout containing reactive MgO probably have a higher degree of hydration, starting from early age, as smaller particles are readily available.

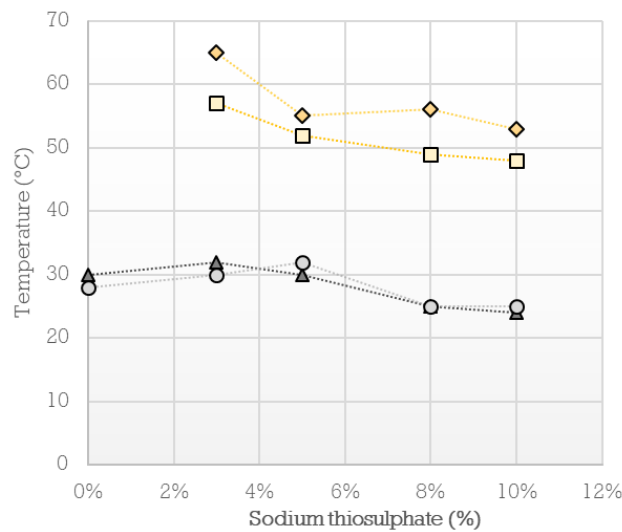


Figure 37. Temperatures measured for the mixes (same legend as for Figure 36).

Increasing the sodium thiosulphate content resulted in a temperature decrease by 8 to 10 °C for reactive magnesia. When 2wt.% of boric acid was present, slightly lower temperatures were measured, but they remained higher compared to dead burned magnesia grouts.

Compression tests were performed at 7 days. Figure 38 plots the effect of retarders on the compressive strength for reactive magnesia grouts. For samples with no or low content of sodium thiosulphate the samples could not be cast for the compression test. Samples with medium sodium thiosulphate content showed good compressive strength, either with or without boric acid. Best results were obtained for the sample with 2wt.% boric acid and 3wt.% of sodium thiosulphate. For higher content of sodium thiosulphate samples presented important efflorescence and important porosity (Figure 38). White precipitate was found, both, on the surface and in the inner part of mortar.

In addition, swelling and cracking were also observed for samples with ratio retarders/cement higher than 5wt.%. Samples without boric acid seemed to have a better behaviour. Obviously, the quantities of sodium thiosulphate were largely oversized in this campaign, as the objective was to study its effect on the microstructure.

REACTIVE MgO

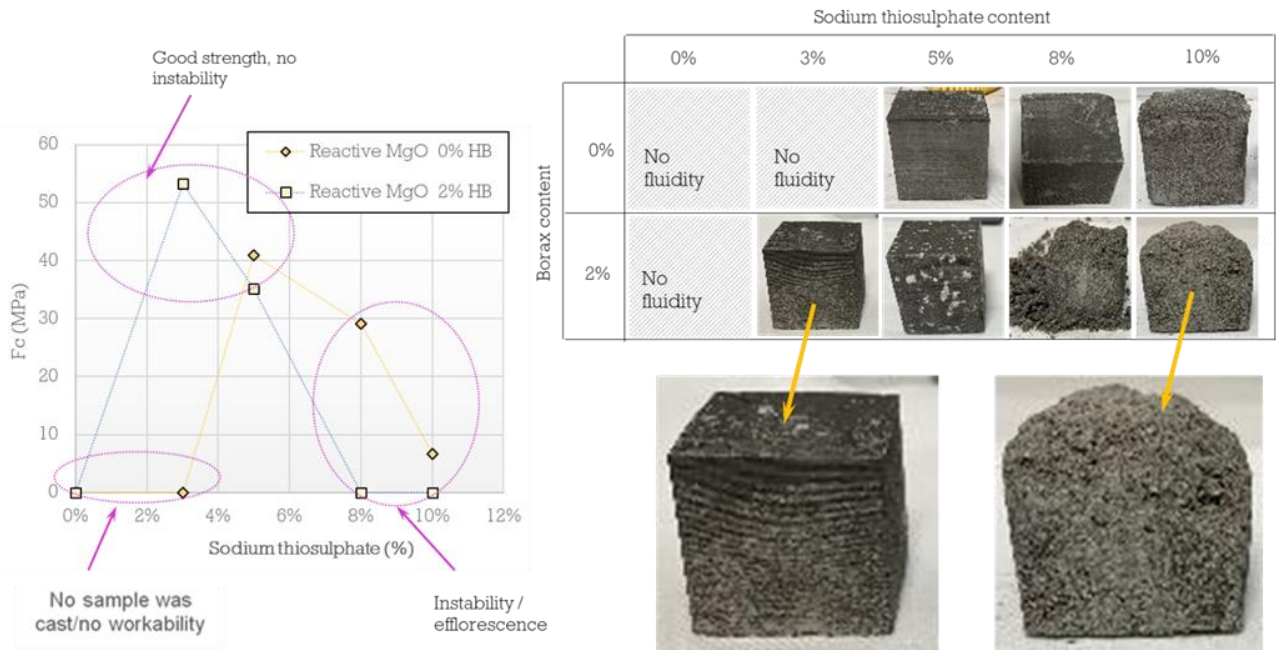


Figure 38. Compression strength for reactive magnesia samples function of retarder content at 7 days (left). Photos of samples (right).

Results for dead-burned magnesia cements are shown in Figure 39. All samples containing at least one retarder, whatever the content, presented efflorescence, which increased with the content of retarder. The reference sample had a lower compressive strength than reactive magnesia samples that properly worked.

DEAD BURNED MgO

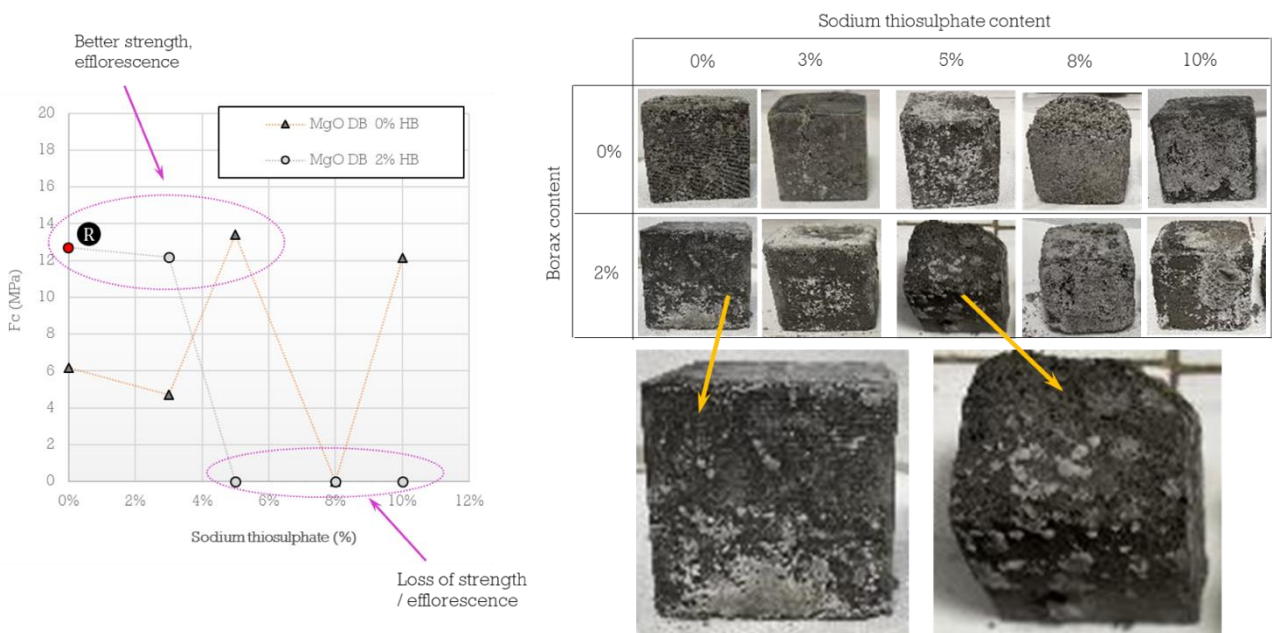


Figure 39. Compression strength for dead burned magnesia samples function of retarder content at 7 days (left) – red point shows the reference formulation. Photos of samples (right).

As previously discussed, (see Figure 33), efflorescence phenomenon was already described in the literature [21]. According to the authors, efflorescence is related to the amount of undissolved KH_2PO_4 in the cement and has negative impact on the overall properties of MPC. In our case samples presenting most efflorescence were:

- Samples containing dead burned magnesia: in this case MgO was not completely hydrated and non-reacted KH_2PO_4 would induce instability and efflorescence in the sample. One way to avoid this phenomenon is to increase the Mg/P ratio. It was shown that the higher Mg/P, the lower efflorescence was present in the matrix.
- Samples containing a high content of sodium thiosulphate: It seems that hydration was significantly hindered by the presence of thiosulphate in important quantities. In this case, unreacted MgO could remain in the matrix due to the inhibiting effect induced by the retarder, which leads to deleterious effects.

XRD diffractograms of mortar R3 and D3 are shown Figure 40, but the results are similar for the other formulations. Anhydrous remaining MgO was detected only in the samples that were prepared with dead-burned magnesia. Grouts prepared with reactive magnesia presented at most trace amounts of MgO (or none at all) meaning that the use of reactive MgO enhanced a complete reaction.

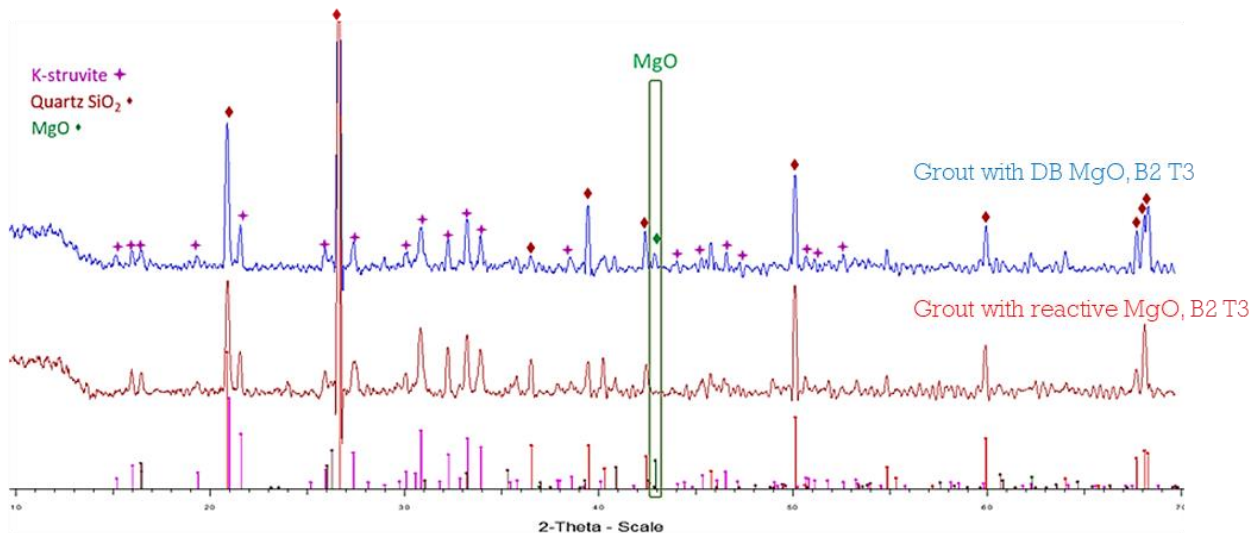


Figure 40. XRD diffractograms at 7 days curing.

Table 22 presents quantitative phase composition data obtained via XRD analysis of MPC mortars after 7 days curing period. For these samples, the only hydrated phase formed was K-struvite. Mullite and quartz are crystalline phases formed from fly ash and sand.

Table 22. Quantitative phase composition.

Sample	Weight content (%) of phase				Sample	Weight content (%) of phase			
	K-struvite	MgO	Quartz	Mullite		K-struvite	MgO	Quartz	Mullite
R1	No sample was cast				D1	Sample not analyzed			
R2	No sample was cast				D2	34.7	3.8	45.9	15.6
R3	50.1	0	40.4	9.5	D3	39.8	2.4	46.7	11.1
R4	42	1.2	50	6.8	D4	Sample not analyzed			
R5	30.3	1.3	55.7	12.6	D5	31.6	5.2	45.6	17.5
R6	No sample was cast				D6	32.2	3.5	52	12.3
R7	45	0	45	10	D7	42.9	3.2	44.9	9
R8	39	0.8	48.5	11.6	D8	29.2	3.9	56.7	10.2
R9	42.5	1.2	50.4	10.2	D9	10.2	13.6	52.5	23.6
R10	35.9	1.8	52.8	9.6	D10	9.5	14.4	52	24.1

From these results, we can observe some trends:

- K-struvite content: As the percentage of sodium thiosulphate in the retarder increases, the percentage of K-struvite generally decreases, indicating that higher sodium thiosulphate content (> 5wt.%) might hinder K-struvite formation. This observation remains consistent for both MPCs prepared with reactive and DB MgO. However, for the same amount of retarder, K-struvite content is higher in MPCs prepared with reactive magnesia.
- Unreacted MgO content: MPCs prepared with reactive MgO display low content, ranging from 0% to 1.8%, while their DB MgO display higher levels, ranging from 2.4% to 14.4%. These results indicate a more complete reaction with KH_2PO_4 in the presence of reactive MgO, in line with its larger specific surface area, which enhances reactivity.
- The percentage of quartz and mullite varies but doesn't show a clear trend. It's important to note that these observations are based on the provided data and may not capture all potential interactions between the components of the MPC mix. The specific mechanisms by which thiosulphate and other additives affect mineral composition in MPC would require further research and analysis.

Reactive and dead burned magnesia at 2wt.% boric acid and 3wt.% sodium thiosulphate have close amount of K-struvite in their composition. However, anhydrous MgO content is higher for dead burned magnesia grout (see Figure 41).

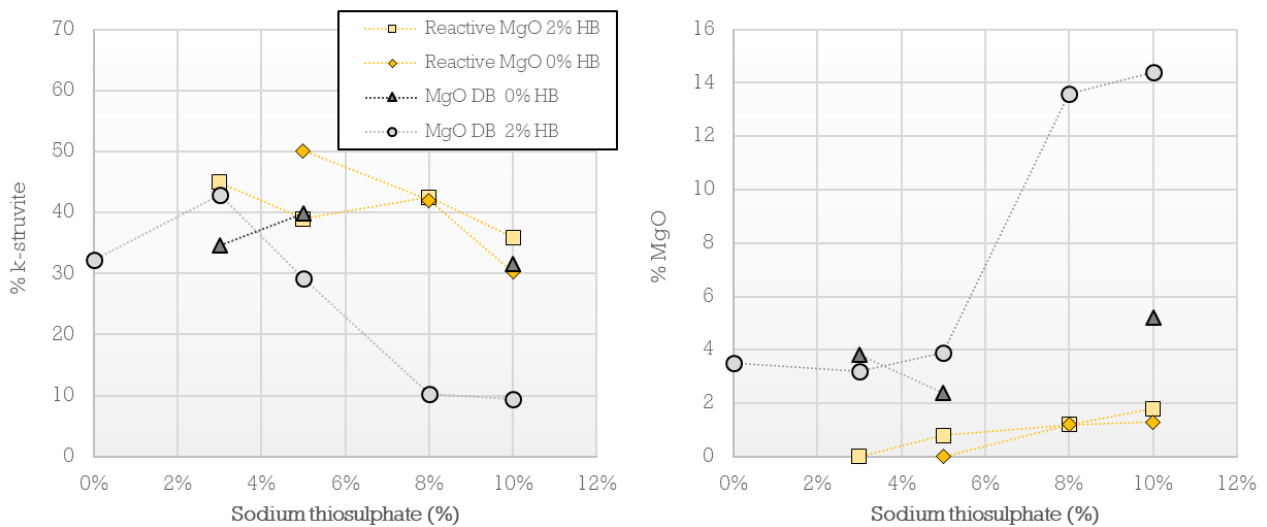


Figure 41. K-struvite and MgO percentage in the matrix function of sodium thiosulphate content at 7 days curing.

The samples were visually different, as for dead-burned magnesia sample efflorescence was present (Figure 42). The non-reacted KH_2PO_4 was thought to be responsible of differences in compressive strength that were observed.

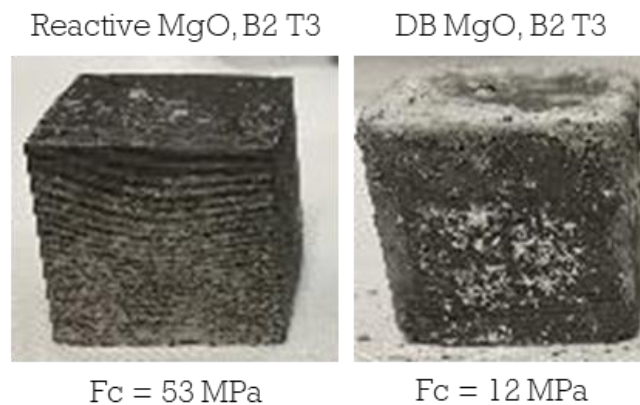


Figure 42. Reactive and dead-burned magnesia samples at 2wt.% boric acid and 3wt.% sodium thiosulphate.

3.1.3 Discussion and conclusions

The experimental results have shown that reactive magnesia can be used in a magnesium phosphate cement, providing that a specific retarder is used. The use of reactive magnesia can have several advantages:

- The high specific surface enhances hydration of MgO, which leads to a better use of the raw material. Whilst in dead-burned based grouts anhydrous MgO can be beneficial in terms of mechanical properties (as does anhydrous cement in OPC high performance concrete), the drawback is that it will also induce anhydrous KH_2PO_4 that leads to efflorescence, instability and low properties for the material. The high specific surface of reactive MgO allows a better consumption of KH_2PO_4 which is mostly linked to a higher hydration degree.
- An interesting point is that the best compressive strength – 53 MPa for a reactive magnesia grout with 2wt.% boric acid and 3wt.% thiosulphate – was obtained for a grout that has a water to cement ratio 0.5, and this should be emphasized as usually much lower compressive strength are obtained for low Mg/P ratios and high water to cement ratios. It was shown that Portland cement matrices seem to have a better behaviour with the increase of water to

cement ratio than other cements (see Figure 43) – this includes collected data on magnesium phosphate materials. The grout prepared with reactive magnesia, at 2wt.% of boric acid and 3wt.% sodium thiosulphate, presented very good compressive strength compared to other mixes at same water to cement value, and for a lower Mg/P ratio. Authors believe that enhanced hydration of this sample is the main factor that impacts the result.

- Less efflorescence and a better durability, as the depletion of KH_2PO_4 is enhanced by the total hydration of high specific surface of reactive MgO .

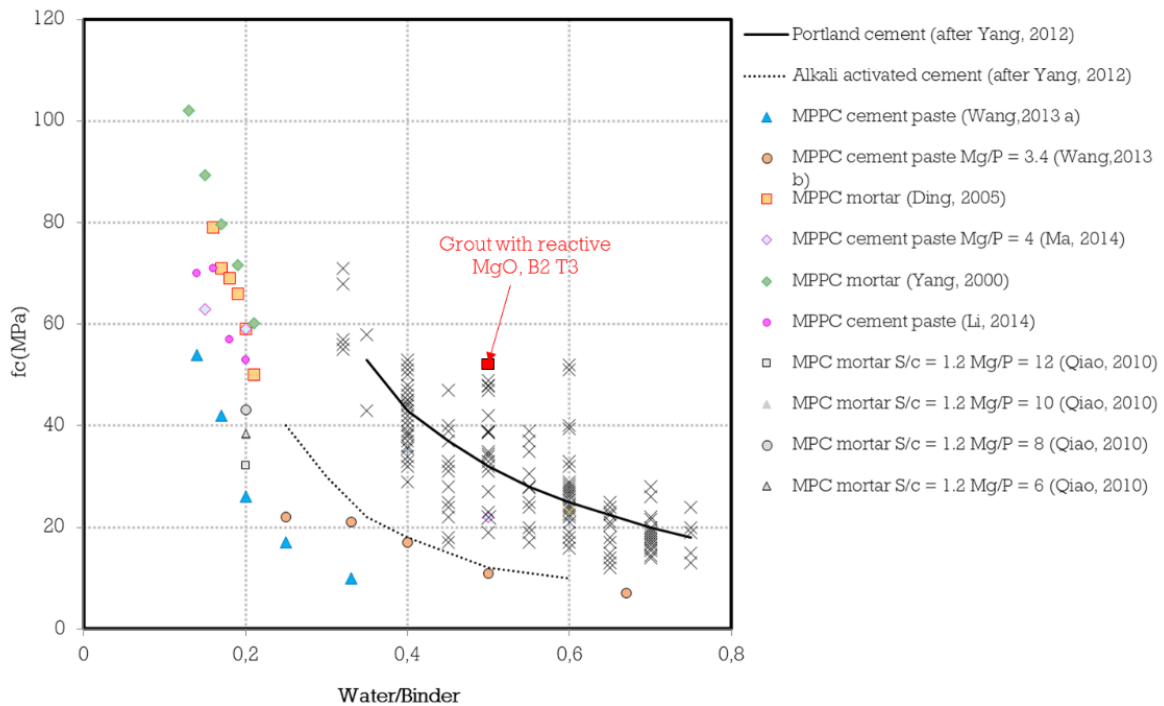


Figure 43. Effect of w/c ratio on the compressive strength of different cementitious materials (compressive strength at 28 days) [23–30].

There is still a considerable amount of work to be done to better understand the effect of the retarder on the hydration mechanisms. When a high amount of sodium thiosulphate is used, the microstructure becomes porous and swells. Obviously, a retarder is not supposed to be used at such high content, but the work will allow to understand its effects on the properties of the material and to assure that no durability issues overcome further on.

Using reactive MgO instead of DB MgO is also an interesting option to reduce overall price. Since reactive MgO has a higher specific surface, it is supposed to better complete reaction with KH_2PO_4 , leaving less anhydrous MgO in the material – fact confirmed by XRD analysis. Reactive MgO would make it possible to reduce the quantity of cement necessary and thus to increase the quantity of filler within the limit of keeping an acceptable mechanical resistance. Future works will aim to design formulations with equal K-struvite volume in the hydrated material compared to the reference formulation, rather than equal volume of initial cement (initial MgO + KH_2PO_4).

3.2 KIPT: effect of mineralogical additives on the structure, the physical and mechanical properties of MKPC

KIPT was engaged in the implementation of WP 4.6.2 “Cost optimization” and participated in an experimental campaign to change the filler of the reference formulation and was associated with the study of the influence of mineralogical additives on the structure and physico - mechanical properties of magnesium potassium phosphate cements (MKPCs). The main objective of task 4.6.2 was to study the properties of MKPC materials using blast furnace slag (BFS) as filler along with fly ash

(FA) for a reference formulation. Considering that BFS, along with FA, is a widely available and inexpensive material at metallurgical plants in Ukraine, the use of BFS as mineral additives in the production of MKPC compounds is very promising. KIPT research activity was related to work on MKPC filler composition instead of/in addition to FA for reference formulation in accordance with the guidelines presented in Figure 44.

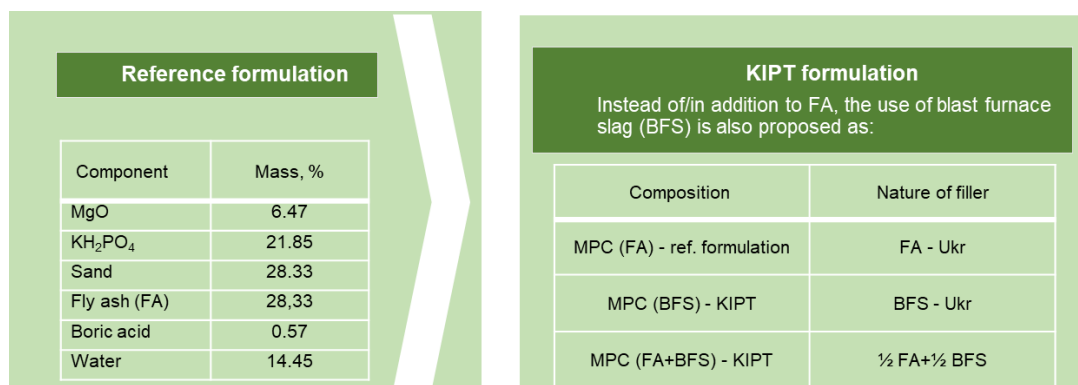


Figure 44. KIPT approach to use of BFS in MKPC reference formulation.

3.2.1 Initial materials and sample preparation

The chemical composition of FA from the Burshtyn thermal power plant (Burshtyn, Ukraine) and BFS from the Mariupol metallurgical plant (Mariupol, Ukraine) are shown in Table 23.

Table 23. Chemical composition of the fly ash and blast furnace slag.

Industrial waste	Weight content, wt.%										
	SiO ₂	Al ₂ O ₃	Fe ₂ O ₃	CaO	MgO	SO ₃	C	MnO	TiO ₂	Na ₂ O +K ₂ O	Other
FA	46.12	18.00	22.17	4.09	1.46	0.21	2.5	0.14	1.78	2.10	1.43
BFS	38.20	4.60	1.65	48.5	4.3	–	–	0.81	–	0.82	1.12

The necessary initial powder components had the following size characteristics:

calcined magnesium oxide (MgO > 97 wt.%), particle size: < 200 μm; potassium dihydrogen phosphate (KH₂PO₄ > 98 wt.%), < 630 μm; sand (SiO₂ > 99.3 wt.%), < 400 μm; FA < 400 μm; BFS < 630 μm.

The main phases of FA were quartz SiO₂ and millite Al₆Si₂O₁₃, and of BFS - akermanite Ca₂MgSi₂O₇, wollastonite CaSiO₃, calcium silicate Ca₂SiO₄, magnesium aluminum spinel MgAl₂O₄ and quartz SiO₂.

In accordance with the proposed recipe, samples of MKPC were prepared, differing in filler: FA, BFS and (½ FA + ½ BFS), called (MKPC-FA), (MKPK-BFS) and (MKPK-FA-BFS), respectively. Raw materials of Ukrainian origin were used as starting materials. Samples, were prepared by mixing the dry powders MgO, KH₂PO₄, sand and filler in lab grinding mill machine Fritch: single pulverising porcelain bowl of 200 g capacity, Ø2.0 cm aluminum oxide balls, speed 150 rpm, mixing time 10 minutes. Next, boric acid H₃BO₃, as a reaction retarder, was dissolved in distilled water, and a mixture of dry components was added to this solution and mixed with a mechanical stirrer in a 250 ml polypropylene can for 5 minutes until a homogeneous paste was obtained. Then, the paste was poured into polypropylene molds and covered with polyethylene film to prevent rapid drying. Samples were demoded after 1 day and kept for at least 28 days to cure at indoor ambient conditions. Figure 45 presents obtained MKPC samples after 28 days of curing.



Figure 45. Samples (3x3x3 cm) of MKPC-FA, MKPC-BFS and MKPC-FA-BFS (from left to right).

3.2.2 XRD analysis of MKPC samples

The crystalline phase composition of all obtained MKPC based samples cured for 28 days was studied by XRD - X-ray diffraction analysis (device DRON-4-07 in copper Cu-K α radiation using a Ni selective absorbing filter). Qualitative crystalline phase analysis was carried out by the angular position and integrated intensity of diffraction peaks using the database of crystallographic compounds ICDD PDF-2. Quantitative analysis was carried out by the Rietveld method using the MAUD software. The method is based on fitting the theoretically calculated diffractogram to the experimental one.

Using XRD analysis, it was found that the main phase of MKPC-FA compound is K-struvite $\text{MgKPO}_4 \cdot 6\text{H}_2\text{O}$ (Figure 46a) and its content, determined by the Rietveld method, was 58 wt.%. To a lesser extent, quartz SiO_2 (38 wt.%) and mullite $\text{Al}_6\text{Si}_2\text{O}_{13}$ (4 wt.%) are represented. The lattice parameters of the $\text{MgKPO}_4 \cdot 6\text{H}_2\text{O}$ phase are following: $a = 6.875\text{\AA}$; $b = 6.160\text{\AA}$; $c = 11.083\text{\AA}$.

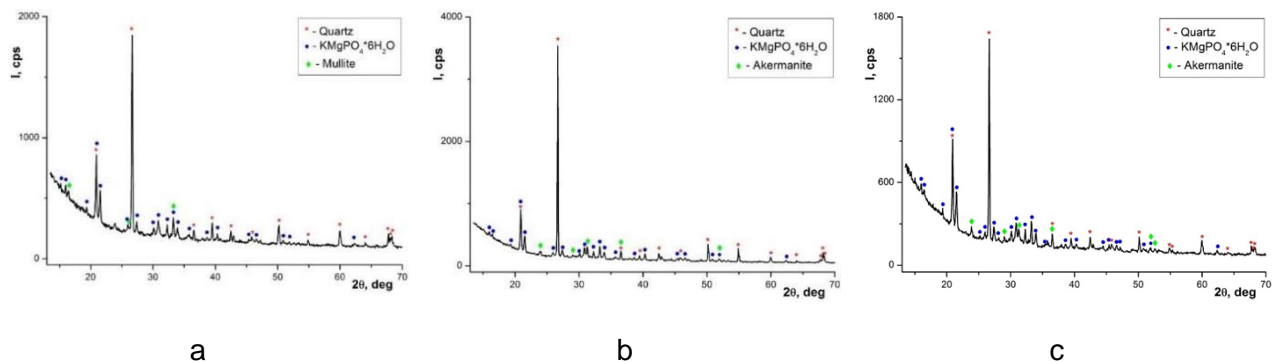


Figure 46. Diffraction patterns for MKPC samples: a – MKPC-FA, b – MKPC-BFS, c – MKPC-FA-BFS.

Three phases were identified in the MKPC-BFS sample (Figure 46b): K-struvite $\text{MgKPO}_4 \cdot 6\text{H}_2\text{O}$ (60 wt.%), quartz SiO_2 (31 wt.%) and akermanite $\text{Ca}_2\text{MgSi}_2\text{O}_7$ (9 wt.%). The crystalline lattice parameters of the K-struvite phase for this compound are following: $a = 6.897\text{\AA}$; $b = 6.188\text{\AA}$; $c = 11.109\text{\AA}$. It should be noted that the lattice parameters of the synthesized K-struvite, as the main phase of MKPC-BFS compound, are increased compared to K-struvite in MKPC-FA. This indicates that, during the preparation of the MKPC-BFS sample, a more significant dissolution of the BFS particles occurs with the release of various elements included in the K-struvite crystal structure with an increase in its lattice parameters.

Three phases were identified in MKPC-FA-BFS sample (Figure 46c): K-struvite $\text{MgKPO}_4 \cdot 6\text{H}_2\text{O}$ (59 wt.%), quartz SiO_2 (34 wt.%) and akermanite $\text{Ca}_2\text{MgSi}_2\text{O}_7$ (7 wt.%). The lattice parameters of the $\text{MgKPO}_4 \cdot 6\text{H}_2\text{O}$ phase are following: $a = 6.874\text{\AA}$; $b = 6.158\text{\AA}$; $c = 11.091\text{\AA}$.

Processing of XRD analysis data using the MAUD program for samples of MKPC-FA, MKPC-BFS, and MKPC-FA-BFS shows that the content of K-struvite in all three cements is almost the same and is equal to 58-60 wt.%. In MKPC-BFS compound, the content of K-struvite is slightly higher than in

other cements. Also, MKPC-BFS is characterized by the presence of K-struvite with the highest crystal lattice parameters in comparison with both MKPC-FA and MKPC-FA-BFS.

3.2.3 Microstructural study of MKPC samples

The study of the microstructure of MKPC based samples was carried out on a JSM-7001F scanning electron microscope (JEOL, Japan) equipped with a thermal field electron gun. The chemical composition of the samples was determined by EDX analysis using an INCA Penta FETx3 analyzer (Oxford Instruments, UK). The typical microstructures of MKPC based samples observed with SEM were subsequently scanned with EDX and elemental statistics were compiled in tables.

MKPC-FA

Figure 47a shows a SEM image of the microstructure of MKPC-FA samples after 28 days of curing the paste.

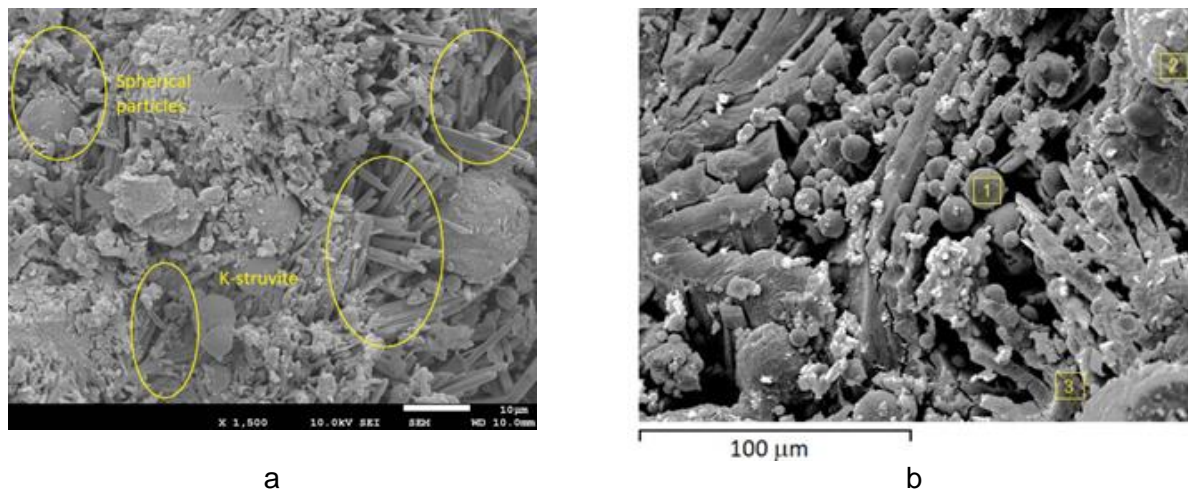


Figure 47. SEM image of the MKPC-FA microstructure.

The sample matrix contains K-struvite crystals in the form of a prism and needles. In addition, encapsulated initial spherical FA particles and reaction products are presented in the obtained product. Unreacted spherical FA particles are observed, which, according to [31,32], differ in chemical activity due to their chemical and mineralogical compositions, as well as in size.

For the EDX analysis, the region of the microstructure near the needle-like crystals of K-struvite was chosen and shown in Figure 47b. The elemental statistics are compiled in Table 24.

Table 24. Elemental statistics in the MKPC-FA compound.

Elements, wt. %	O	Mg	Al	Si	P	K	Ca	Ti	Fe	Total
Area 1	34.17	1.38	20.56	32.78	-	5.32	0.57	1.18	4.04	100.00
Area 2	44.45	4.24	-	8.57	2.62	9.12	0.58	-	30.42	100.00
Area 3	50.84	7.57	5.36	9.92	9.97	12.64	1.34	-	2.36	100.00

Spherical FA particles (Area 1 in Figure 47b) include following elements: mainly Si and, to a lesser extent, Al, Fe, K, Mg, Ti, Ca, and P is absent (Table 24). Therefore, it can be argued that such FA particles are not chemically active in the MKPC environment and are surrounded by needle-like K-struvite crystals and secondary reaction products. Some spherical FA particles, without calcium in their composition, did not react in an acidic environment, and voids form at the location of these particles. K-struvite crystals can grow in these voids.

On the contrary, another particle with shape differs from a spherical one, is characterized by increased chemical activity (Area 2 in Figure 47b). The increased activity of this particle is apparently

due to the fact that its composition contains the maximum amount of Fe (Table 24). This particle is probably a secondary product of the reaction between Ca, Al, Si, and Fe with P.

Wagh et al. [33] noted that calcium, which is represented by oxide, reacts in the same way as MgO, forms phosphate bonds, and promotes the formation of calcium-phosphate cements. It was also reported that Al and Si were incorporated into the MKPC matrix due to the dissolution of the aluminosilicate glassy fraction contained in the FA, which led to the formation of the potassium aluminosilicate phosphate phase **Error! Reference source not found.**]. Furthermore, there is an accumulation of a large number of prismatic K-struvite crystals (Area 3 in Figure 47b). These crystals contain small amounts of Al and Si as well. As can be seen, K-struvite crystals form in large pores or porous regions, which was also noted by Mo et al. [34].

MKPC-FA-BFS

Compared to MKPC-FA microstructure, the microstructure of MKPC-FA-BFS is more complex and denser (Figure 48a).

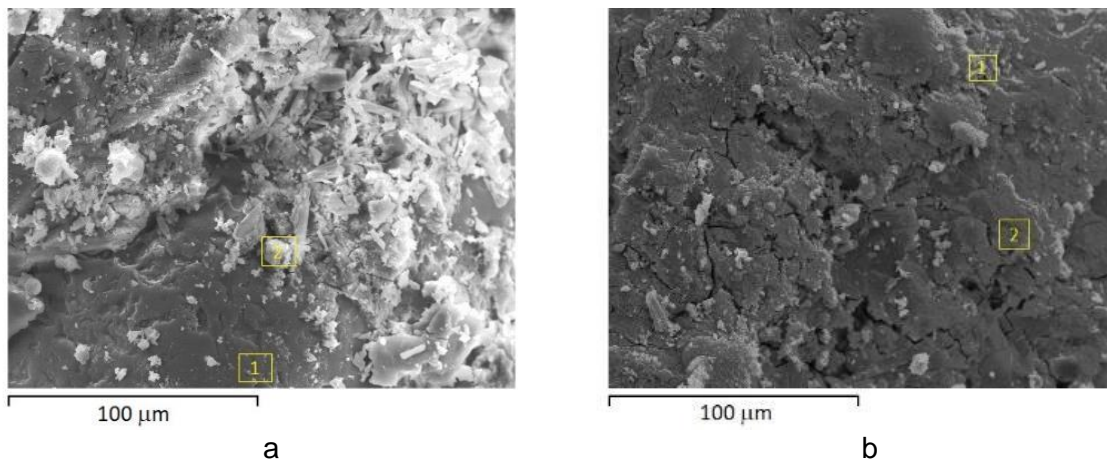


Figure 48. SEM image of the MKPC-FA-BFS (a) and MKPC-BFS (b) microstructure.

SEM/EDX analysis showed a uniform distribution of Mg, K and P, which confirms the formation of K-struvite throughout the MKPC-FA-BFS matrix. It can be seen the Area 1 (Figure 48a) corresponds to unreacted sand particle, the main component of which is quartz SiO_2 (see Table 25). Area 2 corresponds to K-struvite and secondary reaction products on the base of K, P, Mg, Si and Ca.

Table 25. Elemental statistics in the MKPC-FA-BFS matrix.

Elements, wt. %	O	Mg	Al	Si	P	K	Ca	Ti	Fe	Total
Area 1	36.95	0.64	0.1	59.53	-	2.37	0.41	-	-	100.00
Area 2	49.85	10.6	0.2	4.31	16.21	16.86	1.71	-	0.26	100.00

MKPC-BFS

The SEM image of the microstructure of the MKPC-BFS hardened sample after 28 days of curing the paste is shown in Figure 48b.

In general, MKPC-BFS samples have also a denser structure compared to MKPC-FA samples. The presence of microcracks is caused by dehydration of the sample in vacuum during conducting the SEM analysis.

The typical microstructure of MKPC-BFS sample observed with SEM (Figure 48b) was subsequently scanned with EDX and elemental statistics were compiled in Table 26. SEM/EDX analysis showed a uniform distribution of Mg, K and P, which confirms the formation of K-struvite $\text{MgKPO}_4 \cdot 6\text{H}_2\text{O}$ throughout the MKPC-BFS matrix.

Table 26. Elemental statistics in the MKPC-BFS compound.

Elements, wt.%	O	Mg	Al	Si	P	K	Ca	Ti	Fe	Total
Area 1	51.93	6.18	2.08	6.89	7.99	16.04	7.75	-	1.14	100.00
Area 2	45.54	8.10	3.47	7.24	12.59	18.80	1.74	-	2.52	100.00

It should be noted the presence of a large amount of potassium, which is located both areas in a wide (Table 26). A certain amount of potassium is involved in the synthesis of K-struvite, while another part is involved in the formation secondary products enriched by Si and Al. The formation of additional phases, including the secondary phase of potassium aluminosilicate phosphates, can increase the overall compaction and potentially increase the chemical resistance of MKPC [31]. It is easy to see that the Ca content in each of the selected areas differs significantly (Table 25). Calcium is concentrated mainly in Area 1. This region is also enriched in Si. That is, calcium silicates are concentrated in this area, which partially reacted in the initial acidic medium.

As a result, it should be noted that samples of MKPC with the addition of FA as a filler are characterized by a slightly lower density compared to samples with the addition of BFS, namely, both MKPC-FA-BFS and MKPC-BFS. Some spherical FA particles, without calcium in their composition, did not react in an acidic environment, and voids form at the location of these particles. K-struvite crystals can grow in these voids.

In contrast to FA, BFS particles are characterized by increased reactivity in an acidic environment at the initial moment of MKPC formation. This is also evidenced by the absence in the composition of MKPC-BFS compound of most of the phases that were present in the original slag: wollastonite CaSiO_3 , calcium silicate Ca_2SiO_4 and magnesium-containing (MgAl_2O_4). Some elements of these phases are entered in the crystal structure of K-struvite, as indicated by the expansion of its crystal lattice parameters. The rest, apparently, became part of the formed secondary phases, which are involved in the process of production of a dense homogeneous MKPC structure with the addition of BFS. Due to the formation of a denser structure, MKPC-BFS samples show better compressive strength.

3.2.4 Study of mechanical properties

MKPC samples were tested for uniaxial compressive strength. During the tests, the brittle nature of the fracture of the samples was observed. The samples were split into three to five parts. The results of mechanical tests of MKPC samples are shown in Figure 49.



Figure 49. The compressive strength of MKPC based samples.

There is a tendency to increase the compressive strength when introduced BFS into the MKPC mixture. These samples show a maximum compressive strength after 28 days of curing equal to 21.6 MPa. The increase in compressive strength of samples with the addition of granulated BFS compared to samples with the addition of FA was also observed by Gardner et al. [31]. Samples with FA are characterized by the lowest strength values for all test periods - after 7, 14 and 28 days of hardening.

3.2.5 Samples with high content of BFS

Previously, the KIPT formulation used a mixture of (50 wt.% FA + 50 wt.% BFS) as a filler. In addition, a series of experiments were carried out using a higher content of BFS. The samples were tested for mechanical strength after 7, 14 and 28 days of curing. The physico-mechanical characteristics of the obtained samples are presented in Figure 50 (left table).

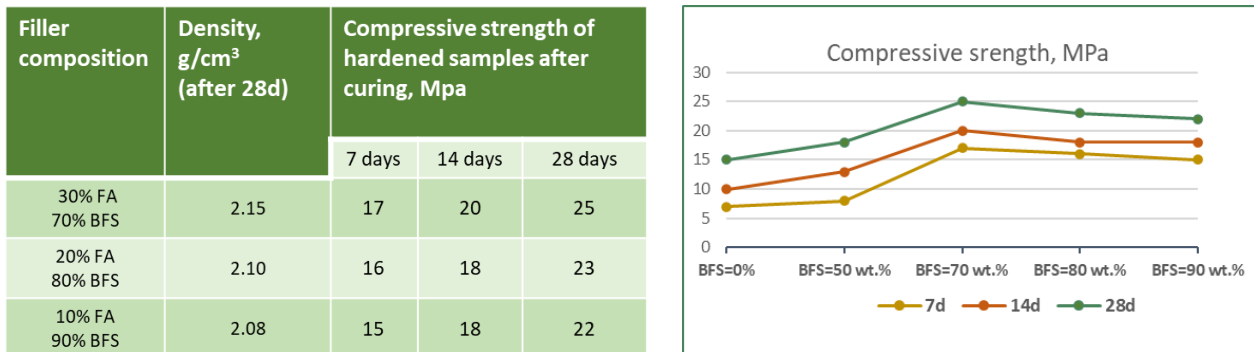


Figure 50. Physico-mechanical characteristics of the BFS containing MPC samples.

Considering the previously obtained mechanical characteristics for samples according to the KIPT formulation with a filler in the form of a mixture (FA+BFS), Figure 50 (right graph) also shows the dependence of the strength of the samples on the BFS content. Measurements have shown that the maximum mechanical strength is possessed by MPC-FA-BFS samples containing 70 wt.% BFS in a mixture of filler (FA + BFS).

3.2.6 Tests with reactive and hard burnt MgO

Experimental studies were carried out to study the process of obtaining MKPCs (with various fillers according to KIPT formulation) if less expensive in price reactive (R) MgO could be used instead of hard burnt (HB) magnesia. As before, raw materials of Ukrainian origin, including FA and BFS, were used in the experiments. FA was used as filler, according to reference formulation, as well as BFS and (½ FA+½ BFS), according to KIPT approach. When obtaining samples, the reaction temperature for the synthesis of phosphates was measured in time and the results are presented in Figure 51.

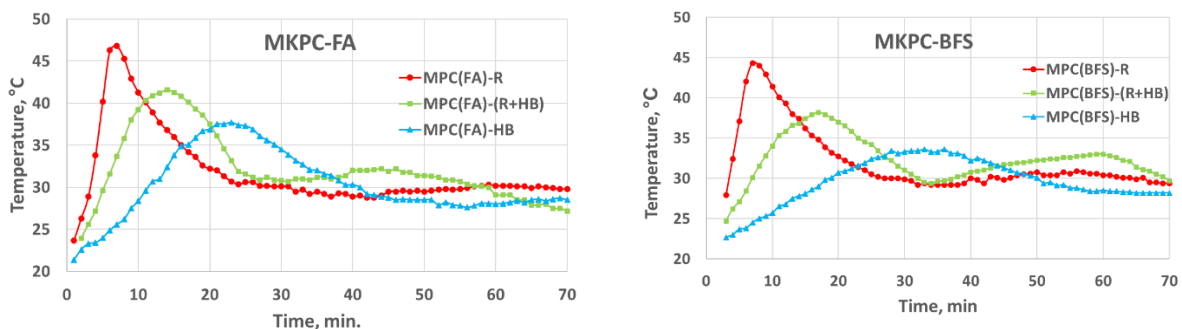


Figure 51. Temperature measurements for MPC sample containing FA (use of MgO as reactive, as well as mix of reactive and hard-burnt, and hard-burnt only).

It has been shown that the magnesium - potassium phosphate formation reaction using reactive MgO occurs significantly faster compared to hard-burnt MgO, regardless of the filler composition: 9 min and about 30 min, respectively, which is clearly shown in Figure 51 for MKPC samples with FA and BFS.

Since blast furnace slag is quite often used to produce MKPC along with fly ash, experiments have been conducted with their use for reactive and hard-burnt MgO. Samples were prepared according to the reference formulation, as well as according to the reference formulation in which BFS was used instead of FA. The physical and mechanical properties of the obtained samples are presented in Table 27.

Table 27. Physico-mechanical characteristics of the MKPC samples containing FA and BFS.

Magnesia	Density, g/cm ³		Compressive strength, MPa	
	FA	BFS	FA	BFS
MgO (HB)	2.0	2.2	19.2	21.5
MgO (½ R+½ HB)	1.9	2.0	18.4	20.1
MgO (R)	1.75	1.9	17.0	17.6

Despite the slight decrease in the compressive strength of the samples with reactive MgO compared to hard burnt one, use of reactive MgO makes it possible to produce the product and to save the quantity of filler within the limit of keeping an acceptable durability property. The use of slag instead of fly ash made it possible to obtain phosphate samples with slightly better mechanical strength characteristics, both for the reaction MgO and the hard burned one.

3.2.7 Conclusions

As part of task 4.6.2 “Cost optimization”, KIPT participated in an experimental campaign to change the filler of the reference formulation and was associated with the study of the influence of mineralogical additives on the properties of MKPCs.

It has been established that when the filler FA is replaced by BFS, the content of K-struvite practically does not change.

The samples were tested for mechanical strength. It is shown that MKPC-BFS samples demonstrate the highest compressive strength compared to MKPC-FA and MKPC-FA-BFS samples.

The increased strength values are explained by the presence of a denser structure of the MKPC-BFS samples, in contrast to the structure of the MKPC-FA and MKPC-FA-BFS samples.

Obtaining a denser structure of MKPC-BFS samples is due to the fact that BFS powder particles are more reactive compared to FA particles.

Experiments on the use of reactive MgO instead of hard-burnt MgO, when preparing MKPC samples according to the KIPT formulation, revealed that the phosphate synthesis reaction proceeded too quickly.

Of course, less expensive in price reactive MgO makes it possible to reduce the price of the final product of keeping an acceptable durability property. At the same time, the problem of fast reaction time of phosphate formation, must be considered when developing industrial - scale technologies.

4 Dissemination

A list of publications, participation in conferences and workshops derived from the work performed in PREDIS under subtask 4.6 are listed below:

- Publications in scientific journals:

Dieguez, M., Ruiz, A. I., Cuevas, J., Alonso, M. C., García-Lodeiro, I. and Fernández, R. (2023). Evaluation of fillers for magnesium potassium phosphate cement (MKPC) for the encapsulation of low and intermediate level metallic radioactive wastes. *Materials*, 16 (2), 679.

Fernández-García, C., Alonso, M. C., Bastidas, J. M., García-Lodeiro, I. and Fernández, R. (2024). MgO/KH₂PO₄ and Curing Moisture Content in MKPC Matrices to Optimize the Immobilization of Pure Al and Al-Mg Alloys. *Materials*, 17(6), 1263. <https://doi.org/10.3390/ma17061263>.

Fernández-García, C., Padilla-Encinas, P., Fernández, R. and Alonso, M. C. (2024). Interaction of aluminium alloys with MKPC and OPC blended cements on the metal – matrix interface. *Applied Geochemistry Journal* (under review).

Padilla-Encinas, P., Dieguez, M., Cuevas, J., Ruiz, A. I. and Fernández, R. (2024). The Influence of the Magnesium-to-Phosphate Molar Ratio on Magnesium Potassium Phosphate Cement Properties Using Either Wollastonite or Volcanic Ash as Fillers. *Minerals*, 14, (1), 103.

Perona, R., Fernández-García, C., García-Lodeiro, I., Criado, M., Bastidas, J. M. and Alonso, M. C. (2023). Corrosion behavior and immobilization of pure aluminum and Al-Mg alloy LLRW in magnesium potassium phosphate cements. *Journal of Nuclear Materials*, 582. <https://doi.org/10.1016/j.jnucmat.2023.154501>.

Sayenko S., Shkuropatenko V., Pylypenko O., Kholomieiev H., Karsim S., Zykova A. Production and Properties of Magnesium Potassium Phosphate Cements Containing Fly Ash and Metallurgical Slag Additives for Radioactive Waste Immobilization. *Nuclear and Radiation Safety (Ukrainian journal)* 2(98), 2023, 30-43, [https://doi.org/10.32918/nrs.2023.2\(98\).03](https://doi.org/10.32918/nrs.2023.2(98).03)

○ Presentations in conferences:

Fernández-García, C. and Alonso, M. C. Corrosion of aluminum alloy in simulated pore systems of magnesium phosphate cements for hydrogen inhibition. IV national congress of construction materials (CNMAT22). Abstracts book, ISBN: 978-84-09-38118-0. June 28 to July 1, 2022, Ciudad Real, Spain.

Fernández-García, C. and Alonso, M. C. Corrosion, and hydrogen evolution of Al/AlMg alloy in mortar of magnesium phosphate and Portland base binders. XLII national congress of RSEQ electrochemistry specialist group meeting (GERSEQ22). Abstracts book, ISBN: 978-84-09-42511-2. July 6-8, 2022, Santander, Spain.

Fernández-García, C. and Alonso, M. C. Physico-chemical stability of Magnesium Potassium Phosphate Cements (MKPC) for aluminium alloy immobilization. 48 Annual meeting of the Spanish Nuclear Society (SNE48). Abstracts book, ISBN: 978-84-090-01616-7. October 4-6, 2023, Toledo, Spain.

Fernández-García, C., Padilla-Encinas, P., Alonso, M. C. and Fernández, R. Interaction of Al alloys with MKPC and OPC based binders on the metal-matrix interface. 6th International Workshop on Mechanisms and Modelling of Waste / Cement Interactions (JCCW2023). Abstracts book. November 20-24, 2023, Prague, Check Republic.

Raúl Fernández, Inés García-Lodeiro, Mikel Dieguez, Ana Isabel Ruiz, María Cruz Alonso (2022). Towards the optimization of magnesium phosphate cements formulations for

reactive metals encapsulation. NUWCEM 2021 – International Symposium on Cement-Based Materials for Nuclear Wastes. France, Avignon – 2022, May 4-6.

Mikel Dieguez, Ana Isabel Ruiz, María Cruz Alonso, Inés García-Lodeiro, Raúl Fernández (2022). Effect of the volcanic ash from La Palma on the properties of magnesium phosphate cements (MPC). CNMAT2022. Spanish National Congress of Materials. Spain, Ciudad Real – 2022, June 28-July 1.

Lavinia Stefan, Kim Le, Davide Rodrigues, Sylvie Delpech, Céline Cannes. Developing a low-cost magnesium phosphate cement formulation for nuclear waste stabilization. 12th ACI/RILEM International conference on cementitious materials and alternative binders for sustainable binders. France, Toulouse – 2024, June 23-26.

Acknowledgments

This project has received funding from the European Union's Horizon 2020 research and innovation program for Nuclear Fission and Radiation Protection Research (Call NFRP-2019-2020) under grant agreement No. 945098 (PREDIS).

REFERENCES

- [1] F. Glasser, Application of inorganic cements to the conditioning and immobilisation of radioactive wastes, in: M.I. Ojovan (Ed.), *Handbook of Advanced Radioactive Waste Conditioning Technologies*, Woodhead Publishing, 2011: pp. 67–135. <https://doi.org/10.1533/9780857090959.1.67>.
- [2] M. Atkins, F.P. Glasser, Application of portland cement-based materials to radioactive waste immobilization, *Waste Management* 12 (1992) 105–131. [https://doi.org/10.1016/0956-053X\(92\)90044-J](https://doi.org/10.1016/0956-053X(92)90044-J).
- [3] M. Pourbaix, *Atlas of electrochemical equilibria in aqueous solutions*, 2nd Edition, National Association of Corrosion Engineers, Houston, Texas, USA, 1974.
- [4] C. Vargel, Chapter B.1 - The corrosion of aluminium, in: C. Vargel (Ed.), *Corrosion of Aluminium (Second Edition)*, Elsevier, Amsterdam, 2020: pp. 41–61. <https://doi.org/10.1016/B978-0-08-099925-8.00008-9>.
- [5] L.J. Gardner, C.L. Corkhill, S.A. Walling, J.E. Vigor, C.A. Murray, C.C. Tang, J.L. Provis, N.C. Hyatt, Early age hydration and application of blended magnesium potassium phosphate cements for reduced corrosion of reactive metals, *Cement and Concrete Research* 143 (2021) 106375. <https://doi.org/10.1016/j.cemconres.2021.106375>.
- [6] I. Odler, *Special Inorganic Cements*, 1st ed., CRC Press, London, 2000. <https://doi.org/10.1201/9781482271942>.
- [7] T. Sugama, L.E. Kukacka, Magnesium monophosphate cements derived from diammonium phosphate solutions, *Cement and Concrete Research* 13 (1983) 407–416.
- [8] H. Lahalle, C. Cau Dit Coumes, C. Mercier, D. Lambertin, C. Cannes, S. Delpech, S. Gauffinet, Influence of the w/c ratio on the hydration process of a magnesium phosphate cement and on its retardation by boric acid, *Cement and Concrete Research* 109 (2018) 159–174. <https://doi.org/10.1016/j.cemconres.2018.04.010>.
- [9] C. Ma, F. Wang, H. Zhou, Z. Jiang, W. Ren, Y. Du, Effect of early-hydration behavior on rheological properties of borax-admixed magnesium phosphate cement, *Construction and Building Materials* 283 (2021) 122701. <https://doi.org/10.1016/j.conbuildmat.2021.122701>.
- [10] R. Liu, B. Fang, G. Zhang, J. Guo, Y. Yang, Investigation of sodium alginate as a candidate retarder of magnesium phosphate cement: Hydration properties and its retarding mechanism, *Ceramics International* 48 (2022) 30846–30852. <https://doi.org/10.1016/j.ceramint.2022.07.038>.
- [11] S.A. Walling, J.L. Provis, Magnesia-Based Cements: A Journey of 150 Years, and Cements for the Future?, *Chemical Reviews* 116 (2016) 4170–4204. <https://doi.org/10.1021/acs.chemrev.5b00463>.
- [12] E. Alvarado, L.M. Torres-Martinez, A.F. Fuentes, P. Quintana, Preparation and characterization of MgO powders obtained from different magnesium salts and the mineral dolomite, *Polyhedron* 19 (2000) 2345–2351. [https://doi.org/10.1016/S0277-5387\(00\)00570-2](https://doi.org/10.1016/S0277-5387(00)00570-2).
- [13] D. Chartier, J. Sanchez-Canet, P. Antonucci, S. Esnouf, J.-P. Renault, O. Farcy, D. Lambertin, S. Parraud, H. Lamotte, C.C.D. Coumes, Behaviour of magnesium phosphate cement-based materials under gamma and alpha irradiation, *Journal of Nuclear Materials* 541 (2020) 152411. <https://doi.org/10.1016/j.jnucmat.2020.152411>.
- [14] S. Huete-Hernández, A. Maldonado-Alameda, J. Giro-Paloma, J.M. Chimenos, J. Formosa, Fabrication of sustainable magnesium phosphate cement micromortar using design of experiments statistical modelling: Valorization of ceramic-stone-porcelain containing waste as filler, *Ceramics International* 47 (2021) 10905–10917. <https://doi.org/10.1016/j.ceramint.2020.12.210>.
- [15] Z. Zhao, M. Chen, J. Xu, L. Li, Y. Huang, L. Yang, P. Zhao, L. Lu, Mix design and rheological properties of magnesium potassium phosphate cement composites based on the 3D printing

- extrusion system, *Construction and Building Materials* 284 (2021). <https://doi.org/10.1016/j.conbuildmat.2021.122797>.
- [16] EN 196-1, Methods of testing cement. Part 1: Determination of strength, (2016).
- [17] M.C. Alonso Alonso, J.L. García-Calvo, C. Walker, M. Naito, S. Pettersson, I. Puigdomenech, M.A. Cuñado, M. Vuorio, H. Weber, H. Ueda, Development of an accurate pH measurement methodology for the pore fluids of low pH cementitious materials, SKB, Stockholm (Sweden), 2012. <https://skb.se/upload/publications/pdf/R-12-02.pdf>.
- [18] C. Fernández-García, M.C. Alonso, J.M. Bastidas, I. García-Lodeiro, R. Fernández, MgO/KH₂PO₄ and Curing Moisture Content in MKPC Matrices to Optimize the Immobilization of Pure Al and Al-Mg Alloys, *Materials* 17 (2024) 1263. <https://doi.org/10.3390/ma17061263>.
- [19] C.A. Strydom, E.M. van der Merwe, M.E. Aphane, The effect of calcining conditions on the rehydration of dead burnt magnesium oxide using magnesium acetate as a hydrating agent, *Journal of Thermal Analysis and Calorimetry* 80 (2005) 659–662. <https://doi.org/10.1007/s10973-005-0710-x>.
- [20] F. Qiao, Reaction Mechanisms of Magnesium Potassium Phosphate Cement and its Application, Hong Kong University of Sciences and Technology, 2010.
- [21] M. Le Rouzic, T. Chaussadent, L. Stefan, M. Saillio, On the influence of Mg/P ratio on the properties and durability of magnesium potassium phosphate cement pastes, *Cement and Concrete Research* 96 (2017) 27–41. <https://doi.org/10.1016/j.cemconres.2017.02.033>.
- [22] L. Stefan, T. Chaussadent, H. Bessaies-Bey, Thiosulphates for use as set retarders in phosphomagnesium cement pastes, WO2021123564a1, 2019.
- [23] K.-H. Yang, A.-R. Cho, J.-K. Song, Effect of water–binder ratio on the mechanical properties of calcium hydroxide-based alkali-activated slag concrete, *Construction and Building Materials* 29 (2012) 504–511. <https://doi.org/10.1016/j.conbuildmat.2011.10.062>.
- [24] A. Wang, Z. Yuan, J. Zhang, L. Liu, J. Li, Z. Liu, Effect of raw material ratios on the compressive strength of magnesium potassium phosphate chemically bonded ceramics, *Materials Science and Engineering: C* 33 (2013) 5058–5063. <https://doi.org/10.1016/j.msec.2013.08.031>.
- [25] A. Wang, J. Zhang, J. Li, A. Ma, L. Liu, Effect of liquid-to-solid ratios on the properties of magnesium phosphate chemically bonded ceramics, *Materials Science and Engineering: C* 33 (2013) 2508–2512. <https://doi.org/10.1016/j.msec.2013.02.014>.
- [26] H. Ma, B. Xu, J. Liu, H. Pei, Z. Li, Effects of water content, magnesia-to-phosphate molar ratio and age on pore structure, strength and permeability of magnesium potassium phosphate cement paste, *Materials & Design* 64 (2014) 497–502. <https://doi.org/10.1016/j.matdes.2014.07.073>.
- [27] Z. Ding, Z. Li, Effect of aggregates and water contents on the properties of magnesium phospho-silicate cement, *Cement and Concrete Composites* 27 (2005) 11–18. <https://doi.org/10.1016/j.cemconcomp.2004.03.003>.
- [28] Y. Li, J. Sun, B. Chen, Experimental study of magnesia and M/P ratio influencing properties of magnesium phosphate cement, *Construction and Building Materials* 65 (2014) 177–183. <https://doi.org/10.1016/j.conbuildmat.2014.04.136>.
- [29] Q. Yang, B. Zhu, S. Zhang, X. Wu, Properties and applications of magnesia–phosphate cement mortar for rapid repair of concrete, *Cement and Concrete Research* 30 (2000) 1807–1813. [https://doi.org/10.1016/S0008-8846\(00\)00419-1](https://doi.org/10.1016/S0008-8846(00)00419-1).
- [30] F. Qiao, C.K. Chau, Z. Li, Property evaluation of magnesium phosphate cement mortar as patch repair material, *Construction and Building Materials* 24 (2010) 695–700. <https://doi.org/10.1016/j.conbuildmat.2009.10.039>.
- [31] L.J. Gardner, S.A. Bernal, S.A. Walling, C.L. Corkhill, J.L. Provis, N.C. Hyatt, Characterisation of magnesium potassium phosphate cements blended with fly ash and ground granulated blast furnace slag, *Cement and Concrete Research* 74 (2015) 78–87. <https://doi.org/10.1016/j.cemconres.2015.01.015>.

- [32] B. Xu, H. Ma, H. Shao, Z. Li, B. Lothenbach, Influence of fly ash on compressive strength and micro-characteristics of magnesium potassium phosphate cement mortars, *Cement and Concrete Research* 99 (2017) 86–94. <https://doi.org/10.1016/j.cemconres.2017.05.008>.
- [33] A.S. Wagh, S.Y. Jeong, D. Singh, High strength phosphate cement using industrial byproducts ashes, in: *The American Society of Civil Engineers*, A. Azizinamini, D. Darwin, and C. French, Kona, Hawaii, 1997: pp. 542–553.
- [34] L. Mo, L. Lv, M. Deng, J. Qian, Influence of fly ash and metakaolin on the microstructure and compressive strength of magnesium potassium phosphate cement paste, *Cement and Concrete Research* 111 (2018) 116–129. <https://doi.org/10.1016/j.cemconres.2018.06.003>.